

ML-TDR-64-195

AD609667



SLIP-CAST FUSED SILICA

TECHNICAL DOCUMENTARY REPORT No. ML-TDR-64-195

| | | | | |
|------------|------------|----|---|----|
| COPY | 2 | OF | 3 | 14 |
| HARD COPY | \$. 4. 00 | | | |
| MICROFICHE | \$. 1. 00 | | | |

OCTOBER 1964

JAN 1 1965

AF MATERIALS LABORATORY
RESEARCH AND TECHNOLOGY DIVISION
AIR FORCE SYSTEMS COMMAND
WRIGHT-PATTERSON AIR FORCE BASE, OHIO

(Prepared by Georgia Institute of Technology,
Engineering Experiment Station, Atlanta, Georgia;
J. D. Walton and N. E. Poulos, Authors)

ARCHIVE COPY

NOTICES

When Government drawings, specifications, or other data are used for any purpose other than in connection with a definitely related Government procurement operation, the United States Government thereby incurs no responsibility nor any obligation whatsoever; and the fact that the Government may have formulated, furnished, or in any way supplied the said drawings, specifications, or other data, is not to be regarded by implication or otherwise as in any manner licensing the holder or any other person or corporation, or conveying any rights or permission to manufacture, use, or sell any patented invention that may in any way be related thereto.

Qualified requesters may obtain copies of this report from the Defense Documentation Center (DDC), (formerly ASTIA), Cameron Station, Bldg. 5, 5010 Duke Street, Alexandria, Virginia, 22314.

This report has been released to the Office of Technical Services, U.S. Department of Commerce, Washington 25, D. C., in stock quantities for sale to the general public.

Copies of this report should not be returned to the Research and Technology Division, Wright-Patterson Air Force Base, Ohio, unless return is required by security considerations, contractual obligations, or notice on a specific document.

500 - December 1964 - 448-18-448

FOREWORD

This report was prepared by J. D. Walton and M. E. Foulcs of the Engineering Experiment Station, Georgia Institute of Technology, Atlanta, Georgia. It was offered for publication at no charge to the Government. Since the subject matter conforms to that with which the Air Force Materials Laboratory is concerned, the report is being published as a Technical Documentary Report.

Acknowledgment is made of the cooperation of the Georgia Institute of Technology in releasing this report for publication and distribution. This cooperative effort is very much appreciated.

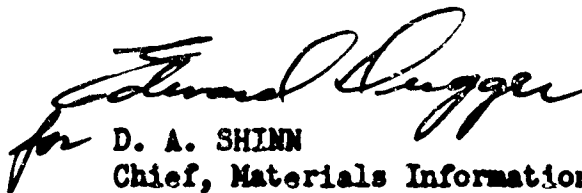
Considerable information on the properties and manufacture of fused silica has been published since its discovery by M. Gadin in 1839. However, no information was available on a new method of fabricating items from fused silica which has been under development at Georgia Tech since 1956. This new development involves the process of slip-casting fused silica. It provides fabrication techniques for forming large and intricate shapes to close tolerances which are prohibitive with the conventional molten fused silica forming techniques. Also, some of the physical properties of this new fused silica form are considerably different from the parent material. These differences require that slip-cast fused silica be considered as an entirely new material, and not as the same fused silica which has been so well studied and about which so much is known.

Since 1956, Georgia Tech has published information in technical reports and bulletins that it has generated from its scientific work on slip-cast fused silica. Also, other investigators have recently published work on slip-cast fused silica. Therefore, it was thought that a collection of this information into a workbook would be of value to those who are interested in slip-cast fused silica.

ABSTRACT

This workbook provides a collection of technical data and information on the slip-cast fused silica work of the Georgia Institute of Technology. It is intended to provide scientists and engineers with thermo-physical, mechanical, electrical, and nuclear properties of slip-cast fused silica. Fabrication techniques and engineering data related to the use of this material for thermal protection systems and radomes are presented. A comprehensive bibliography is also included.

This technical documentary report has been reviewed and is approved.

A handwritten signature in cursive script, appearing to read "D. A. Shinn", with a small "for" written to the left of the main signature.

D. A. SHINN
Chief, Materials Information Branch
Materials Applications Division
AF Materials Laboratory

TABLE OF CONTENTS

| | Page |
|--|------|
| I. FUSED SILICA. | 1 |
| II. SLIP-CASTING FUSED SILICA | 4 |
| A. The Slip. | 4 |
| B. Slip-Casting. | 4 |
| C. Firing. | 4 |
| D. Shrinkage | 8 |
| III. THERMO-PHYSICAL PROPERTIES OF SLIP-CAST FUSED SILICA. | 11 |
| A. Thermal Conductivity. | 11 |
| B. Bulk Density and Porosity | 16 |
| C. Coefficient of Thermal Expansion and Specific Heat. | 16 |
| D. Young's Modulus of Elasticity | 16 |
| IV. MECHANICAL PROPERTIES OF SLIP-CAST FUSED SILICA | 21 |
| A. Modulus of Rupture. | 21 |
| B. Tensile Strength. | 21 |
| C. Compressive Strength. | 26 |
| V. ELECTRICAL PROPERTIES OF SLIP-CAST FUSED SILICA | 26 |
| A. Dielectric Constant and Loss Tangent. | 26 |
| B. Volume Resistivity. | 28 |
| C. Dielectric Strength | 28 |
| VI. NUCLEAR PROPERTIES OF SLIP-CAST FUSED SILICA. | 31 |
| VII. SLIP-CAST FUSED SILICA FOR THERMAL PROTECTION SYSTEMS AND RADOMES . | 33 |
| A. Fabrication. | 34 |
| B. Surface Sealing | 37 |

(Continued)

TABLE OF CONTENTS (Continued)

| | Page |
|--|------|
| 1. Surface melting | 37 |
| 2. Teflon coating | 42 |
| C. High Temperature Environment Simulation | 42 |
| 1. Laboratory testing | 42 |
| a. Oxy-hydrogen rocket motor. | 42 |
| b. Oxy-acetylene torch-facility | 54 |
| 2. Arc Plasma Testing | 54 |
| 3. Testing Full-scale nose cone | 62 |
| D. Improving the Refractoriness of Slip-Cast Fused Silica | 68 |
| 1. Ablation Rate | 68 |
| E. Electrical Evaluation of Slip-Cast Fused Silica Radomes | 78 |
| F. Attachment of Slip-Cast Fused Silica Radomes | 78 |
| G. Improving the Strength of Slip-Cast Fused Silica | 80 |
| H. Rain Erosion Testing of Slip-Cast Fused Silica | 83 |
| VIII. BIBLIOGRAPHY | 85 |
| IX. APPENDIXES. | 88 |
| A. Effective Emittance Calculation | 89 |
| B. Thermal Shock Considerations | 91 |
| C. Rain Erosion Sled Tests | 98 |

LIST OF FIGURES

| | Page |
|---|------|
| 1. Specific Volume of Different Forms of Silica (Ref 1, page 365) . . . | 2 |
| 2. Specific Heat vs. Temperature for Fused Silica, Graphite, Air, and Copper | 3 |
| 3. Particle Size Distribution of Fused Silica Slip (Ref 2, page 9). . . | 5 |
| 4. Cast Wall Thickness vs. Casting Time for Fused Silica Slip (Ref 3, page 47) | 6 |
| 5. Relation Between Cast Wall Thickness and Time for Fused Silica Slip Pressure Cast at 0, 20, 40, and 60 psig Applied Pressure (Ref 4, page 47) | 7 |
| 6. Cristobalite Content of Slip-Cast Fused Silica Fired Under One Atmosphere of Air (Ref 5, page 30) | 9 |
| 7. Slip-Cast Fused Silica Ash Tray Compared With Ash Tray Slip-Cast from Cone 01 Whiteware Body to Illustrate Low Shrinkage of Slip- Cast Fused Silica (Ref 3, page 57) | 10 |
| 8. Shell and Tube Heat Exchanger Slip-Cast from Fused Silica (Ref 4, page 53) | 12 |
| 9. Sectional View of Thermal Conductivity Apparatus (Ref 7, page 55). . | 13 |
| 10. Thermal Conductivity of Clear Fused Silica, Slip-Cast Fused Silica, and Foamed Fused Silica Slip as a Function of Mean Specimen Temperature (Ref 3, page 57) | 14 |
| 11. Thermal Diffusivity of Slip-Cast Fused Silica and Foamed Fused Silica (Ref 8, page 35). | 15 |
| 12. Thermal Conductivity Test Specimen Design Used by Midwest Research Institute (Ref 7, page 95) | 17 |
| 13. Effect of Temperature and Time at Temperature on Thermal Conductivity of Slip-Cast Fused Silica Studied by Midwest Research Institute (Ref 7, page 96) | 18 |
| 14. Bulk Density of Slip-Cast Fused Silica Fired Under One Atmosphere of Air (Ref 6, page 21). | 19 |
| 15. Porosity of Slip-Cast Fused Silica Under One Atmosphere of Air (Ref 6, page 18) | 20 |

(Continued)

LIST OF FIGURES (Continued)

| | Page |
|---|------|
| 16. Modulus of Rupture as a Function of Firing Conditions (Ref 2, page 25) | 22 |
| 17. Modulus of Rupture Contour for Slip-Cast Fused Silica Fired Under One Atmosphere of Air (Ref 6, page 13) | 23 |
| 18. Time to Reach Maximum Strength in Slip-Cast Fused Silica During One Atmosphere Air Firing vs. Reciprocal of Absolute Sintering Temperature (Ref 9, page 10) | 24 |
| 19. Tensile Strength of Slip-Cast Fused Silica vs. Firing Time at 2200° F for Various Testing Temperatures (Ref 10, in Press). | 25 |
| 20. Compressive Strength of Slip-Cast Fused Silica as a Function of Firing Time Fired Under One Atmosphere of Air (Ref 6, page 10) . . . | 27 |
| 21. Resistivity of Clear Fused Silica and Slip-Cast Fused Silica as a Function of Temperature (Ref 11, page 191) | 29 |
| 22. Dielectric Strength of Fused Silica Glass as a Function of Temperature (Ref 12, page 424) | 30 |
| 23. Effect of Irradiation on the Modulus of Rupture of Slip-Cast Fused Silica (Ref 13, page 43) | 32 |
| 24. Nose Cone Configurations Sent to Redstone Arsenal (Ref 7, page 104). . | 35 |
| 25. Radomes Which Have Been Slip-Cast from Fused Silica (Ref 5, page 9 11) | 36 |
| 26. Pressure Casting Set-Up for Slip-Casting Fused Silica Radome (Ref 14, page 50). | 38 |
| 27. Photograph of Set-Up for Tip-Up Pressure Casting of Radome (Ref 14, page 93). | 39 |
| 28. Artist Conception of Modified Flame Glazing Device (Ref 5, page 97). . | 40 |
| 29. Insertion Phase Difference for Slip-Cast Fused Silica (Ref 15) . . . | 41 |
| 30. Set-Up for Evaluating Ceramic Materials in Exhaust of Oxy-Hydrogen Rocket Motor (Ref 16, page 156). | 43 |
| 31. Stagnation Temperature and Stagnation Enthalpy in Rocket Motor Exhaust as a Function of Distance from the Exit Plane (Ref 17, page 20). | 44 |

(Continued)

LIST OF FIGURES (Continued)

| | Page |
|--|------|
| 32. Copper Calorimeter for Heat Flux Measurements (Ref 8, page 52) . . . | 45 |
| 33. Heat Flux of Exhaust of Oxy-Hydrogen Rocket Motor (Ref 8, page 55) | 47 |
| 34. Backside Temperature Change as a Function of Thickness of Slip-Cast Fused Silica Plates Exposed to Oxy-Hydrogen Rocket Motor (Ref 18, page 22). | 49 |
| 35. Backside Temperature Change for Grooved and Ungrooved Flat Plate Samples of Slip-Cast Fused Silica Exposed to Oxy-Hydrogen Rocket Motor (Ref 18, page 24). | 50 |
| 36. Temperature Profiles and Backside Temperature for 1/2-Inch Thick Plate of Slip-Cast Fused Silica (Ref 8, page 37) | 53 |
| 37. Temperature Measurements on a 1/4-Inch Thick Slip-Cast Fused Silica Plate Located 14-Inches from the Exit Plane of the Oxy-Hydrogen Rocket Motor (Ref 8, page 64). | 55 |
| 38. Temperature Measurements on a 1/4-Inch Thick Pyroceraam Plate Located 14-Inches from the Exit Plane of the Oxy-Hydrogen Rocket Motor (Ref 8, page 65) | 56 |
| 39. Temperature Measurements on a 1/4-Inch Thick Aluminum Oxide Plate Located 14-Inches from the Exit Plane of the Oxy-Hydrogen Rocket Motor (Ref 8, page 63) | 57 |
| 40. Artist Rendering of Oxy-Acetylene Test Facility (Ref 14, page 110) . | 58 |
| 41. Relative Heat Flux vs. Distance for 40, 60, and 80 CFH Acetylene at Oxygen-to-Acetylene Ratio of 1.5 (Ref 19, page 9). | 59 |
| 42. Surface Temperature, Weight Change and Length Change of Slip-Cast Fused Silica as a Function of Time Exposed to Oxy-Acetylene Test Facility (Ref 14, page 46) | 60 |
| 43. Simulated Capability of LAS Arc-Vacuum Facility, Altitude vs. Velocity Including Radiation Equilibrium Data Points for Fused Silica (Ref 14, page 19). | 63 |
| 44. Fused Silica Nose Cone Showing Mounting Brackets Cemented in Place With Adhesive Resin (Ref 7, page 47) | 64 |
| 45. 164 HT Facility (Ref 14, page 14). | 65 |

(Continued)

LIST OF FIGURES (Concluded)

| | Page |
|--|------|
| 46. Slip-Cast Fused Silica Nose Cone after Test (Elevation) (Ref 14, page 15) | 69 |
| 47. Slip-Cast Fused Silica Nose Cone after Test (Plan) (Ref 14, page 16) | 70 |
| 48. Surface Temperature, Weight Change and Length Change of Slip-Cast 2.5 w/o Chromium Oxide - 97.5 w/o Fused Silica as a Function of Time Exposed to Oxy-Acetylene Test Facility (Ref 14, page 47) | 71 |
| 49. Drawing Illustrating Flame Shield-Test Bar Arrangement (Ref 14, page 55) | 73 |
| 50. Surface Temperature and Length Change of Slip-Cast Fused Silica with Flame Shield as a Function of Time Exposed to Oxy-Acetylene Test Facility (Ref 14, page 56) | 74 |
| 51. Surface Temperature and Length Change of Slip-Cast 2.5 w/o Chromium Oxide - 97.5 w/o Fused Silica with Flame Shield as a Function of Time Exposed to Oxy-Acetylene Test Facility (Ref 14, page 57) | 75 |
| 52. Effective Emittance vs. Corrected Surface Temperature for Slip-Cast Fused Silica (Ref 14, page 70) | 76 |
| 53. Effective Emittance vs. Corrected Surface Temperature for Slip-Cast 2.5 w/o Chromium Oxide - 97.5 w/o Fused Silica (Ref 14, pages 71-73) | 77 |
| 54. Comparison of Effective Emittance vs. Corrected Surface Temperature of Slip-Cast Fused Silica With and Without Chromium Oxide | 79 |
| 55. Experimental Ring Configuration for Mounting Slip-Cast Fused Silica Radome | 81 |
| 56. Apparent Tensile Strength of Fused Silica Cylinders Wrapped with Fiberglas Yarn Using Constant Tension Device | 84 |

LIST OF TABLES

| | Page |
|---|------|
| I. PROPERTIES OF FUSED SILICA SLIP. | 4 |
| II. EFFECT OF TEMPERATURE ON DIELECTRIC CONSTANT AND LOSS TANGENT OF SLIP-CAST FUSED SILICA | 26 |
| III. CRISTOBALITE CONTENT OF SLIP-CAST FUSED SILICA SAMPLES AFTER IRRADIATION. | 33 |
| IV. NUCLEAR PROPERTIES OF FUSED SILICA | 33 |
| V. OPERATIONAL DATA FOR OXYGEN-HYDROGEN ROCKET MOTOR. | 46 |
| VI. TEST CONDITIONS EMPLOYED FOR MATERIALS TEST WORK | 61 |
| VII. TEST DATA OF SLIP-CAST FUSED SILICA UNDER TEST CONDITIONS LISTED IN TABLE III | 61 |
| VIII. TEST CONDITIONS AND RESULTS FOR FUSED SILICA SPECIMENS EXPOSED TO AN ARC-PLASMA JET EFFLUENT | 66 |

I. Fused Silica

Fused silica is usually produced by melting quartz, but may be obtained by melting any of the crystalline forms of silica. Fused silica is the least dense form of silica, as can be seen from Figure 1. The common crystalline forms of silica have high and low temperature forms. The crystalline structure changes from one form to the other at a definite temperature, resulting in a sudden change in volume $1/$. This change is known as an inversion and causes the material to be very sensitive to thermal shock in the temperature range of the inversion. From Figure 1 it can be seen that vitreous (fused) silica has no inversion, and also essentially no thermal expansion. The coefficient of thermal expansion of fused silica is $0.54 \times 10^{-6}/^{\circ}\text{C}$ or $0.3 \times 10^{-6}/^{\circ}\text{F}$. This unusually low coefficient of thermal expansion is responsible for its excellent thermal shock resistance.

The specific heat of fused silica is shown as a function of temperature in Figure 2. Also shown in Figure 2 are the specific heat of copper, air, and graphite as a function of temperature.

Sosman has presented data which indicate that the modulus of elasticity of fused silica increases with temperature up to about 1200°F where it is approximately 30 per cent above the room temperature value. Above this temperature the modulus of elasticity decreases. At 1500°F it is approximately 15 per cent below the room temperature value.

A summary of elastic constants for vitreous (fused) silica are given by Sosman as follows:

| | |
|------------------------|-------------------------------|
| Modulus of Compression | $5.3 \times 10^6 \text{ psi}$ |
| Rigidity | $4.4 \times 10^6 \text{ psi}$ |

Manuscript released by the authors June 1964 for publication as an RTD Technical Documentary Report.

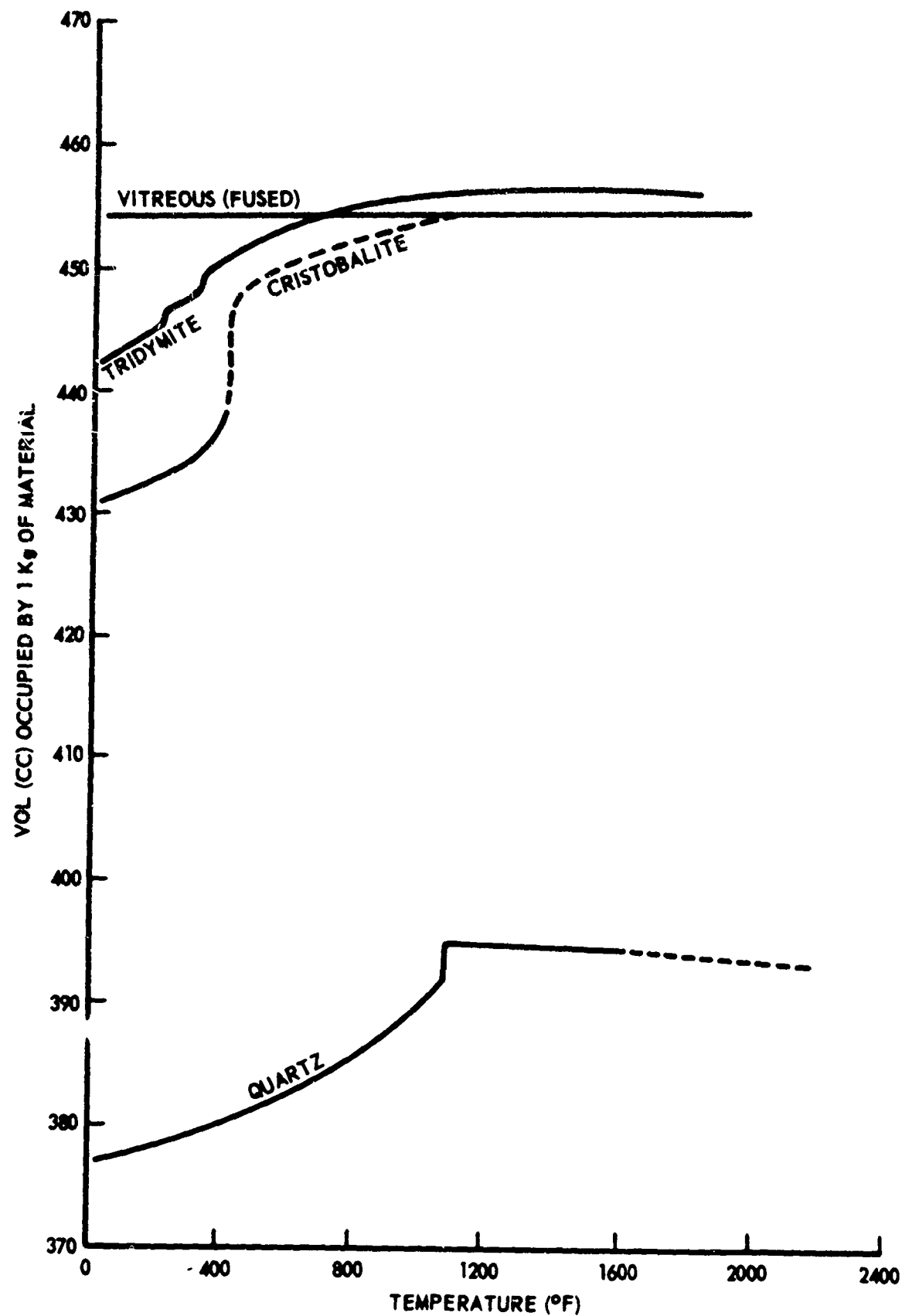
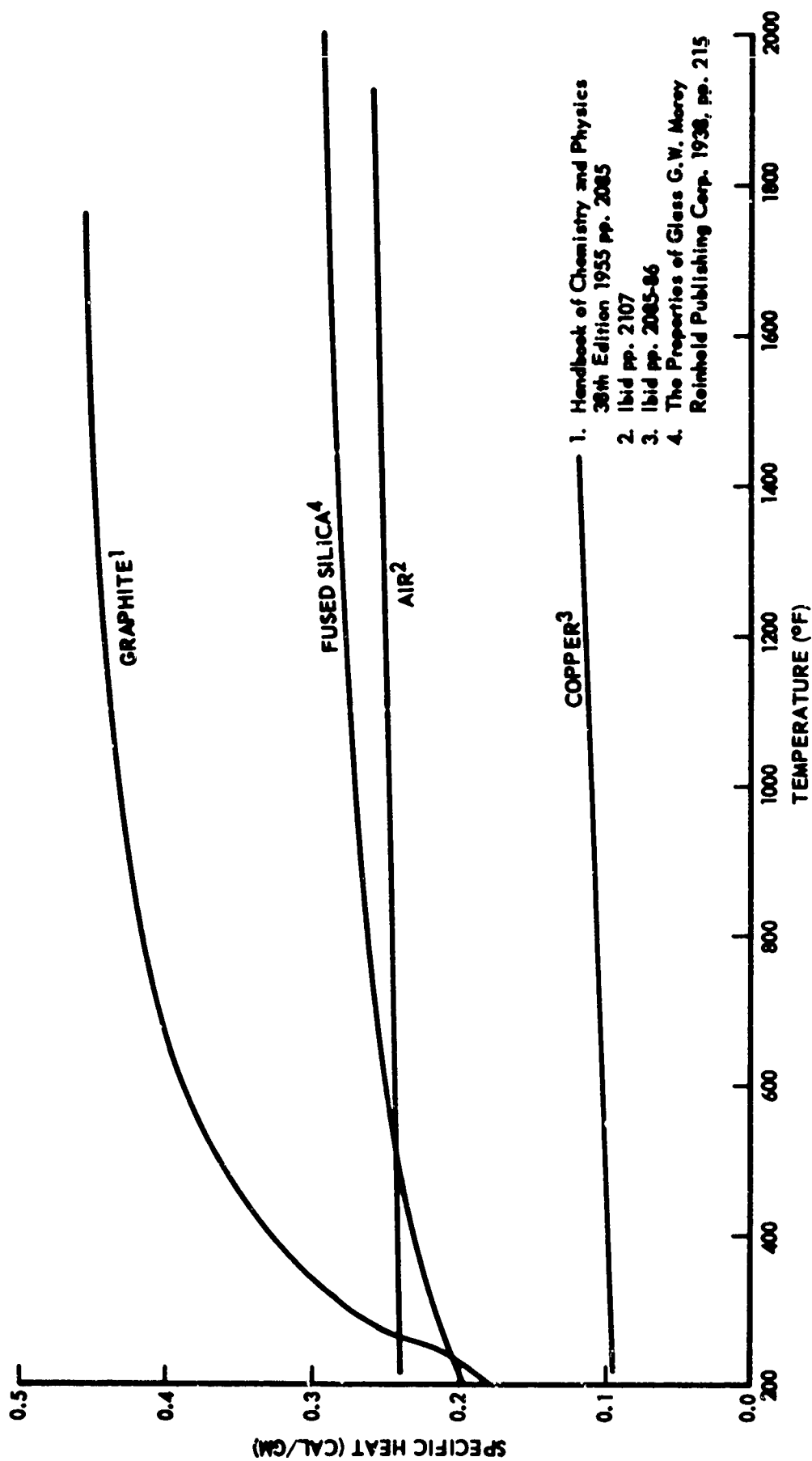


Figure 1. Specific Volume of Different Forms of Silica (Ref 1, page 365).



1. Handbook of Chemistry and Physics
38th Edition 1955 pp. 2085
2. Ibid pp. 2107
3. Ibid pp. 2085-86
4. The Properties of Glass G.W. Morey
Reinhold Publishing Corp. 1938, pp. 215

Figure 2. Specific Heat vs. Temperature for Fused Silica, Graphite, Air, and Copper.

| | |
|------------------------|------------------------|
| Young's Modulus | 10.0×10^6 psi |
| Poisson's Ratio | 0.14 |
| Modulus of Penetration | 10.0×10^6 psi |

II. Slip-Casting Fused Silica

A. The Slip

A fused silica slip may be prepared by wet grinding fused silica 2/ to the particle size range shown in Figure 3. Properties of the slip are shown in Table I.

TABLE I
PROPERTIES OF FUSED SILICA SLIP

| | |
|------------------------|--------|
| Weight Per Cent Solids | 82.6 |
| Apparent Viscosity | 131 cp |
| pH | 5.2 |

B. Slip-Casting

Slip-casting is carried out in plaster molds. The cast wall thickness as a function of casting time 3/ is shown in Figure 4. The effect of applied pressure to the slip during casting 4/ is shown in Figure 5.

C. Firing

The usual firing temperature for slip-cast fused silica is between 2100° and 2300° F. An attractive characteristic of slip-cast fused silica is its ability to be rapid-fired to these temperatures and subsequently

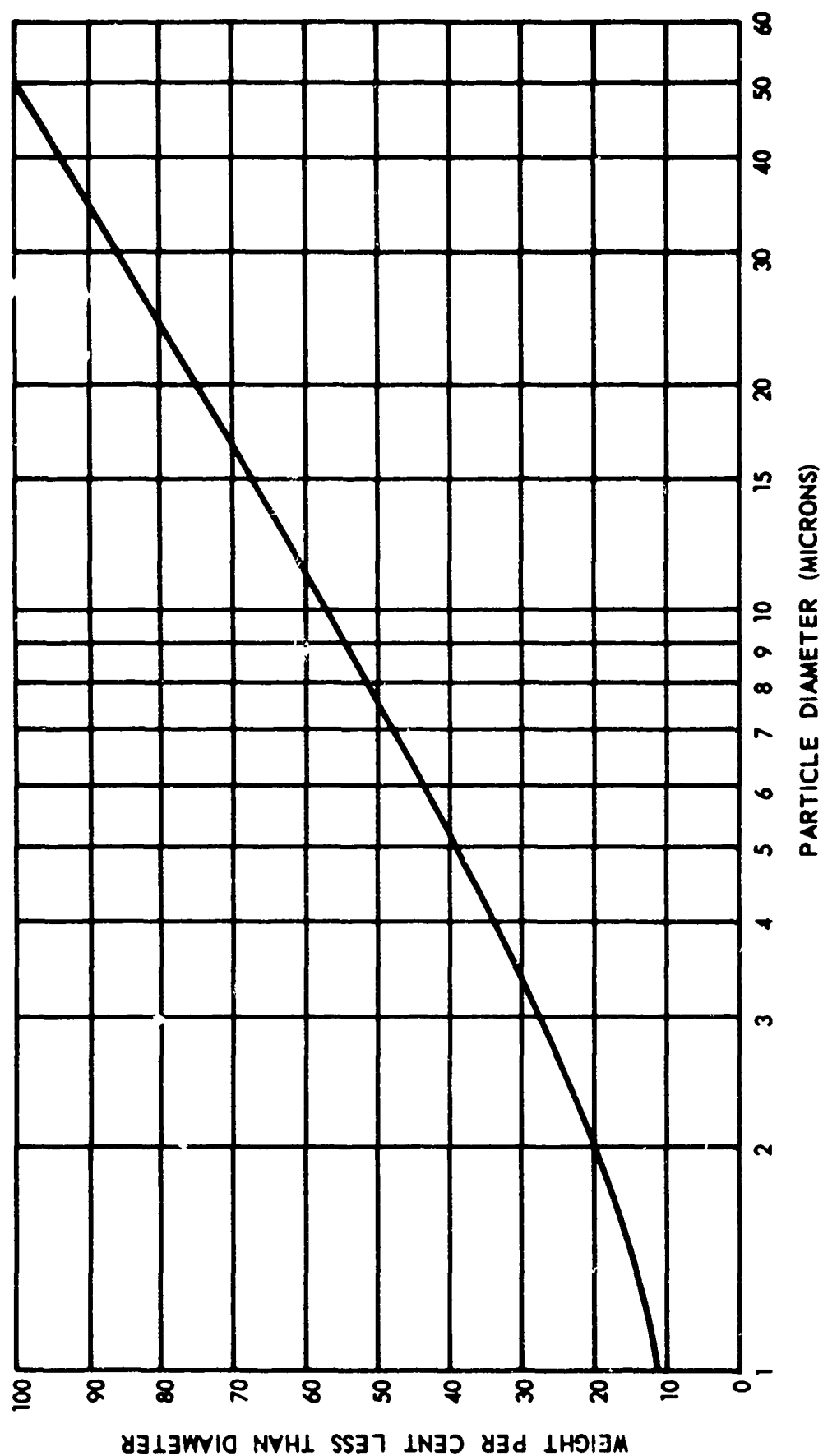


Figure 3. Particle Size Distribution of Fused Silica Slip (Ref 2, page 9).

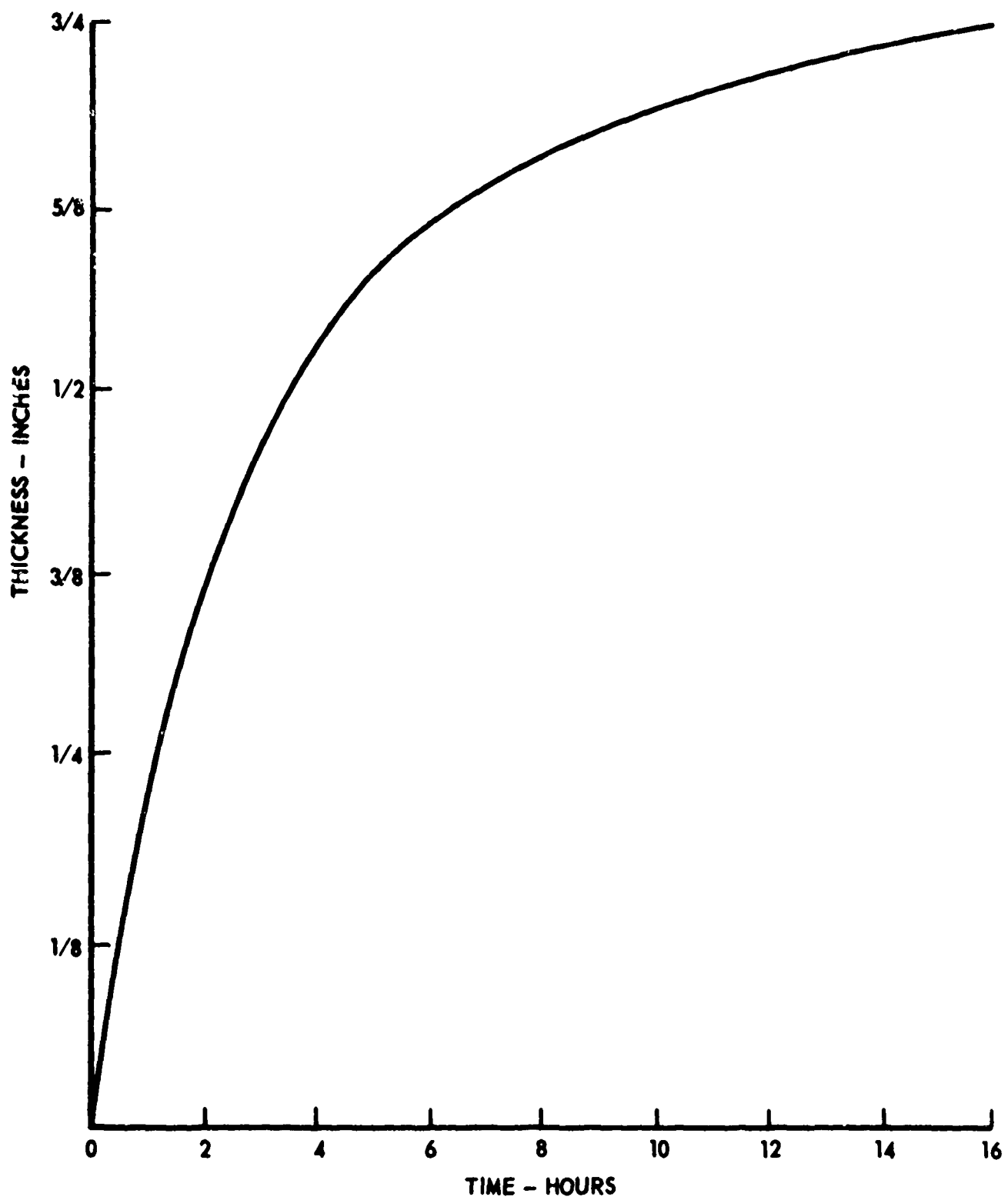


Figure 4. Cast Wall Thickness vs. Casting Time for Fused Silica Slip (Ref 3, page 47).

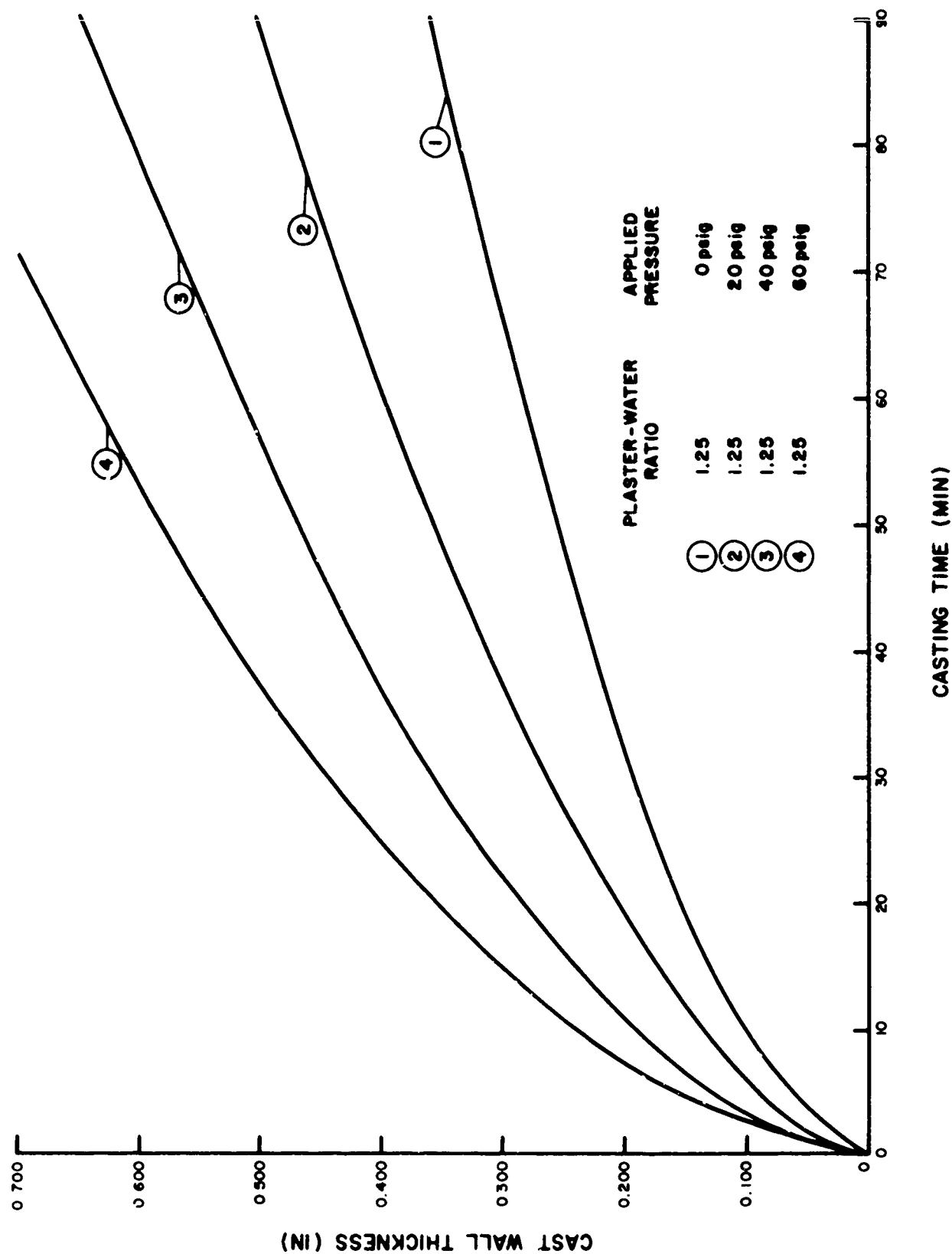


Figure 5. Relation Between Cast Wall Thickness and Time, for Fused Silica Slip Pressure Cast at 0, 20, 40, and 60 psig Applied Pressure (Ref 4, page 47).

air quenched with no cracking due to thermal shock. Fused Silica transforms to cristobalite in this temperature range which makes it necessary to control firing time very carefully. A small percentage of cristobalite is required to obtain maximum strength. However, since cristobalite has an undesirable thermal inversion as shown in Section I and Figure 1 excessive amounts must be avoided to prevent an appreciable decrease in thermal shock capability. Cristobalite content of fired slip-cast fused silica is shown as a function of firing time for firing temperatures of 2100°, 2200°, and 2300° F 5/ in Figure 6. For thin wall (< 1/2-inch) slip-cast fused silica articles, a firing schedule of 3-1/3 hours at 2200° F has been found optimum using an electric kiln. The rate of devitrification increases with increasing moisture content in the furnace atmosphere. Therefore, when firing in an unmuffled gas fired kiln the firing time and/or temperature must be reduced to compensate for the increased devitrification rate.

The relationship between firing conditions and electrical thermal and mechanical properties is discussed in the following sections.

D. Shrinkage

The combined drying and firing linear shrinkage of slip-cast fused silica is between 1 to 2 per cent. This shrinkage is unique among ceramic materials and allows for a much greater degree of control over final dimensions than is possible with conventional slip-cast ceramic materials which exhibit shrinkage between 15 to 20 per cent. This difference in shrinkage is illustrated in Figure 7 which shows two ash trays cast in the same plaster mold 3/. The high shrinkage of the conventional ceramic body is evident when compared with the ash tray on the right slip-cast from fused

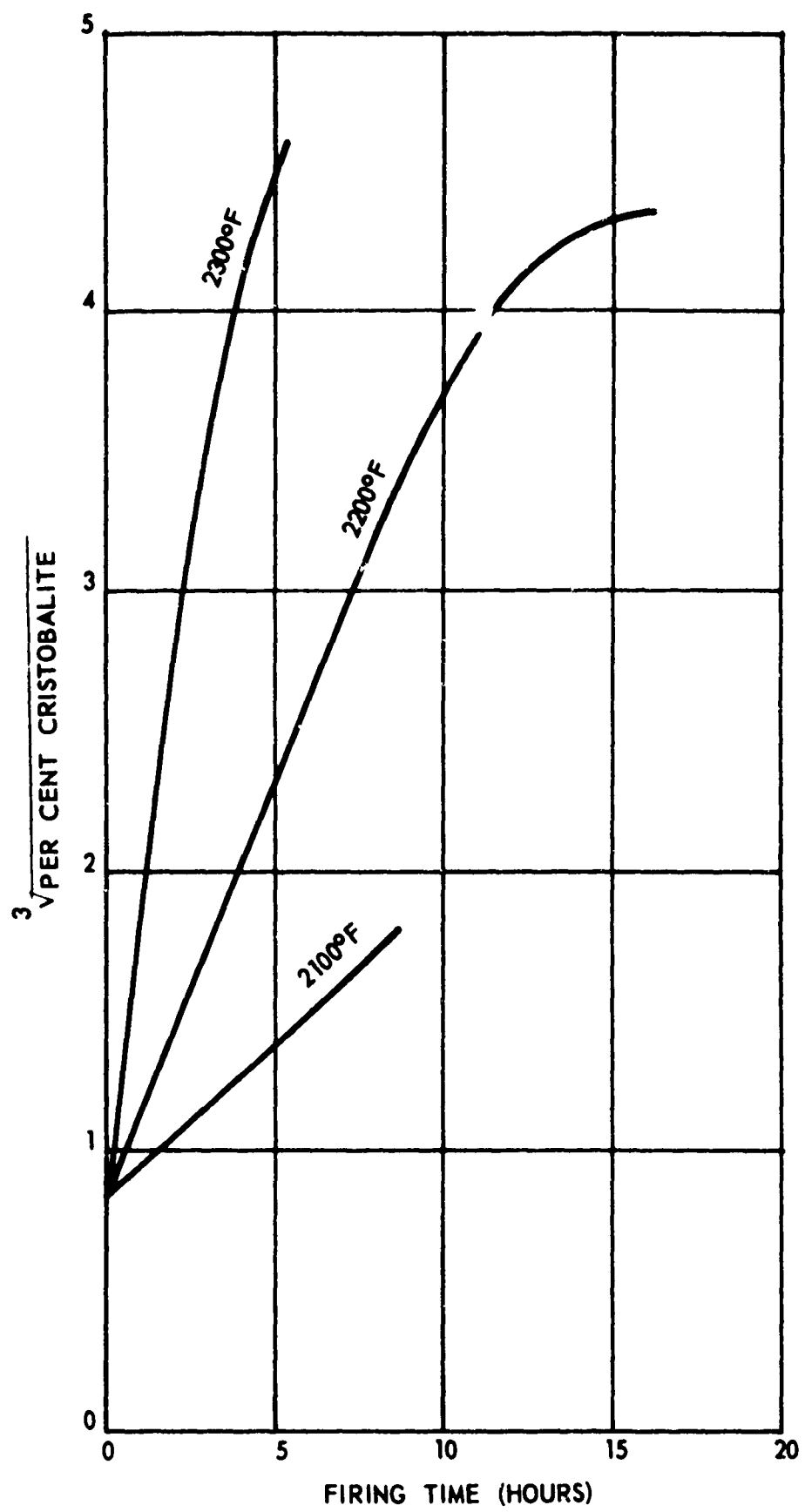


Figure 6. Cristobalite Content of Slip-Cast Fused Silica Fired Under One Atmosphere of Air (Ref 5, page 30).

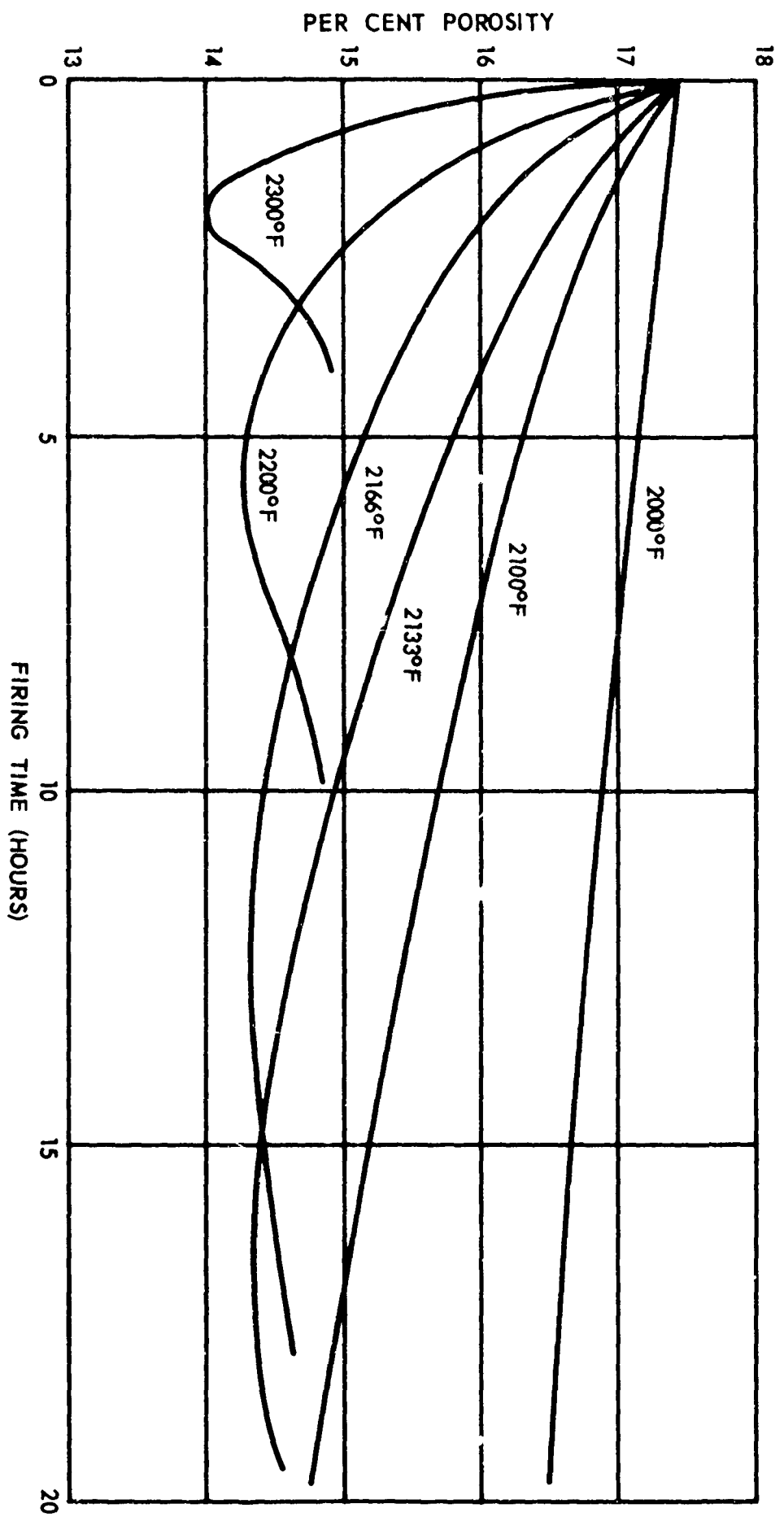


Figure 15. Porosity of Slip-Cast Fused Silica Under One Atmosphere of Air (Ref 6, page 18).



Figure 7. Slip-Cast Fused Silica Ash Tray Compared With Ash Tray Slip-Cast from Cone 01 Whiteware Body to Illustrate Low Shrinkage of Slip-Cast Fused Silica (Ref 3, page 57).



Figure 8. Shell and Tube Heat Exchanger Slip-Cast from Fused Silica (Ref 4, page 53).

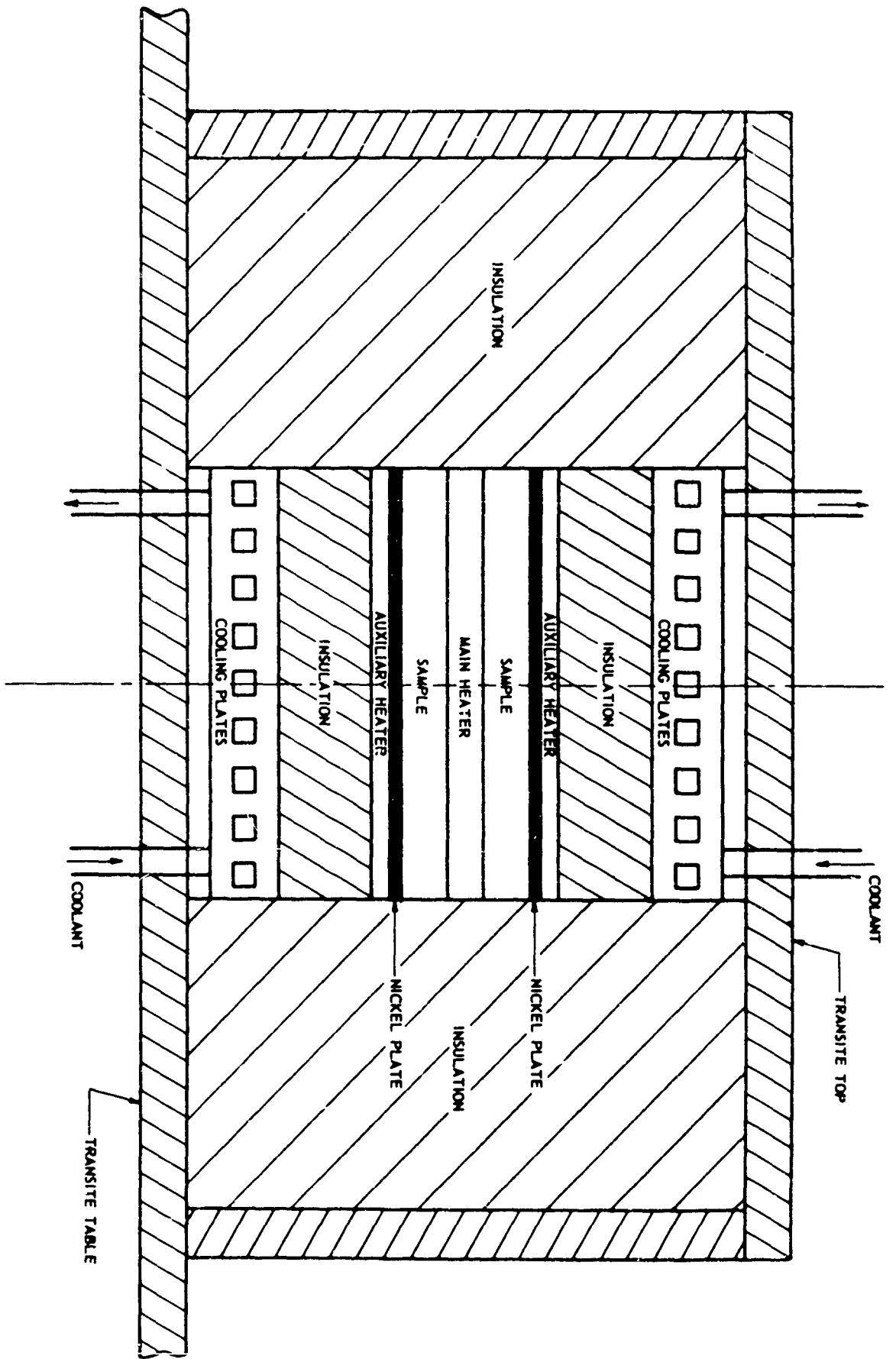


Figure 9. Sectional View of Thermal Conductivity Apparatus (Ref 7, page 55).

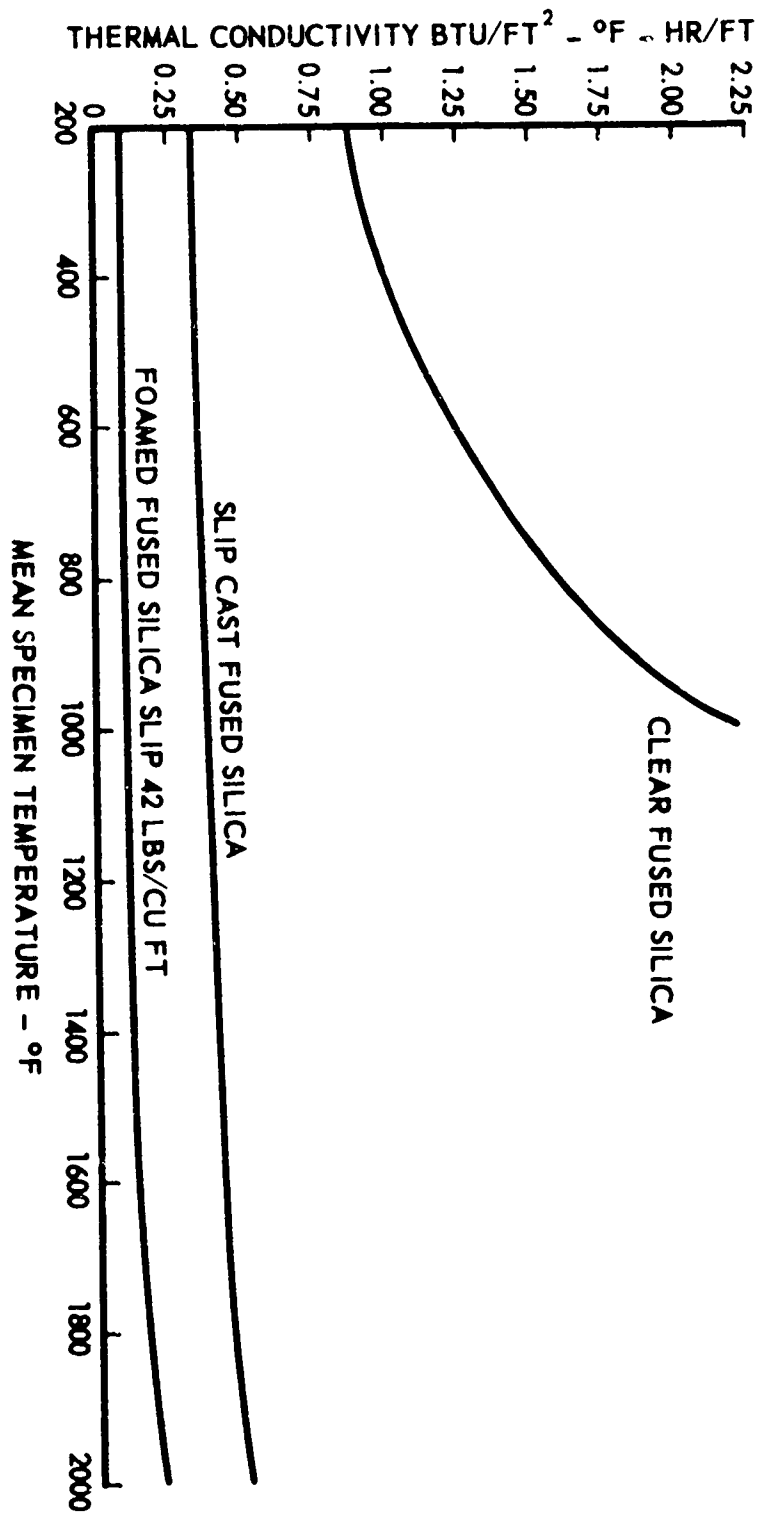


Figure 10. Thermal Conductivity of Clear Fused Silica, Slip-Cast Fused Silica, and Foamed Fused Silica Slip as a Function of Mean Specimen Temperature (Ref 3, page 57).

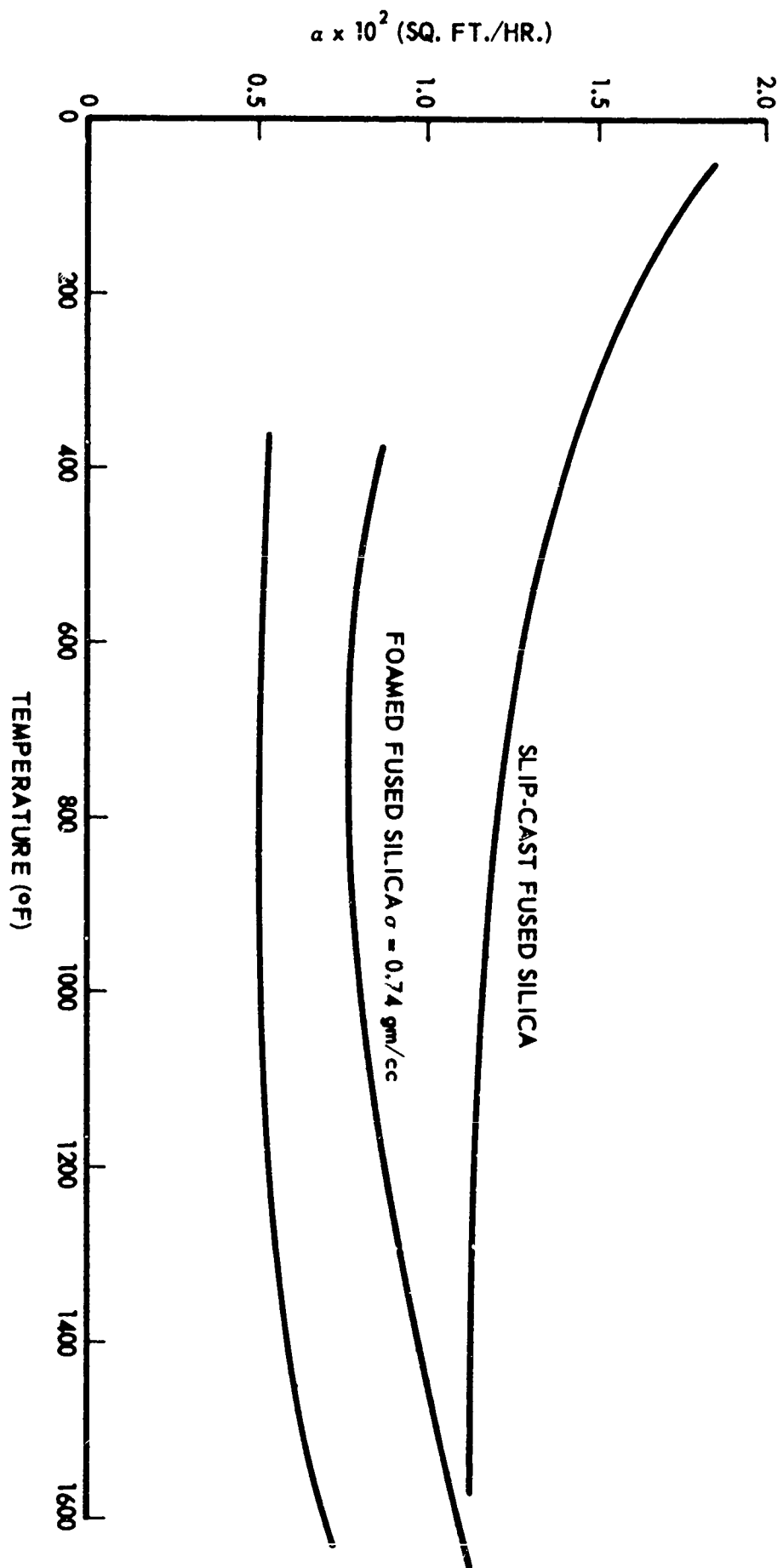


Figure 11. Thermal Diffusivity of Slip-Cast Fused Silica and Foamed Fused Silica (Ref 8, page 35).

Midwest Research Institute (MRI) has also determined the thermal conductivity of slip-cast fused silica 7/. The apparatus used by MRI is shown in Figure 12. Figure 13 presents the thermal conductivity data obtained from MRI. The increased thermal conductivity above 2000° F is due to the long time heating employed by MRI in obtaining their data. The specimen was above 2000° for 6 days, and above 2400° F for about 48 hours. During this time the fused silica was almost completely transformed into cristobalite as determined by x-ray analysis. Also, the cooling curve shows that the material being cooled is not the same as that being heated. For short time use, even at temperatures above 2500° F it would be expected that the thermal conductivity of slip-cast fused silica would follow the dashed line shown in Figure 13.

B. Bulk Density and Porosity

The effect of firing time and temperature on the bulk density of slip-cast fused silica 6/ is shown in Figure 14. Per cent porosity is shown plotted as a function of firing time 6/ in Figure 15.

C. Coefficient of Thermal Expansion and Specific Heat

The coefficient of thermal expansion and specific heat of fused silica are determined by the basic material and are not affected by the method of fabrication. The values for these properties were given in Section I.

D. Young's Modulus of Elasticity

The value of Young's Modulus or Elasticity for slip-cast fused silica has been determined at Georgia Tech. The room temperature value is approximately 3.8×10^6 psi. Similar values were reported by Raytheon for slip-cast fused silica specimens supplied by Georgia Tech.

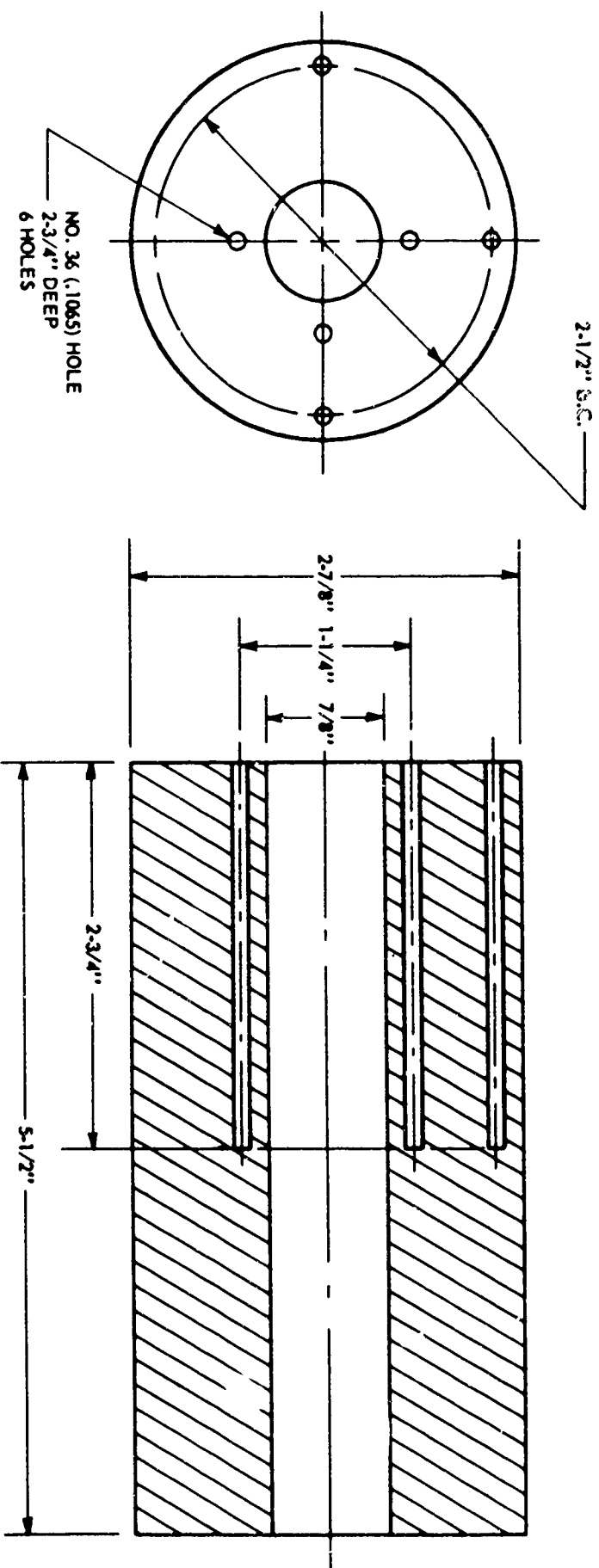


Figure 12. Thermal Conductivity Test Specimen Design Used by Midwest Research Institute (Ref 7, page 95).

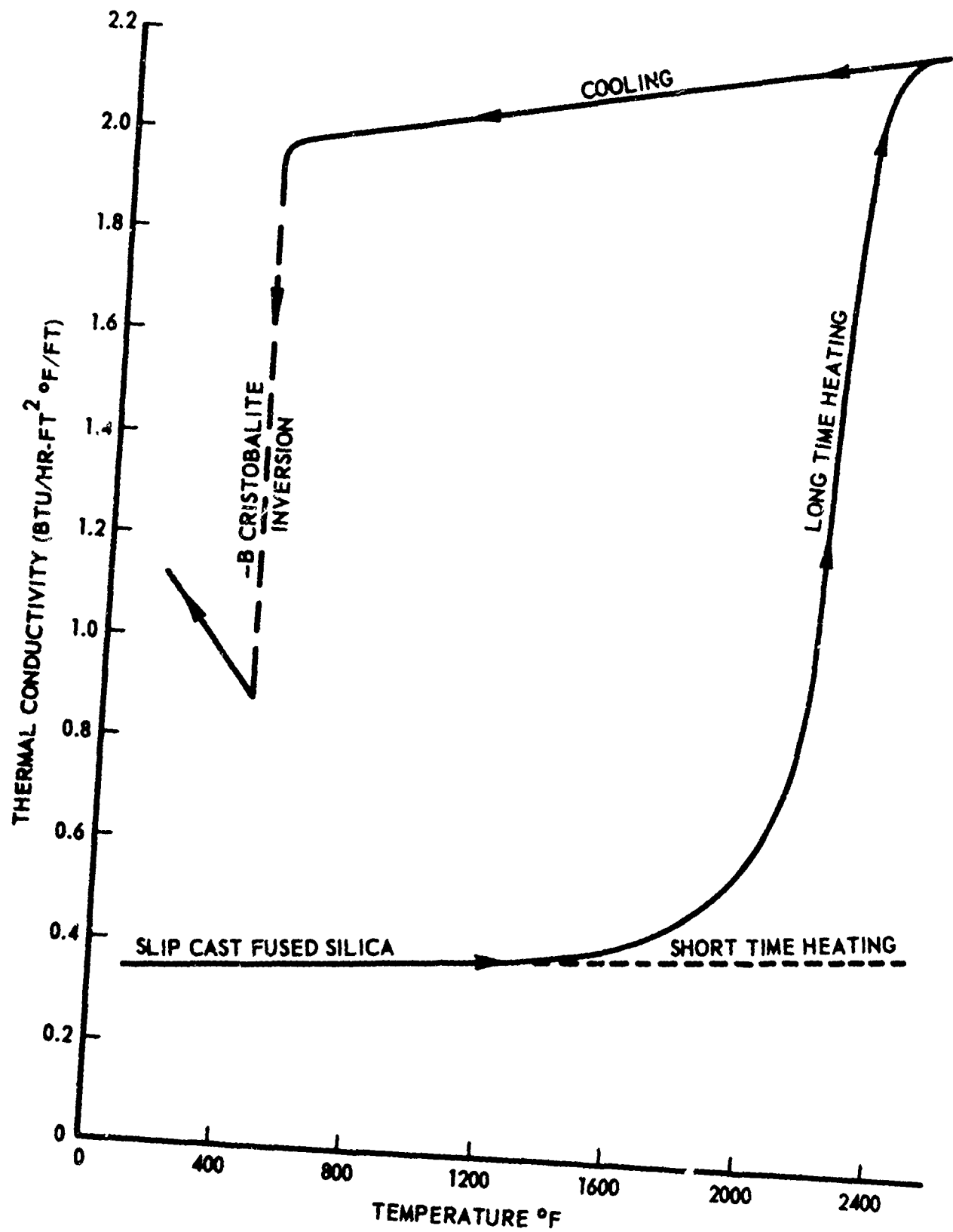


Figure 13. Effect of Temperature and Time at Temperature on Thermal Conductivity of Slip-Cast Fused Silica Studied by Midwest Research Institute (Ref 7, page 96).

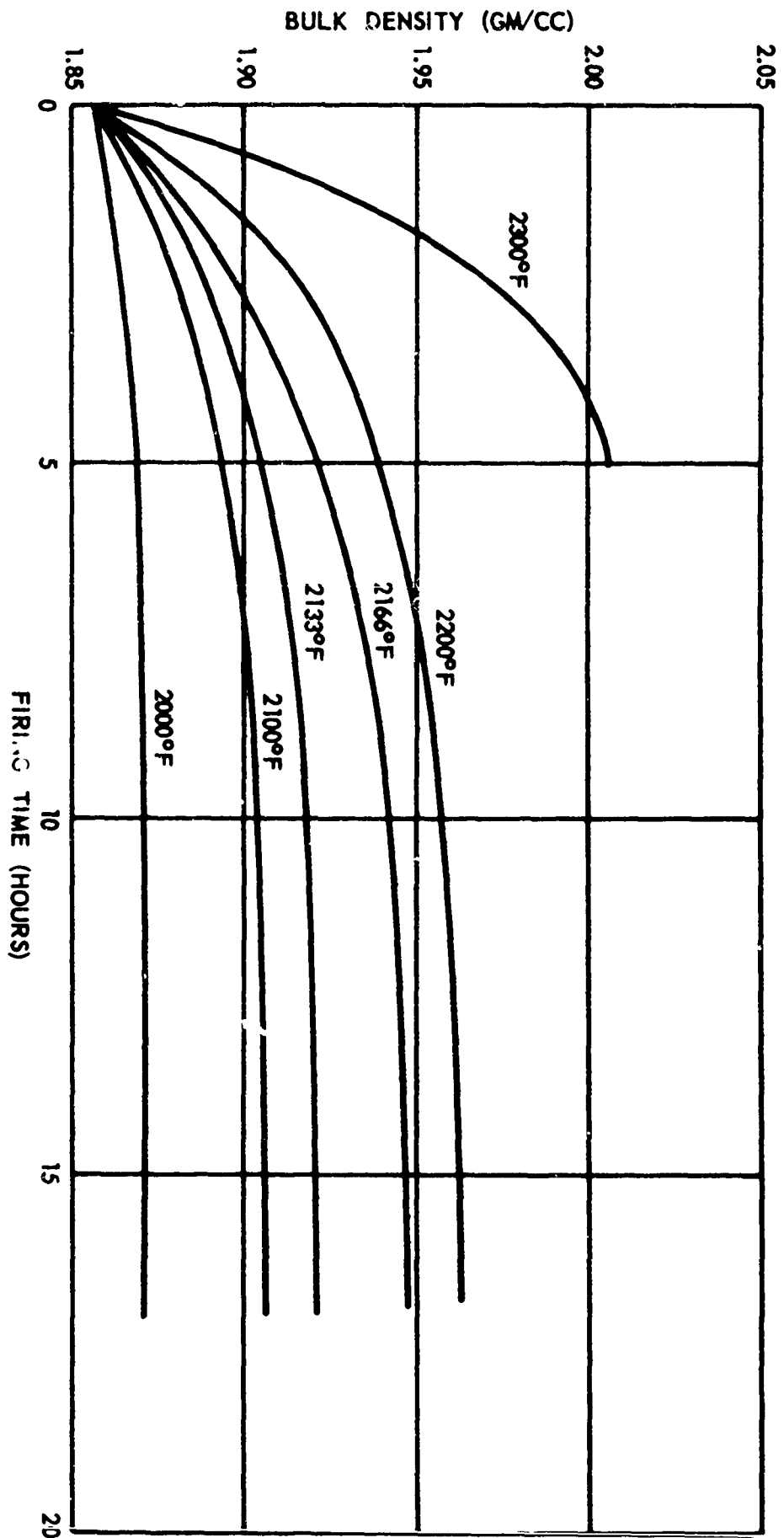


Figure 14. Bulk Density of Slip-Cast Fused Silica Fired Under One Atmosphere of Air (Ref 6, page 21).

NOTE: θ_c IS THE CORRECTED FIRING TIME

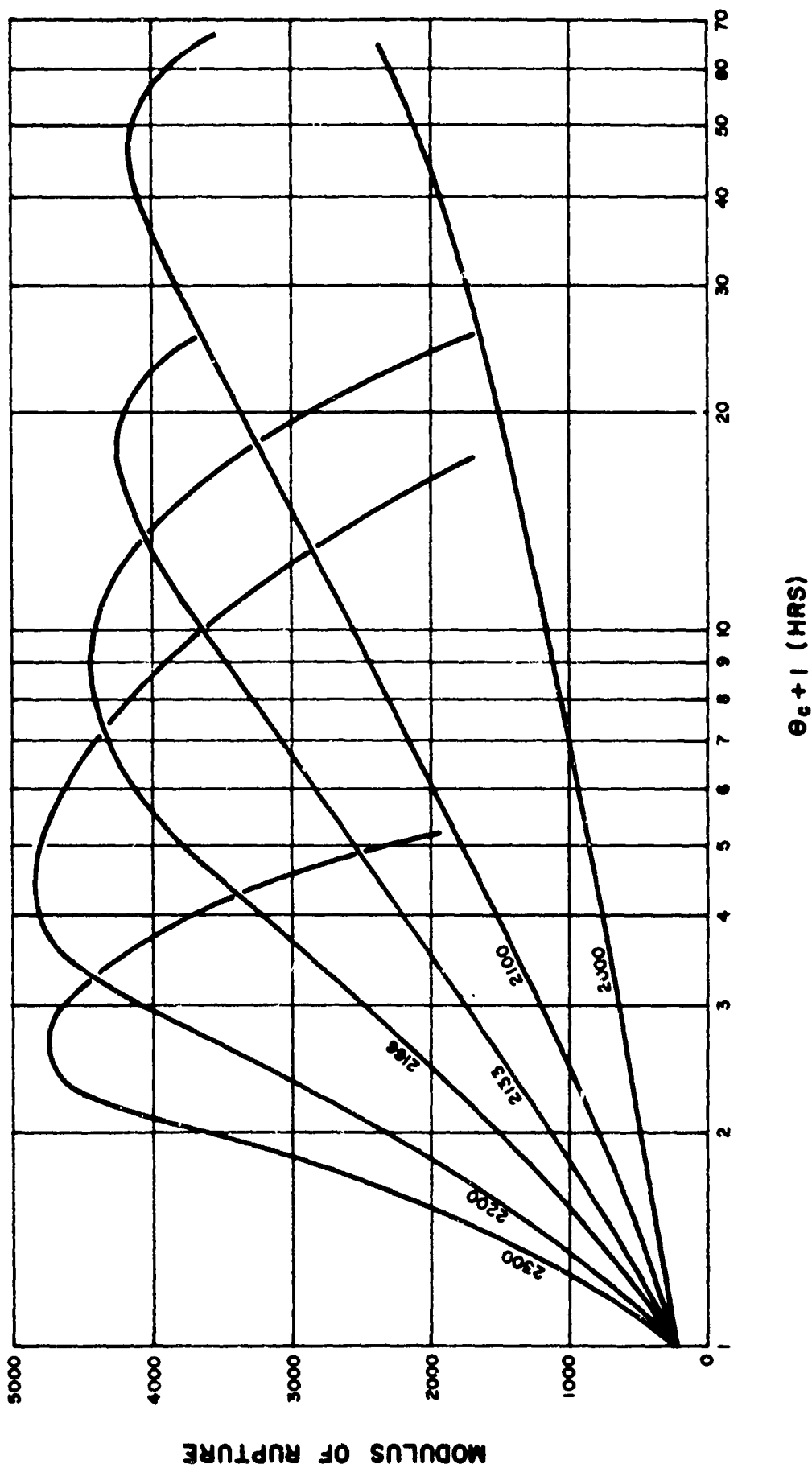


Figure 16. Modulus of Rupture as a Function of Firing Conditions (Ref 2, page 25).

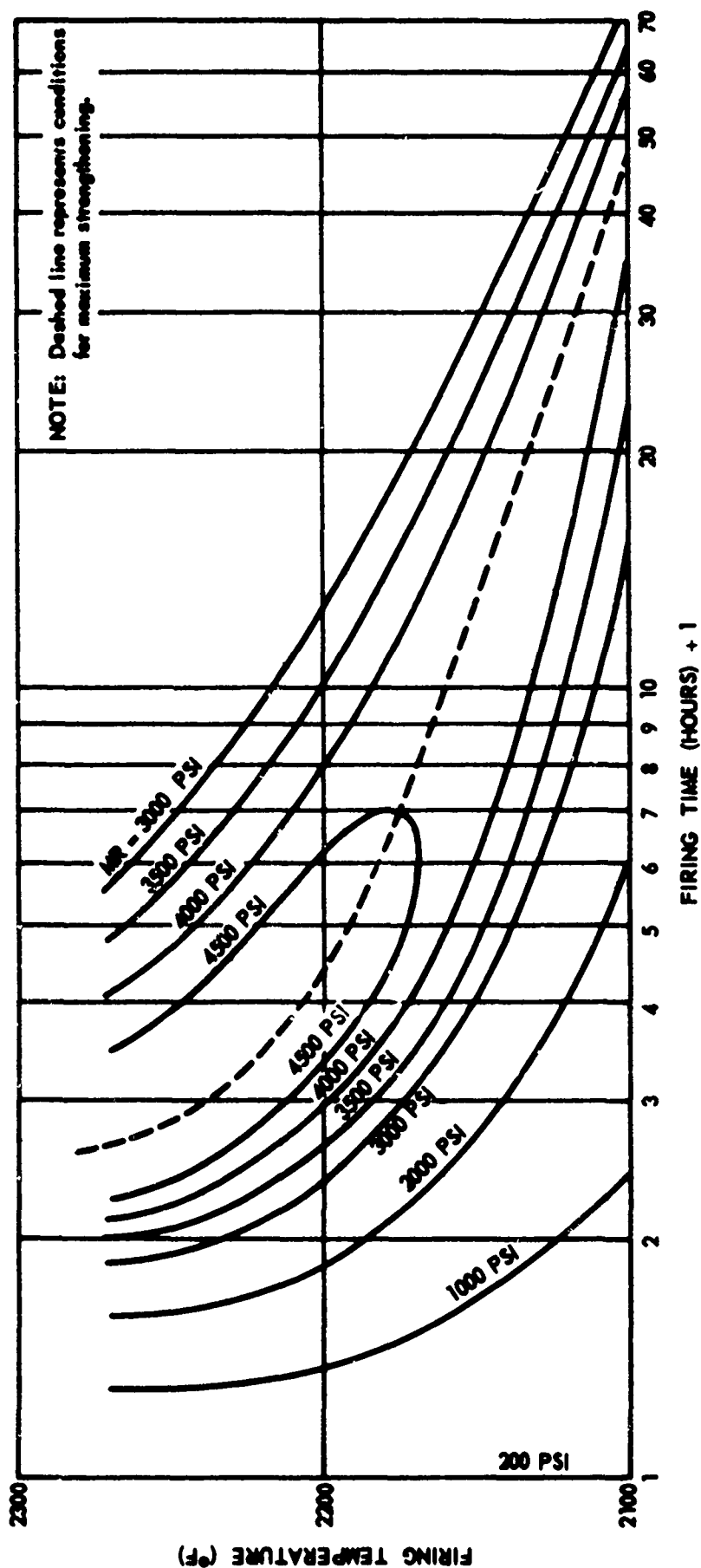


Figure 17. Modulus of Rupture Contour for Slip-Cast Fused Silica Fired Under One Atmosphere of Air (Ref 6, page 13).

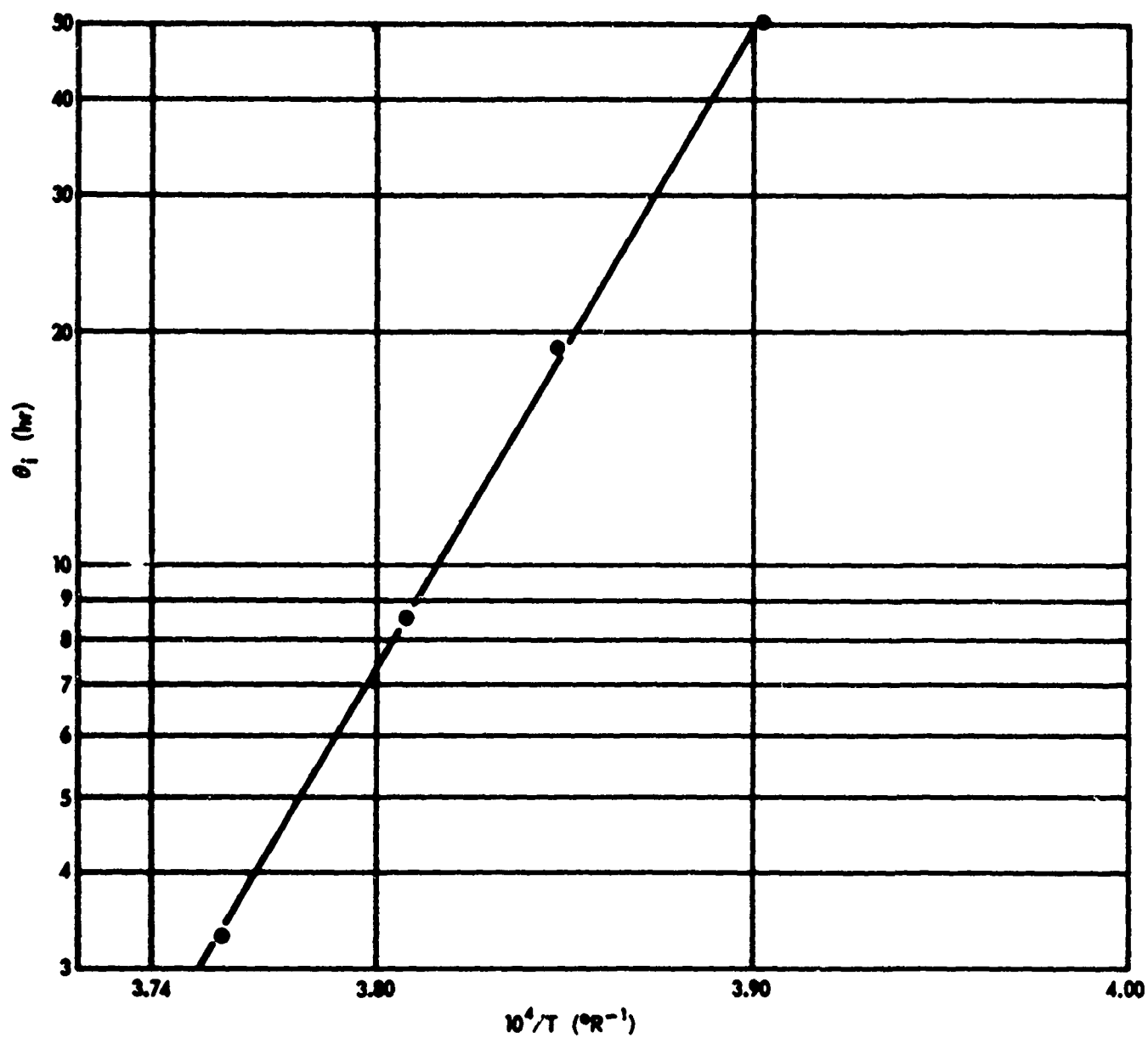


Figure 18. Time to Reach Maximum Strength in Slip-Cast Fused Silica During One Atmosphere Air Firing vs. Reciprocal of Absolute Sintering Temperature (Ref 9, page 10).

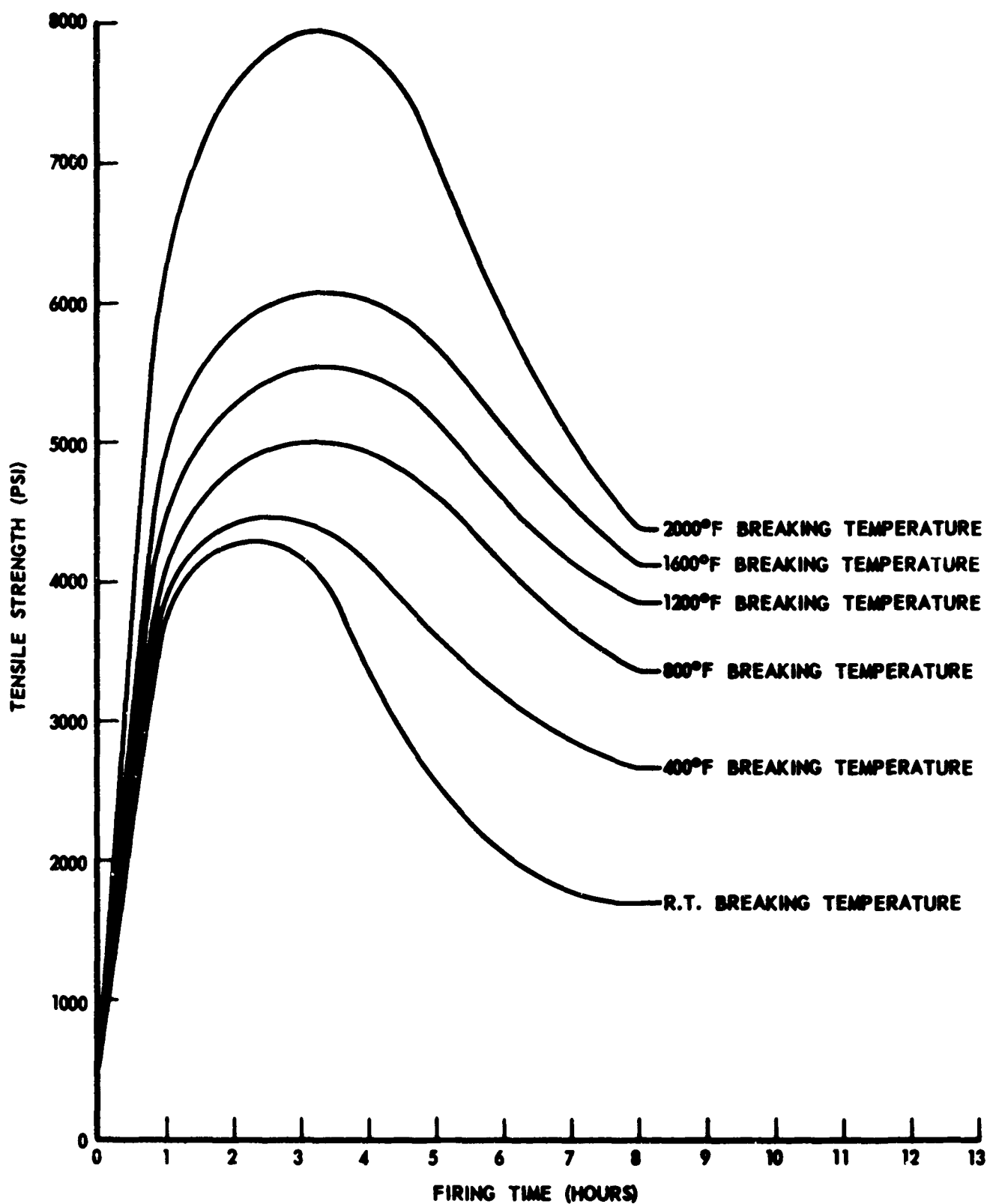


Figure 19. Tensile Strength of Slip-Cast Fused Silica vs. Firing Time at 2200° F for Various Testing Temperatures (Ref 10, in Press).

C. Compressive Strength

The room temperature compressive strength of slip-cast fused silica is shown as a function of firing time for several firing temperatures 6/ in Figure 20. It should be noted that the firing time required to give maximum compressive strength is longer for temperatures above 2166° F than that required to give maximum modulus of rupture. Below 2166° F the firing time that gives maximum compressive strength also gives maximum modulus of rupture.

V. Electrical Properties of Slip-Cast Fused Silica

A. Dielectric Constant and Loss Tangent

The dielectric constant and loss tangent have been determined at 10^{10} cps for slip-cast fused silica from room temperature to 2500° F. These data are presented in Table II.

TABLE II

EFFECT OF TEMPERATURE ON DIELECTRIC CONSTANT AND LOSS TANGENT
OF SLIP-CAST FUSED SILICA*

| | <u>75°F</u> | <u>1500°F</u> | <u>2000°F</u> | <u>2500°F</u> |
|--|-------------|---------------|---------------|---------------|
| Dielectric Constant | 3.17 | 3.18 | 3.28 | 3.42 |
| Per Cent Change from Room Temperature Value | - | 0.315 | 3.15 | 7.9 |
| Loss Tangent | 0.0002 | 0.0006 | 0.007 | 0.012 |

*Private Correspondence with Mr. Ed Abrams, NOL, White Oak S. S., Maryland, December 1958.

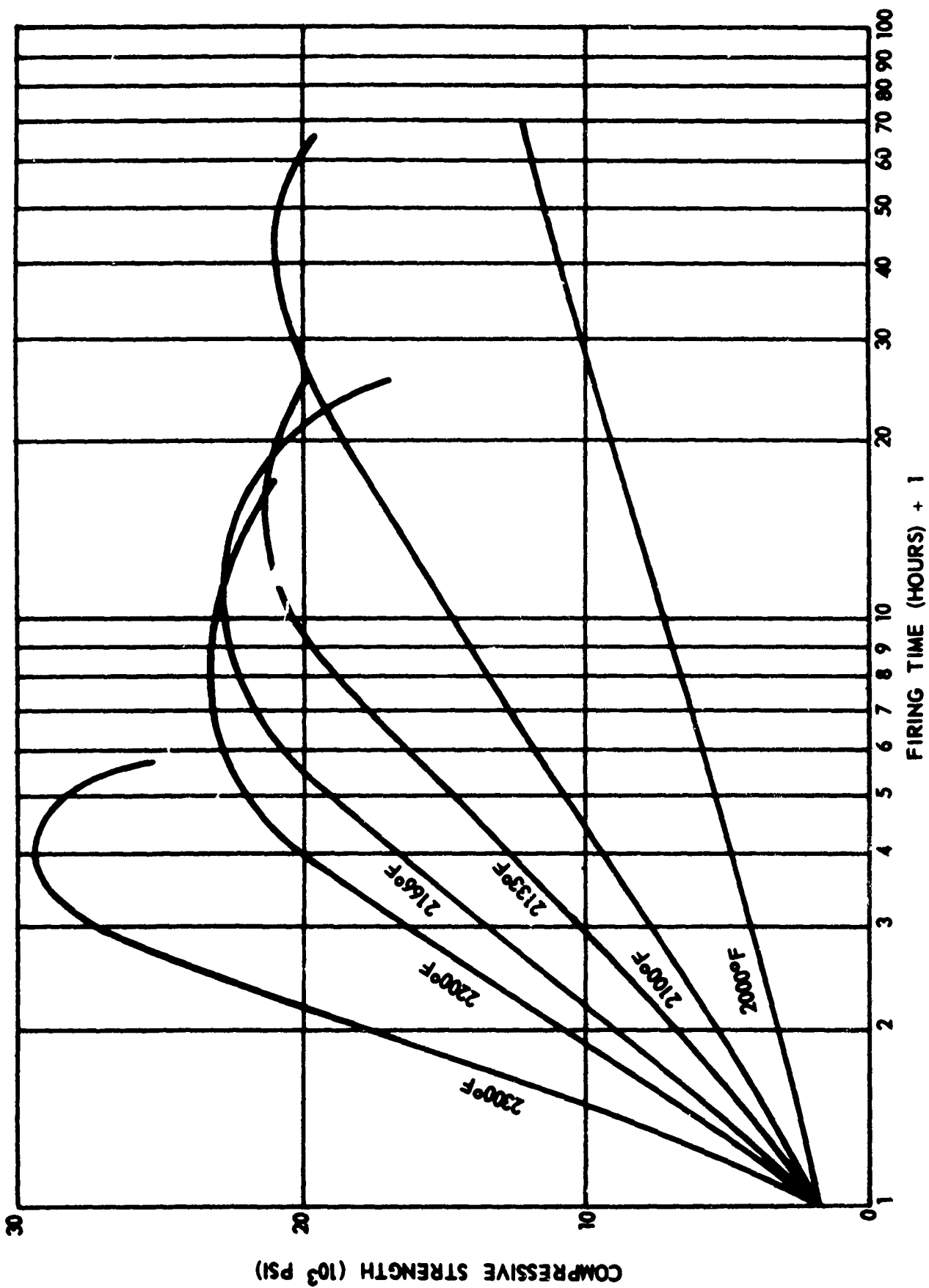


Figure 20. Compressive Strength of Slip-Cast Fused Silica as a Function of Firing Time Fired Under One Atmosphere of Air (Ref 6, page 10).

It should be remembered that these values are for a uniformly heated test section under conditions approaching equilibrium. Under actual high temperature flight or other environmental conditions the low thermal conductivity of slip-cast fused silica should allow a considerable time to pass before the material reaches equilibrium. Therefore, these values might be considered applicable for short periods of time in temperature environments above 2500° F.

B. Volume Resistivity

The volume resistivity of slip-cast fused silica was determined at Georgia Tech 11/. Resistance was measured across a 1/4-inch thick specimen at 1000 volts. The results of these tests are shown in Figure 21. The low value of resistance at room temperature was probably due to the presence of moisture in the pores. As the temperature was increased, and the moisture was expelled, the resistance increased. Also shown in Figure 19 are the resistance vs. temperature data for clear fused quartz reported by Frankel.

C. Dielectric Strength

The dielectric strength of fused silica glass is of the order of 17,000 volts/mil. The dielectric strength of slip-cast fused silica has not been determined. However, its dielectric strength should be less than 17,000 volts/mil since it contains 14-15 per cent connected pores and would be affected considerably by the composition and pressure of gases in the pores.

The dielectric strength of fused silica glass is presented as a function of temperature 12/ in Figure 22.

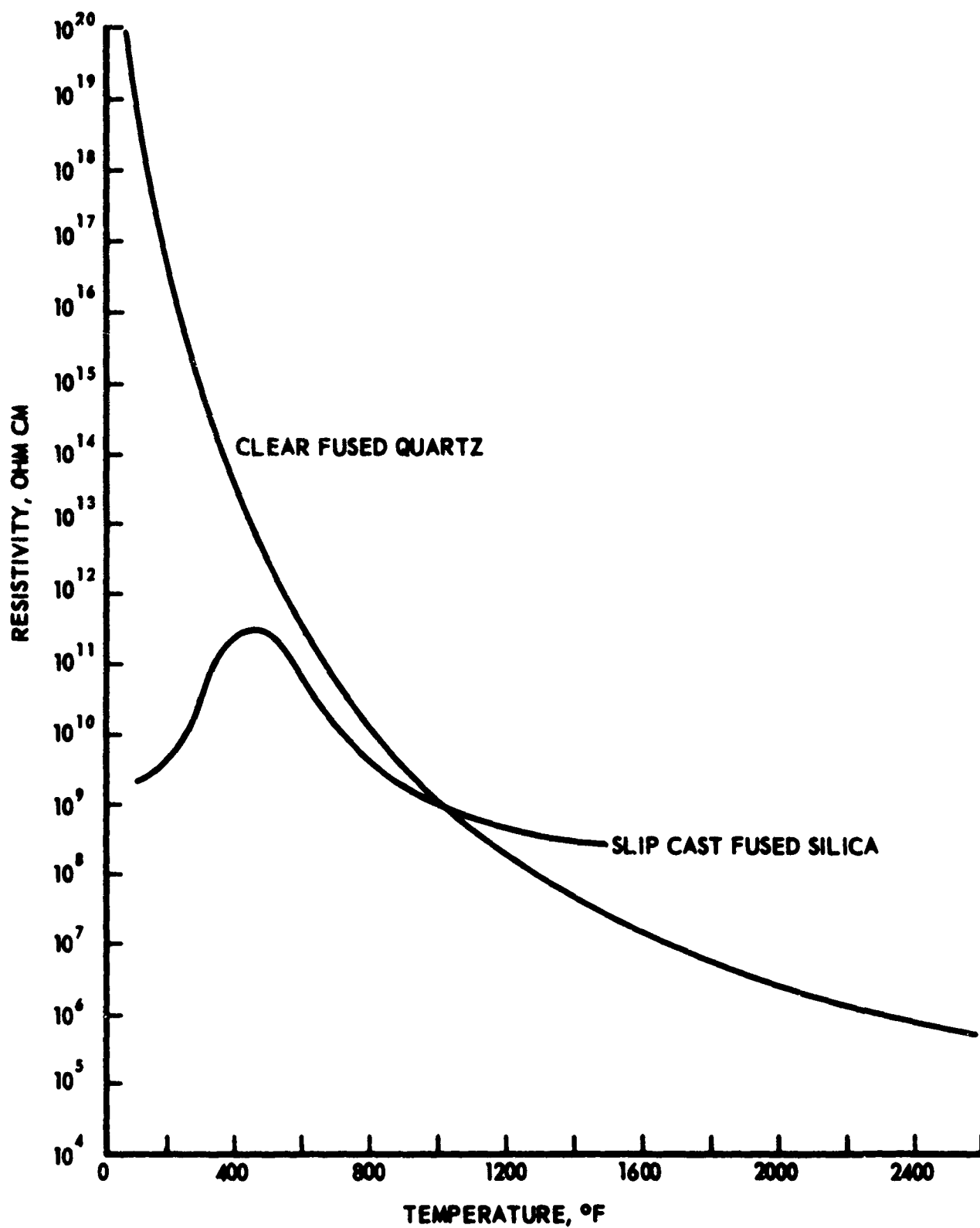


Figure 21. Resistivity of Clear Fused Silica and Slip-Cast Fused Silica as a Function of Temperature (Ref 11, page 191).

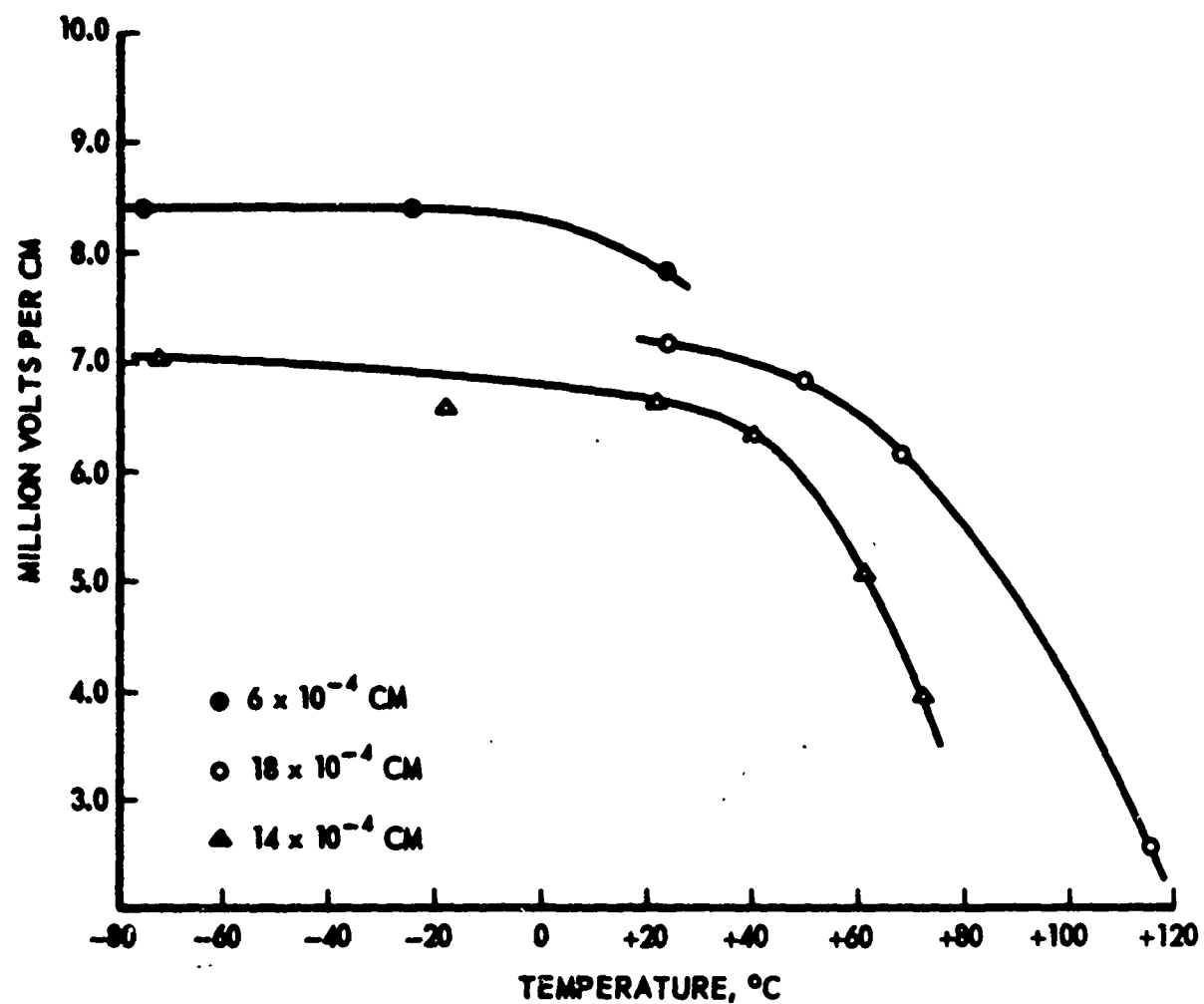


Figure 22. Dielectric Strength of Fused Silica Glass as a Function of Temperature (Ref 12, page 424).

VI. Nuclear Properties

The effect of nuclear radiation on the strength of slip-cast fused silica was determined at Georgia Tech 13/. The radiation was carried out at Westinghouse Test Reactor (WTR). Figure 23 presents the Modulus of Rupture as a function of radiation dose for slip-cast fused silica. The overall average of the transverse strengths of the irradiated bars was 5700 psi as compared with 6050 psi for the unirradiated bars. This difference implies that the irradiation of the order of 2×10^{20} nvt has little influence on the strength of slip cast fused silica, probably causing no change greater than 10 per cent. Bars used in this investigation were 0.375-inch diameter, and were broken over a 1-inch span.

The effect of nuclear radiation on cristobalite in slip-cast fused silica was also determined. Slip-cast fused silica test bars fired at 2200° F for 3-1/3 hours, and overfired at 2300° F for over 24 hours to develop large amounts of cristobalite were irradiated in the WTR. The cristobalite in the overfired bars was completely transformed to an amorphous state except for five samples irradiated in the lower flux positions in the reactor. The cristobalite content of these five samples is listed in Table III. Cristobalite in the 3-1/3 hour fired bars was completely transformed to an amorphous state.

Other nuclear properties of fused silica are shown in Table IV.

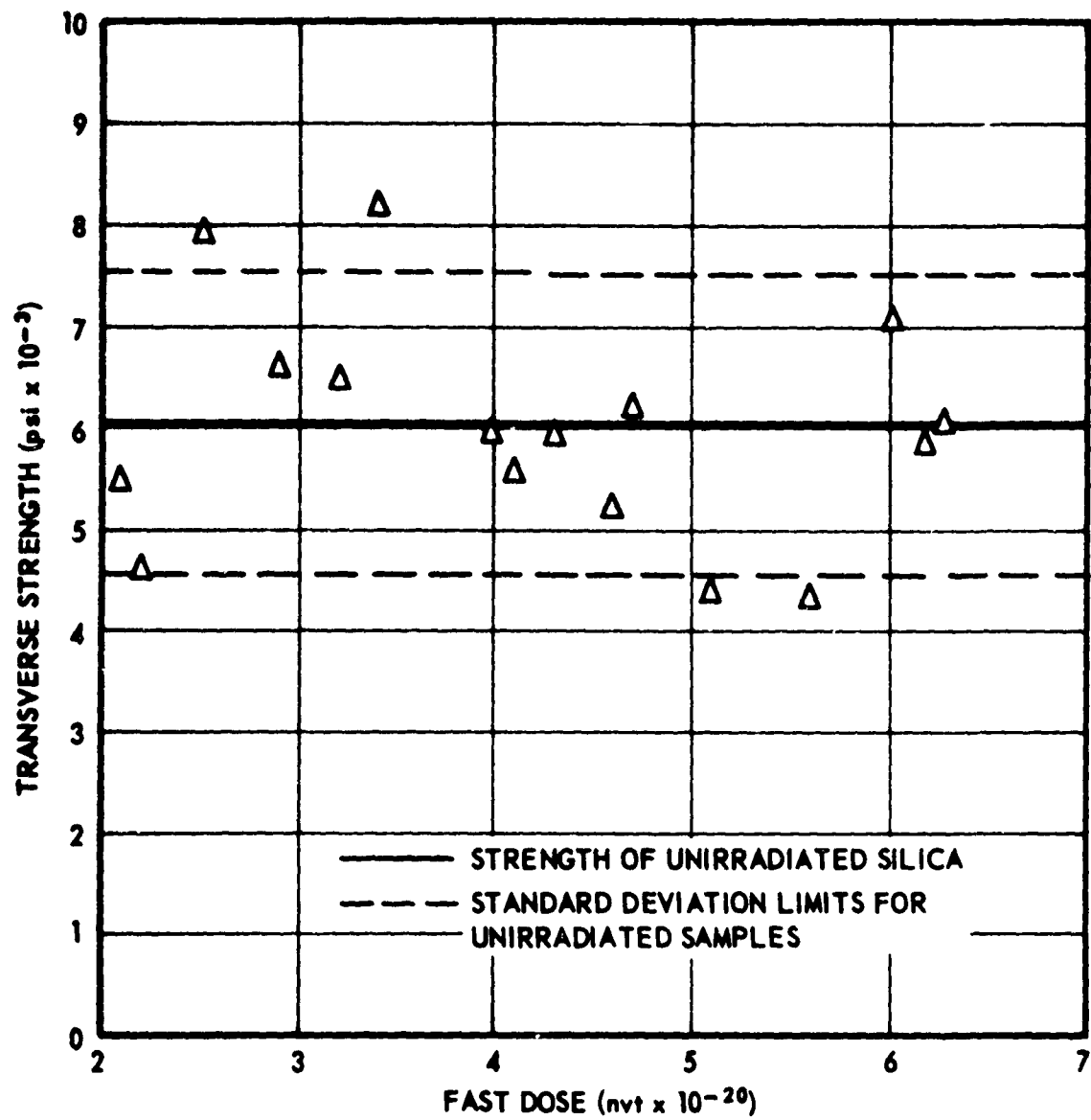


Figure 23. Effect of Irradiation on the Modulus of Rupture of Slip-Cast Fused Silica (Ref 13, page 43).

TABLE III

CRISTOBALITE CONTENT OF SLIP-CAST FUSED SILICA SAMPLES
AFTER IRRADIATION

| Sample No. | Dose (nvt) | Cristobalite Content | |
|------------|----------------------|---------------------------|--------------------------|
| | | Before Irradiation (%) | After Irradiation (%) |
| 62 | 2.9×10^{20} | 88 | 5 |
| 67 | 2.2×10^{20} | 51 | 5 |
| 69 | 2.2×10^{20} | 41 | 3 |
| 71 | 2.1×10^{20} | 40 | 8 |
| 72 | 2.1×10^{20} | 21 | 3 |

Note: All slip-cast fused silica samples subjected to an irradiation dose in excess of approximately 3×10^{20} nvt did not exhibit any cristobalite.

TABLE IV

NUCLEAR PROPERTIES OF FUSED SILICA

| | |
|--|--------------------------|
| Thermal Neutron Absorption Cross Section | 0.161 Barns |
| Macroscopic Absorption Cross Section | 0.0035 cm^{-1} |
| Scattering | 10.1 Barns |

VII. Slip-Cast Fused Silica for Thermal Protection Systems and Radomes

The previously discussed properties of slip-cast fused silica suggested its use for applications where excellent thermal shock resistance, low

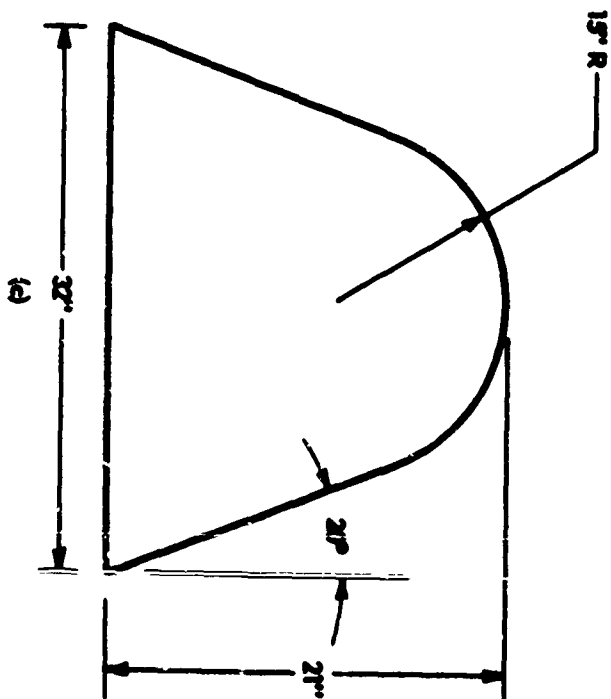
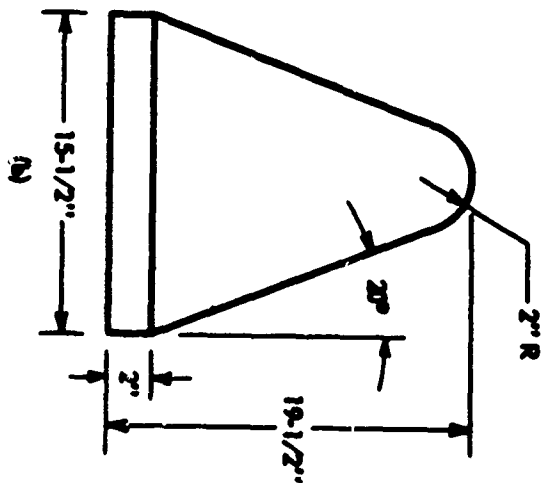
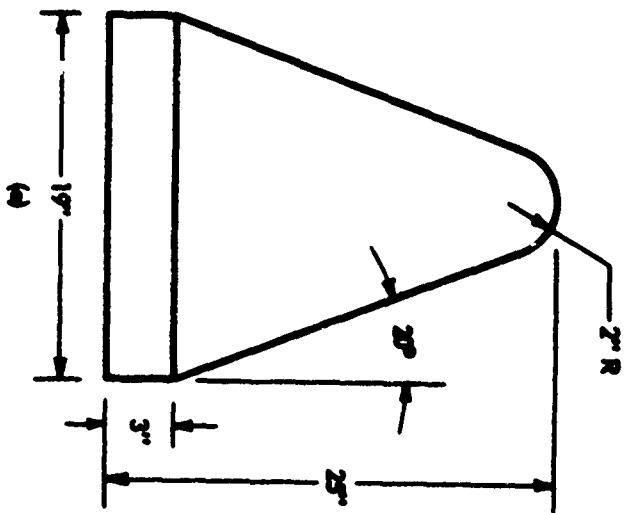
density, low thermal conductivity and ease of fabrication were required. Combining these properties with the low dielectric constant and loss tangent which are unusually stable with temperature suggested an excellent radome material for hypersonic and reentry applications. The unique combination of properties of slip-cast fused silica offered to provide a radome which would also serve as a thermal protection system.

A. Fabrication

Prior to the consideration of slip-cast fused silica as a radome material it was first considered for nose cone applications. The three shapes shown in Figure 24 were satisfactorily slip-cast from fused silica 7/. For this particular application a 3/4-inch wall thickness was cast.

As interest developed in the use of slip-cast fused silica for radomes the shapes shown in Figure 25 were slip-cast 5/. These shapes provided no difficulty in slip-casting. However, when conventional slip-casting procedures were used it was found that the wall thickness varied over the length of the radome to an unacceptable degree. The wall thickness at the base of a radome 13-inches tall with a nominal wall thickness of 0.375 would be approximately 0.080-inches thinner than the wall near the tip.

The conventional slip-casting technique provide for the mold to be filled with the radome tip down, and remain in that position for the duration of the casting time. Naturally, there is a tendency for the suspended particles of silica to settle with time, producing a thicker casting near the tip. By reducing the casting time the difference in thickness between the base and the tip could be reduced. As pointed out in Section II, the cast wall thickness at any given time can be increased



NOTE: DRAWING NOT TO SCALE

Figure 24. Nose Cone Configurations Sent to Redstone Arsenal (Ref 7, page 104).



Figure 25a. Radomes Which Have Been Slip-Cast from Fused Silica.
(Ref 5, page 9-11).



Figure 25b. Radomes Which Have Been Slip-Cast from Fused Silica.
(Ref 5, page 9-11).

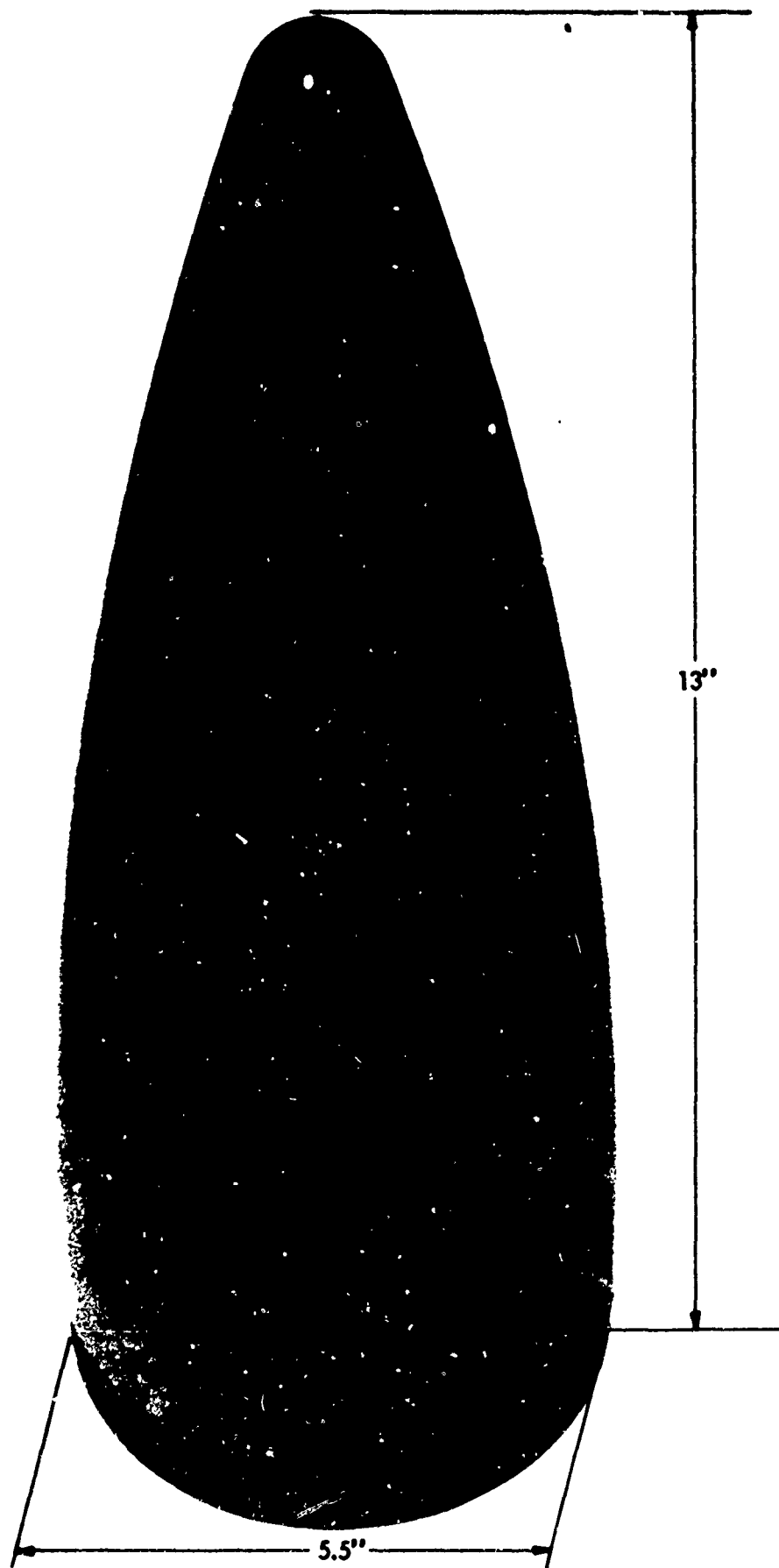


Figure 25c. Radomes Which Have Been Slip-Cast from Fused Silica.
(Ref 5, page 9-11).

by applying a pressure to the slip. This was accomplished by using the set-up 14/ shown in Figure 26. By using this technique and an applied pressure of 20 psi it was possible to reduce the wall thickness variation to 0.040-inches in a 0.375-inch thick wall.

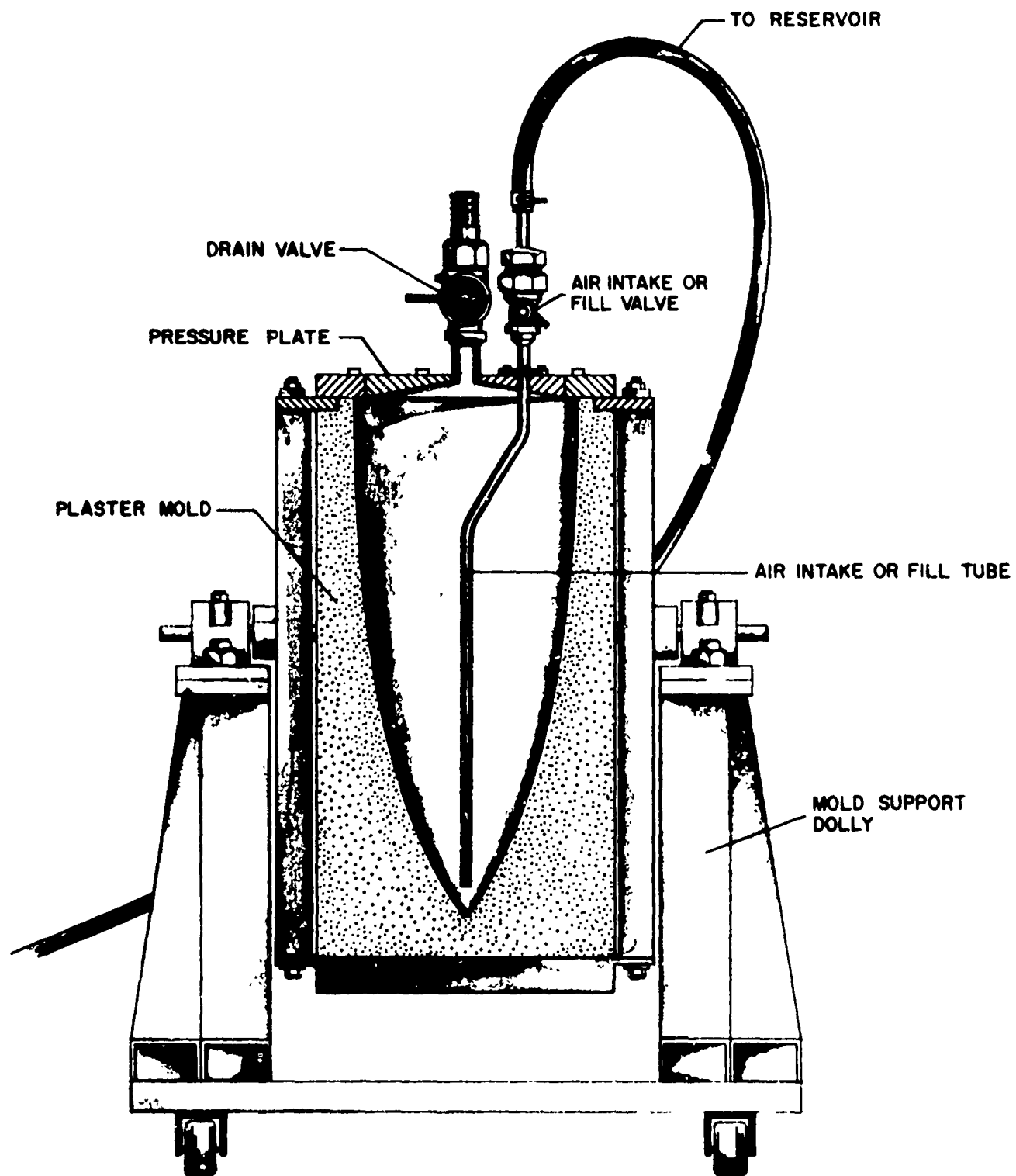
A "tip-up" pressure casting technique was developed to further improve the uniformity of the wall thickness 14/. Figure 27 shows the set-up used to cast a 31-inch tall radome. In this process the mold is filled with the tip pointed up rather than down. As the slip is pumped into the bottom of the mold, the air above the slip is forced through the pores in the plaster. A 13-inch tall radome slip-cast in this manner exhibited a wall thickness variation no greater than $\pm .001$ -inch from the base to the tip.

B. Surface Sealing

Several methods of sealing the surface of slip-cast fused silica have been considered. Only two methods appear practical at this time. These are: surface melting, and Teflon coating.

1. Surface Melting. By using an arc-plasma jet or oxygen-acetylene torch it is possible to flame seal the surface of slip-cast fused silica 5/. This process is referred to as flame glazing. A sketch of the apparatus which has been used to satisfactorily flame glaze slip-cast fused silica radomes is shown in Figure 28. After glazing, the fused surface is annealed by holding at 2150° F for 15 minutes, followed by cooling at 4° F per minute to 1900° F, and then removed from the glazing furnace.

The effect of surface melting on the IPD (Insertion Phase Difference) for slip-cast fused silica has been determined 15/, and is shown in Figure 29.



p. matrangoes ee

Figure 26. Pressure Casting Set-Up for Slip-Casting Fused Silica Radome (Ref 14, page 38).

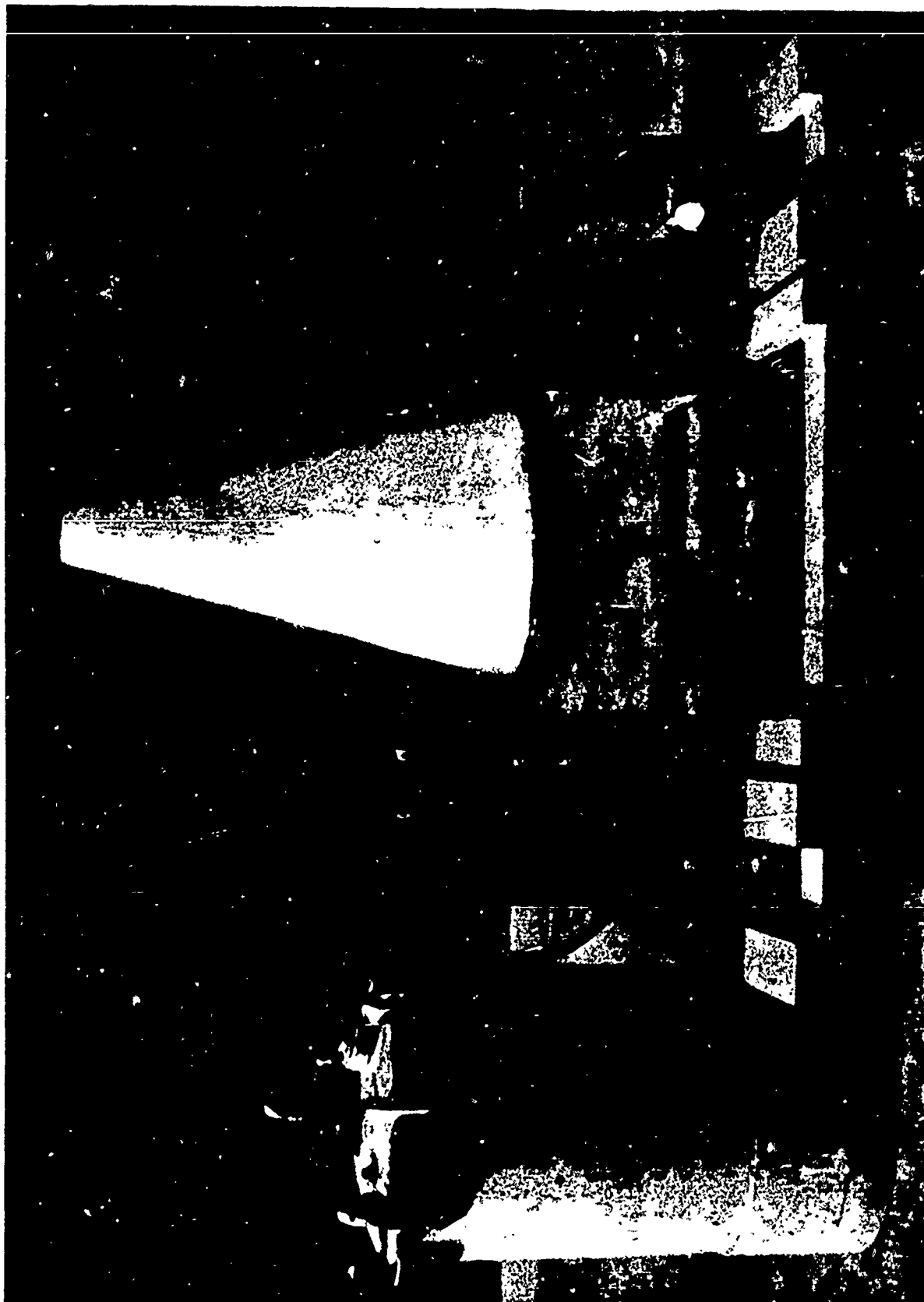


Figure 27. Photograph of Set-Up for Tip-Up Pressure Casting of Radome
(Ref 14, page 93).

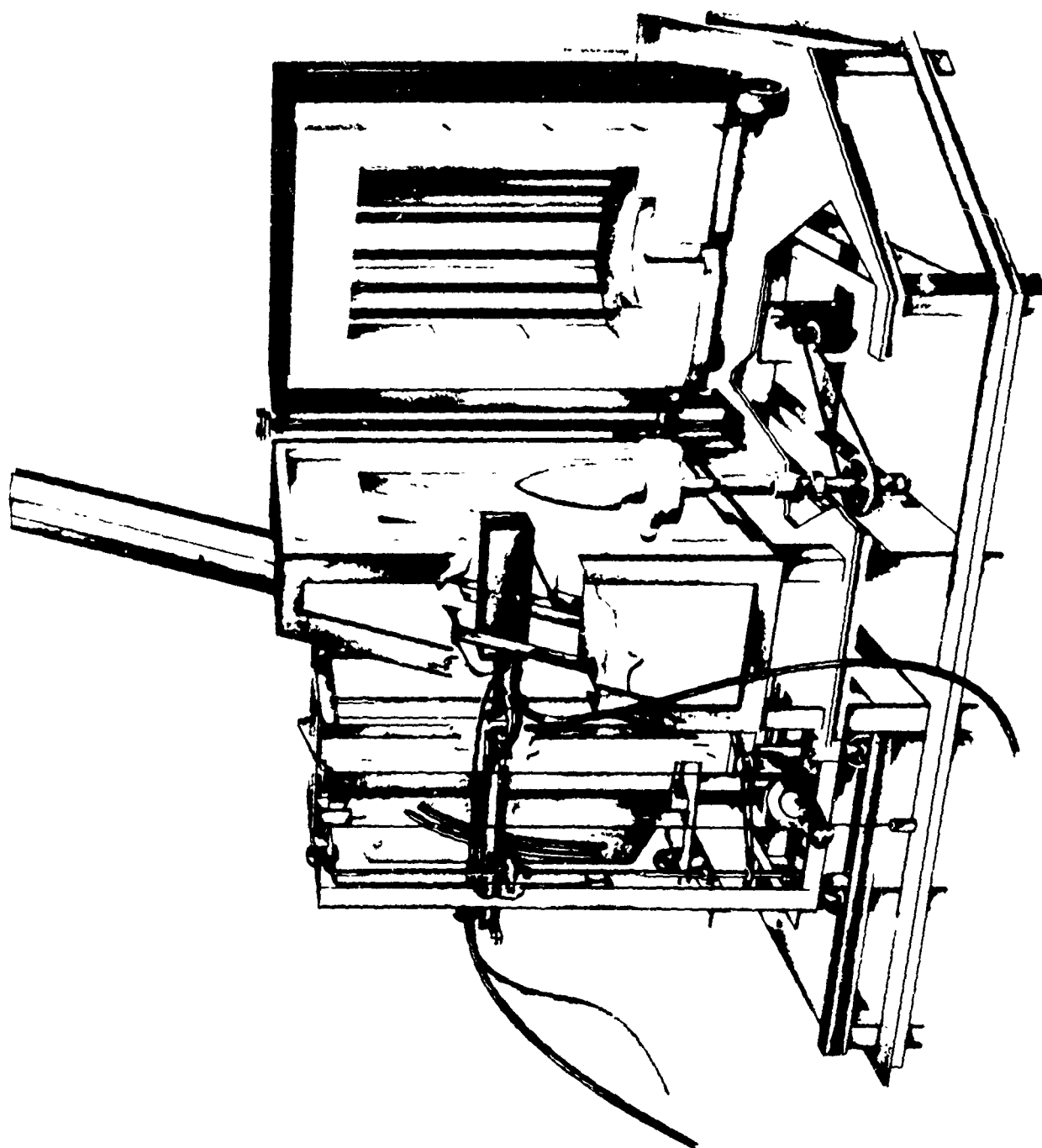


Figure 28. Artist Conception of Modified Flame Glazing Device
(Ref 5, page 97).

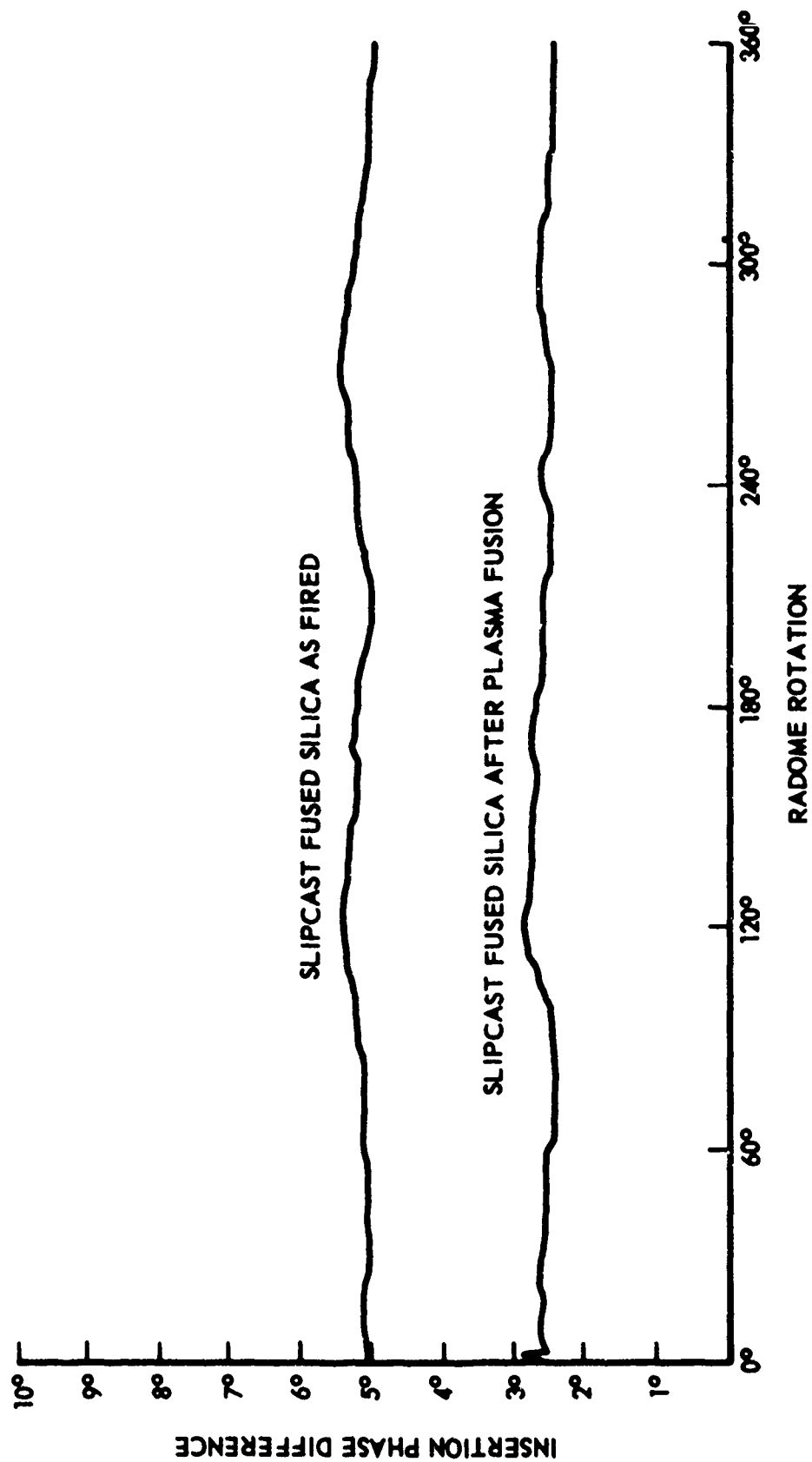


Figure 29. Insertion Phase Difference for Slip-Cast Fused Silica (Ref 15).

2. Teflon Coating. A Teflon coating is being considered for use as a simpler and more economical method of sealing. DuPont's TFE Resin, Clear Finish 852-201, is sprayed on to the surface of the radome to a thickness of approximately 0.001-inch. After drying, it is heated to 750° F. At this temperature the Teflon melts producing a continuous coating. Teflon is a non-charring, low-temperature ablator, with a dielectric constant of 3. Therefore, it is expected that no radome electrical performance difficulties will arise since the thin coating would be completely ablated away almost immediately in any hyperthermal environment.

C. High Temperature Environment Simulation

1. Laboratory Testing. At Georgia Tech two high temperature heat sources have been used to study slip-cast fused silica under severe thermal shock conditions. These are an oxy-hydrogen rocket motor and an oxy-acetylene torch facility.

a. Oxy-Hydrogen Rocket Motor. A typical set-up for evaluating materials in the exhaust of the oxy-hydrogen rocket motor is shown in Figure 30. The impingement angle of the exhaust on the sample can be varied from 45° to 90°. The sample surface-to-motor distance can be varied from 6 to 20-inches. The operational parameters for this motor are shown in Table V. Calculated stagnation enthalpy and stagnation temperature are shown as a function of distance from the exit plane 17/ of the motor in Figure 31. The calorimeter shown in Figure 32 was used to determine the cold calorimeter heat flux provided by the exhaust of this motor 8/. Cold wall calorimeter heat flux is shown as a function of

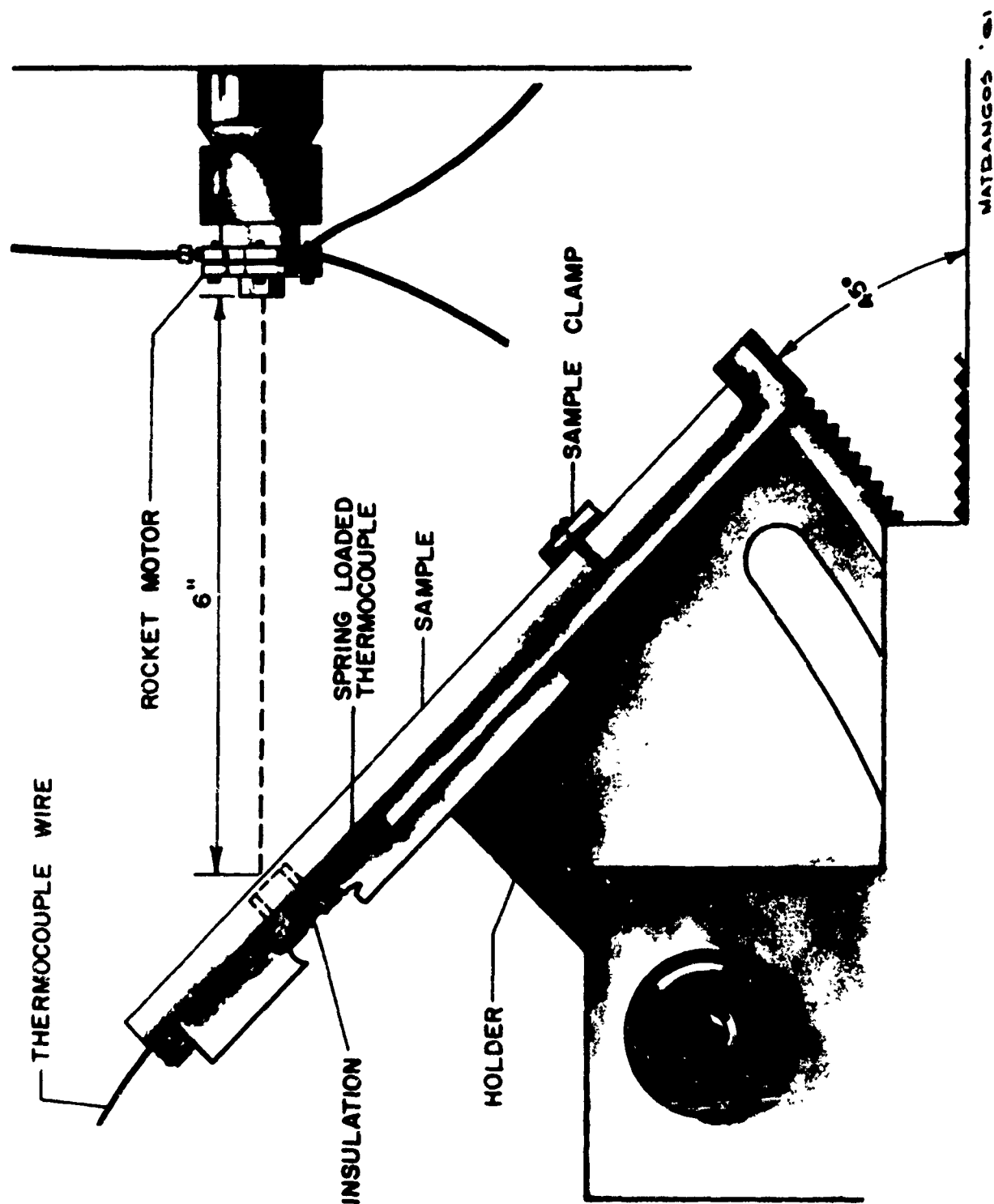


Figure 30. Set-Up for Evaluating Ceramic Materials in Exhaust of Oxy-Hydrogen Rocket Motor (Ref 16, page 156).

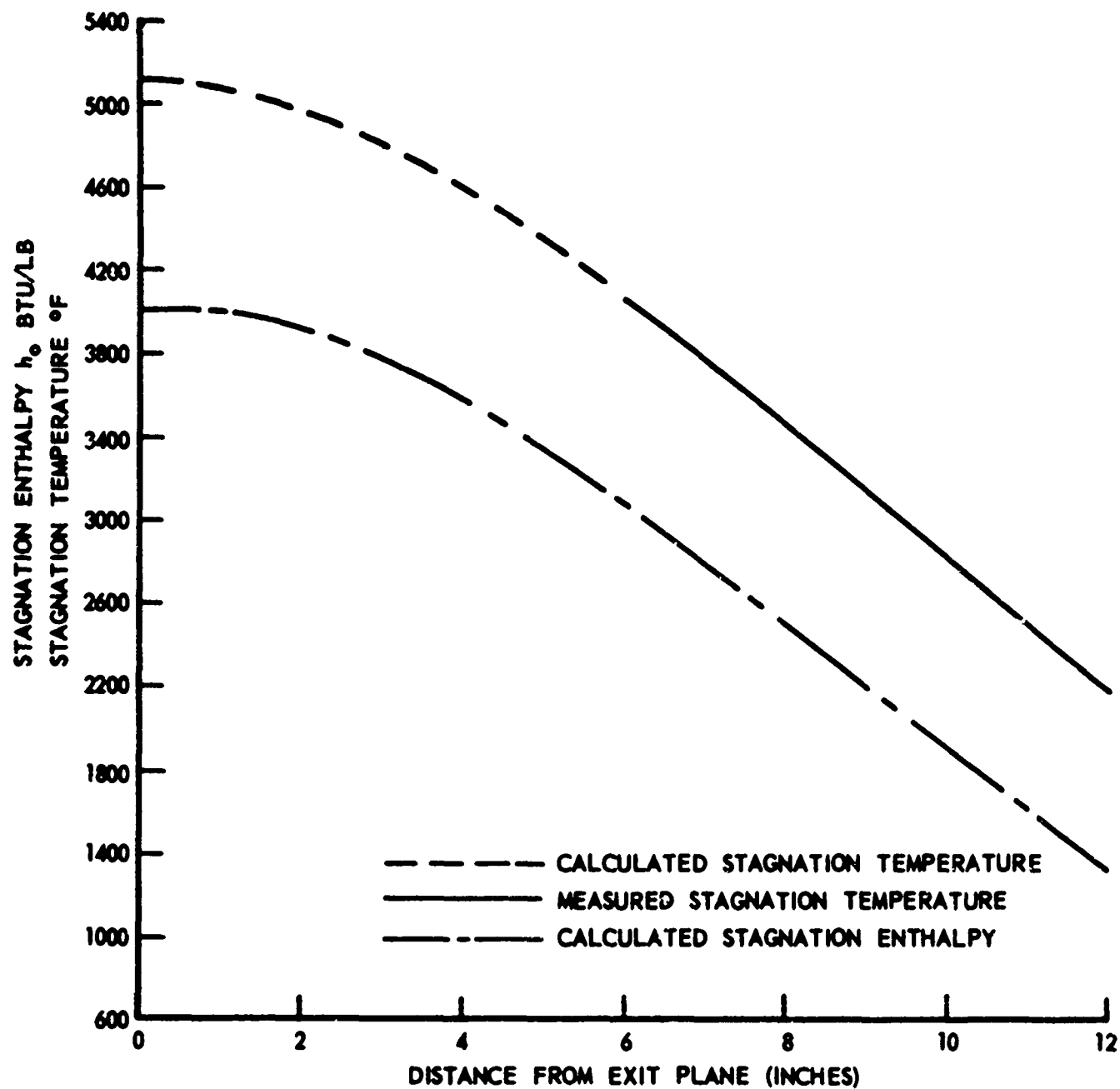


Figure 31. Stagnation Temperature and Stagnation Enthalpy in Rocket Motor Exhaust as a Function of Distance from the Exit Plane (Ref 17, page 20).

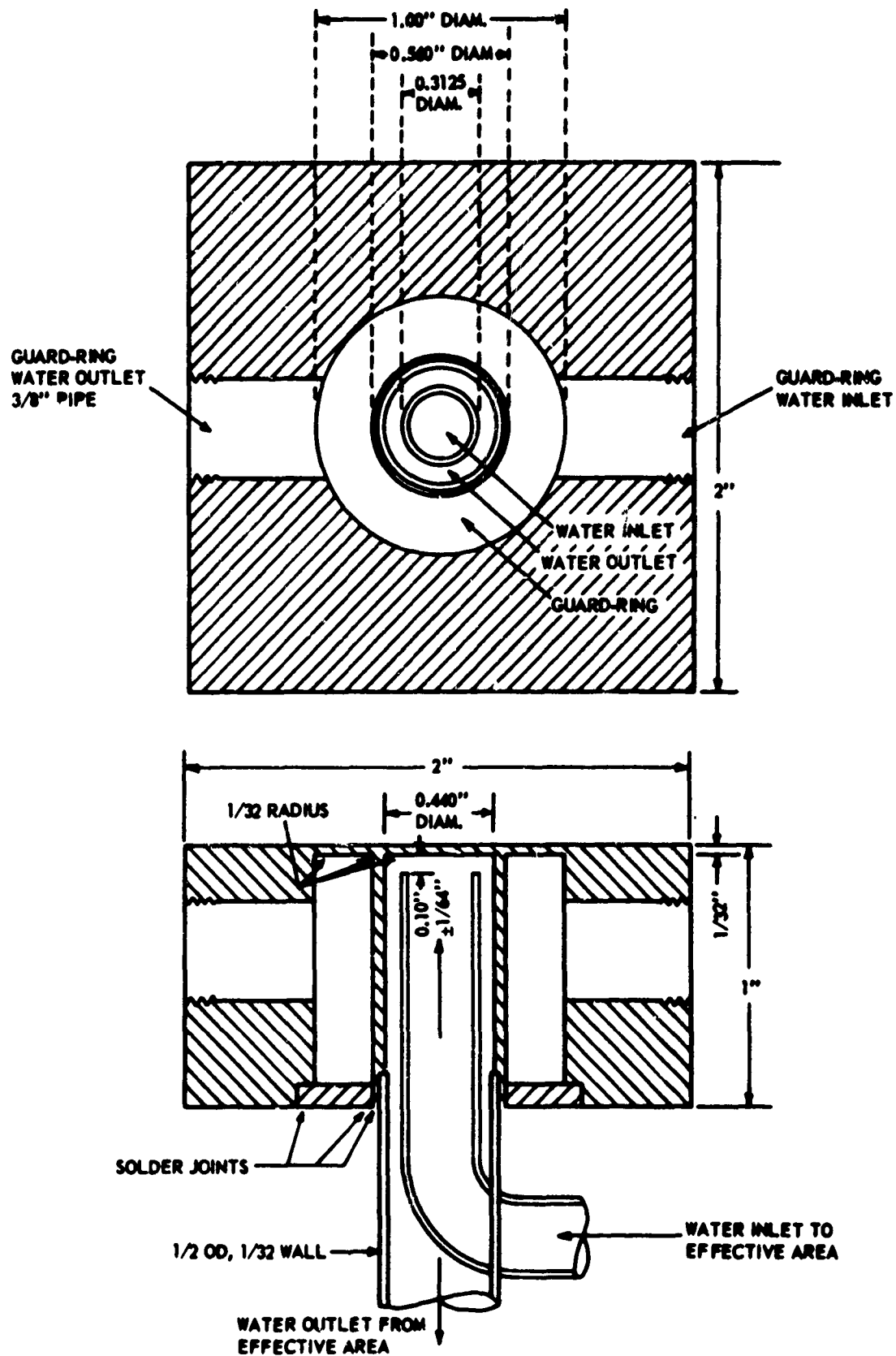


Figure 32. Copper Calorimeter for Heat Flux Measurements (Ref 8, page 52).

distance from the exit plane for an exhaust incidence angle of 90° and 45° in Figure 33.

TABLE V
OPERATIONAL DATA FOR OXYGEN-HYDROGEN ROCKET MOTOR

| | |
|---------------------------------------|------|
| <u>Motor</u> | |
| Fuel mixture ratio, $V_{H_2}:V_{O_2}$ | 4:1 |
| Hydrogen flow rate, S.C.F.M. | 36 |
| Oxygen flow rate, S.C.F.M. | 9 |
| Chamber pressure, psia | 275 |
| <u>Exhaust gas at exit plane</u> | |
| Pressure, psia | 15.1 |
| Velocity, ft/sec | 7966 |
| Temperature, °R | 3214 |
| Stagnation temperature, °R | 5400 |
| Mach No. | 2.5 |

A series of flat plates of fused silica, 2-inch x 7-inch, of various thicknesses were slip-cast for evaluation in the exhaust of the oxy-hydrogen rocket motor. The samples were fired between two blocks of foamed silica in an electric kiln at 2200° F for 2 hours. Each sample was placed 6-inches to the rear of the exhaust nozzle and inclined at 45° to the direction of flow. The backside was insulated with kaolin wool and a spring-loaded iron-constantan thermocouple was placed against the silica surface opposite the point of flame

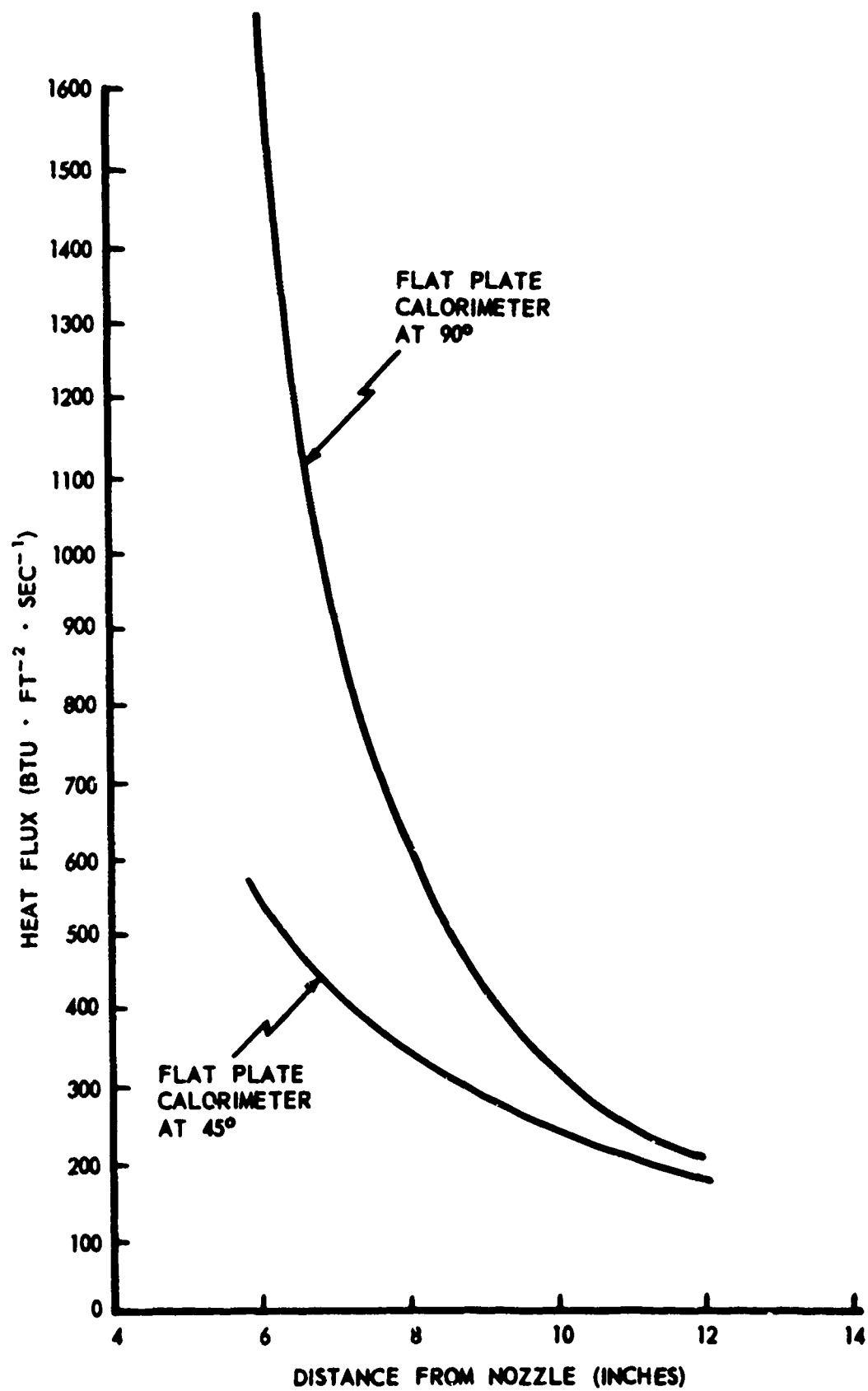


Figure 33. Heat Flux of Exhaust of Oxy-Hydrogen Rocket Motor (Ref 8, page 55).

impingement. A schematic of the sample positioning, thermocouple location, etc., is shown in Figure 30. Temperature was automatically recorded on a strip chart recorder. The backside temperature increase versus sample thickness for various time intervals is shown in Figure 34.

A second series of test plates were cast with various thicknesses to determine the approximation to one dimensional heat flow in a sample of low conductivity exposed to the high velocity gases of the rocket motor. One test plate of each set had a circular guard ring on the backside opposite the point of flame impingement. The dimensions of this guard ring were 1/2-inch I.D. x 3/4-inch O.D. The guard ring was cut with a core drill to a depth of approximately two-thirds of the thickness of the piece. Each of these samples was exposed to the exhaust gases exactly as before. The results of six of these runs are shown in Figure 35. Several other runs were made as a check on these results. The temperature-time curves were practically identical with the first runs.

An effort was made to determine whether the temperature-time data from the flat plate sample evaluation could be used to estimate the thermal diffusivity and thermal conductivity of the sample material. Since the surface of the sample became molten very quickly, did not ablate severely, and the backside was well insulated, an ideal model could be described which would approximate the test conditions and allow a relatively simple mathematical analysis.

If the model selected is an infinite flat plate of finite thickness with its surfaces suddenly heated to and held at a constant temperature, an expression for the temperature at the center of the plate is

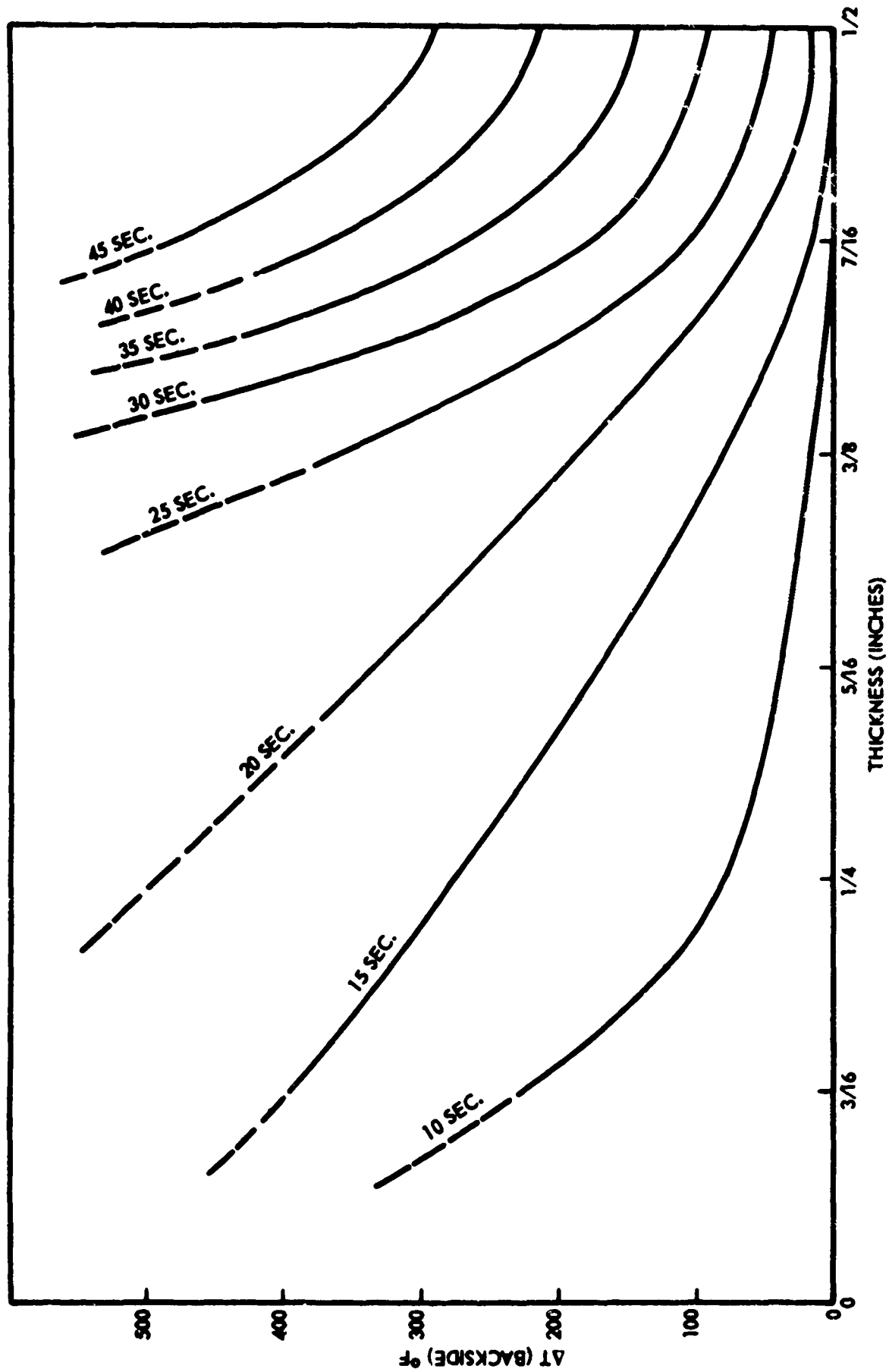


Figure 34. Backside Temperature Change as a Function of Thickness of Slip-Cast Fused Silica Plates Exposed to Oxy-Hydrogen Rocket Motor (Ref 18, page 22).

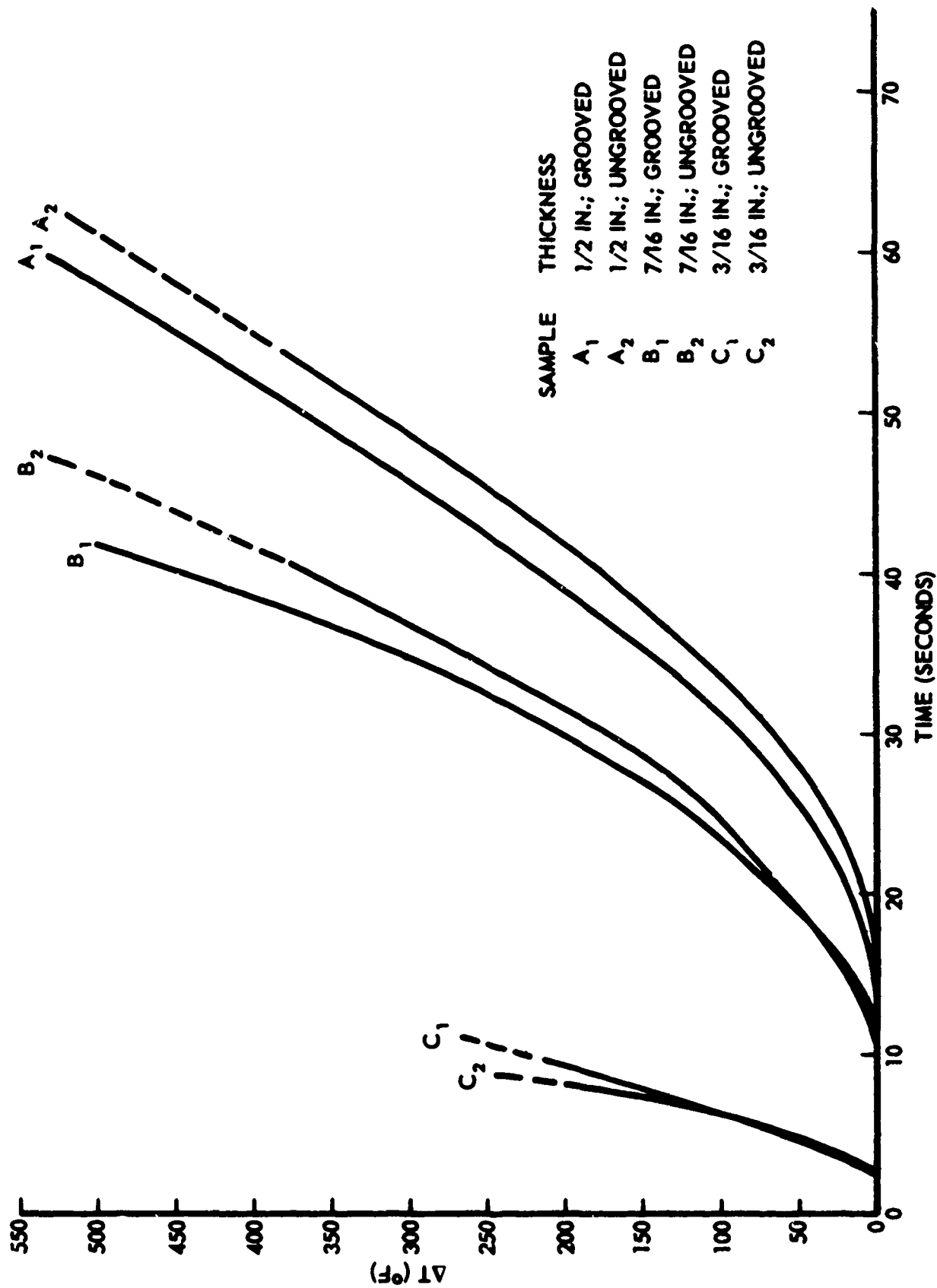


Figure 35. Backside Temperature Change for Grooved and Ungrooved Flat Plate Samples of Slip-Cast Fused Silica Exposed to Oxy-Hydrogen Rocket Motor (Ref 18, page 24).

$$T = T_s + \frac{4}{\pi} (T_i - T_s) \left(e^{-\frac{\pi^2}{4} \frac{\alpha t}{L^2}} - \frac{1}{3} e^{-\frac{9\pi^2}{4} \frac{\alpha t}{L^2}} + \frac{1}{5} e^{-\frac{25\pi^2}{4} \frac{\alpha t}{L^2}} - \dots \right)$$

where:

T_s = surface temperature

T_i = initial temperature

α = thermal diffusivity ($\rho \frac{K}{C_p}$)

t = time

$2L$ = thickness of plate

K = thermal conductivity

C_p = heat capacity

ρ = density

Using a graphic solution and data from Figure 34 for the 1/2-inch grooved sample with

$$T_s = 3100^\circ \text{ F}$$

$$T_i = 80^\circ \text{ F}$$

$$L = 1/24 \text{ ft}$$

$$T = 1/90 \text{ hr}$$

$$C_p = 0.18 \text{ Btu} \cdot \text{lb}_m^{-1} \cdot ^\circ\text{F}^{-1}$$

$$\rho = 115 \text{ lb}_m \cdot \text{ft}^{-3}$$

gives

$$\frac{\alpha t}{L^2} = 0.113$$

$$\alpha = 0.0176 \text{ ft}^2 \cdot \text{hr}^{-1}$$

Thus

$$K = \alpha C_p$$

$$K = (0.0176)(115)(0.18)$$

$$K = 0.37 \text{ (Btu ft)/(ft}^2 \text{ hr } ^\circ\text{F)}.$$

Using the same method and data from Figure 35 for the 7/16-inch grooved sample with

$$L = \frac{7}{(16)(12)} \text{ ft}$$

$$t = 35/3600 \text{ hr}$$

gives

$$\frac{\alpha t}{L^2} = 0.131$$

$$\alpha = 0.0179 \text{ ft}^2/\text{hr}.$$

Thus

$$K = \alpha PC_p$$

$$K = (0.0179) (115) (0.18)$$

$$K = 0.37 \text{ (Btu ft)/(ft}^2 \text{ hr } ^\circ\text{F)}$$

These values are in excellent agreement with the values determined in the steady state thermal conductivity apparatus. It appears that a thin sample of low conductivity which will not ablate rapidly can be easily and quickly evaluated in the micro-motor exhaust to yield thermal diffusivity data which are surprisingly accurate. These data were used to generate the temperature profiles and backside temperature for a 1/2-inch thick slab of slip-cast fused silica 8/ as shown in Figure 36.

To compare the thermal response of slip-cast fused silica, Pyroceram 9606 and Al_2O_3 , 1/4-inch thick plates of all three materials were exposed

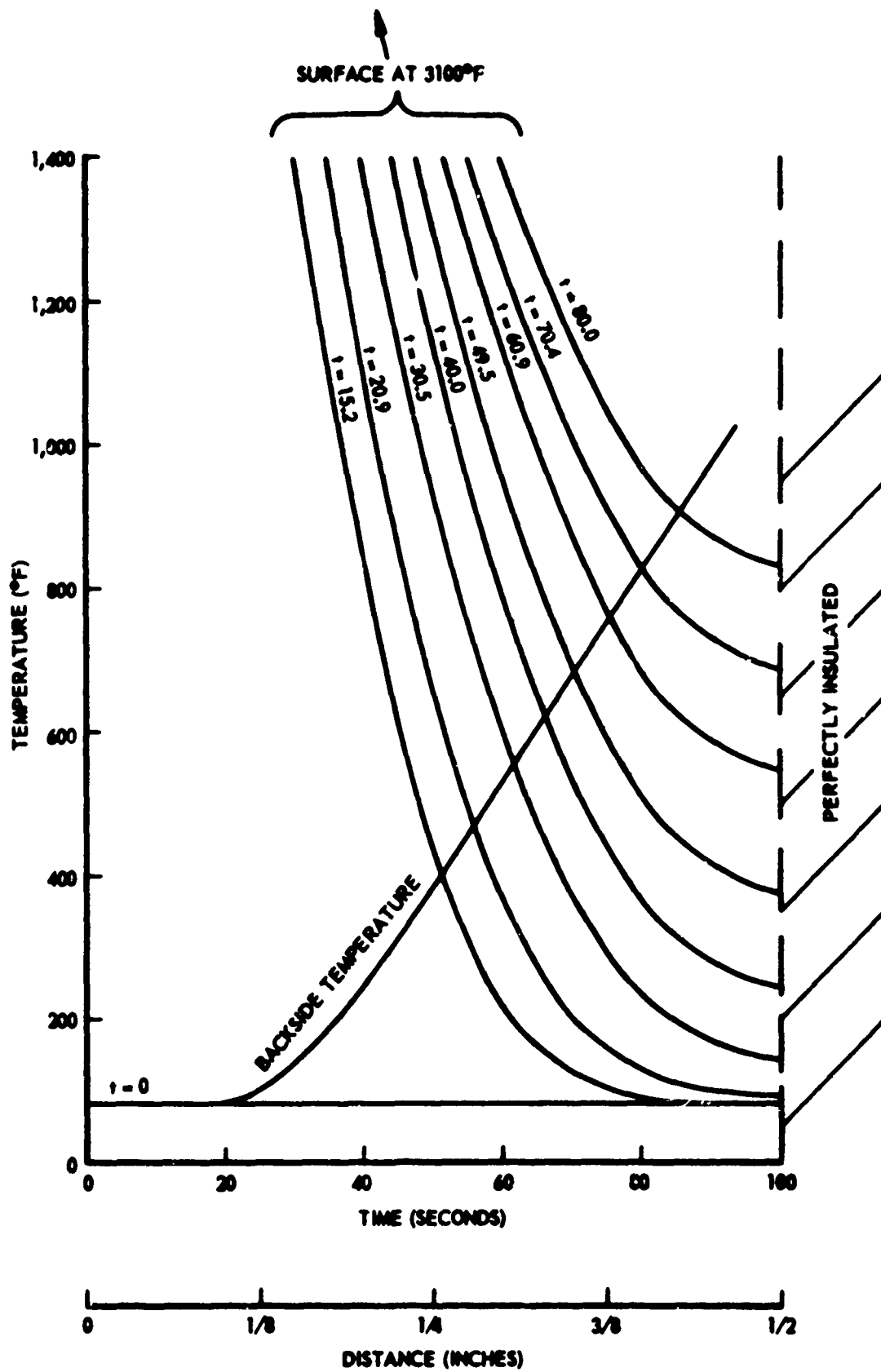


Figure 36. Temperature Profiles and Backside Temperature for 1/2-Inch Thick Plate of Slip-Cast Fused Silica (Ref 8, page 37).

to the exhaust of the oxy-hydrogen rocket motor at a distance of 14-inches from the exit plane 8/. This distance was selected since it was the closest distance at which Pyrocera 9606 and Al_2O_3 could survive the thermal shock. The frontside temperature, backside temperature and temperature difference between these two surfaces for all three materials are shown in Figures 37, 38, and 39.

b. Oxy-Acetylene Torch-Facility. The oxy-acetylene torch facility shown in Figure 40 was constructed to thermally evaluate large numbers of samples 14/. The water calorimeter heat flux provided by this facility at three different gas flow rates is shown as a function of distance from the torch 19/ in Figure 41.

The sample configuration was a 3/4-inch diameter bar, 2-1/2-inches long. The distance from the exposed end of the test bar to the torch tip was 3-inches. Cold wall heat-flux at this point was approximately 1500 Btu/ft²-sec using oxygen flow of 90 CFH at 25 psig and acetylene flow of 60 CFH at 15 psig.

The optical surface temperature, change in weight and change in length for slip-cast fused silica 14/ are shown as a function of time exposed to the oxy-acetylene torch facility in Figure 42.

2. Arc Plasma Testing. Slip-cast fused silica has been evaluated in the LAS High Temperature Arc Facility 19/. Test conditions are shown in Table VI. The performance of slip-cast fused silica under these conditions is shown in Table VII.

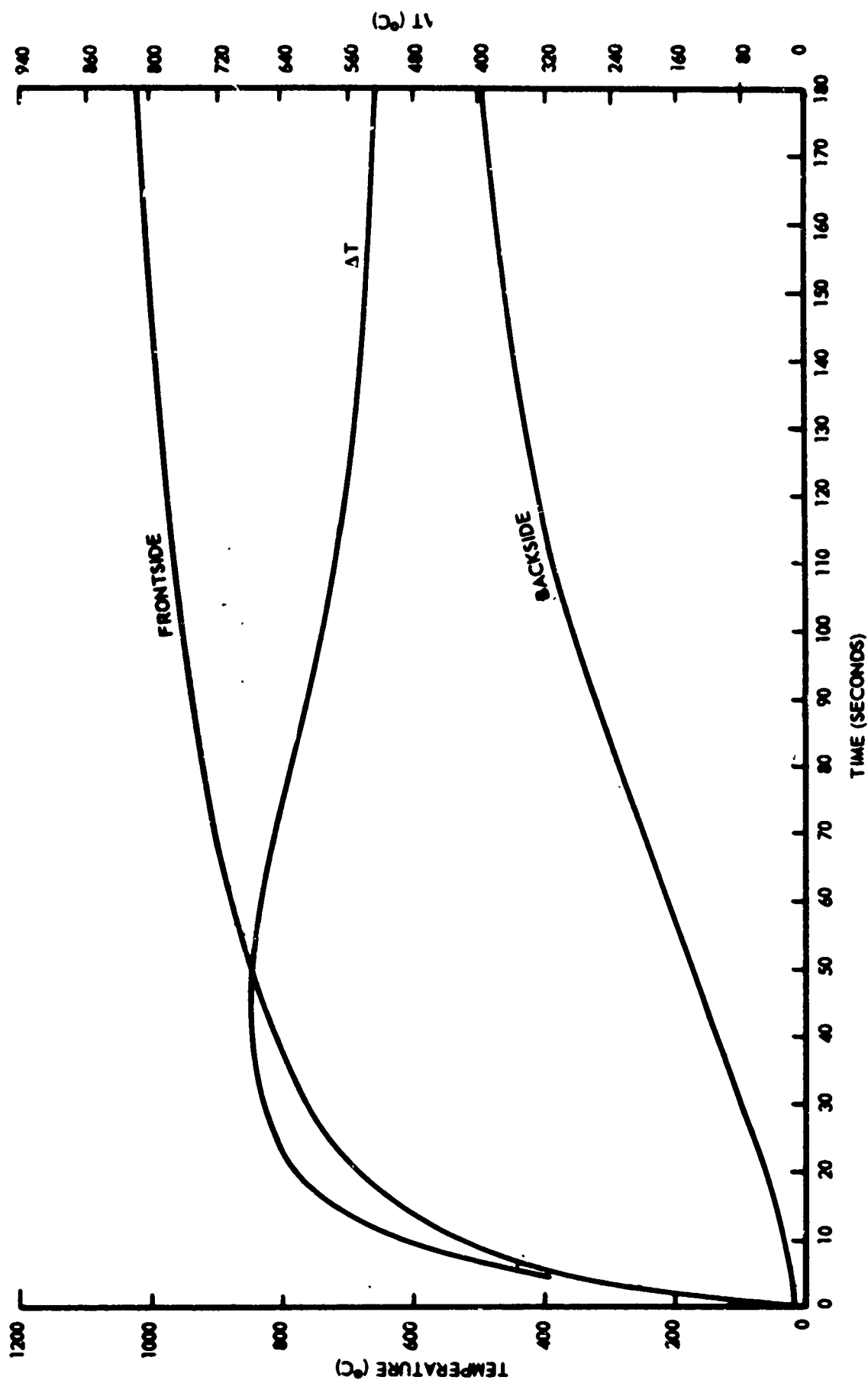


Figure 37. Temperature Measurements on a 1/4-Inch Thick Slip-Cast Fused Silica Plate Located 14-Inches from the Exit Plane of the Oxy-Hydrogen Rocket Motor (Ref 8, page 64).

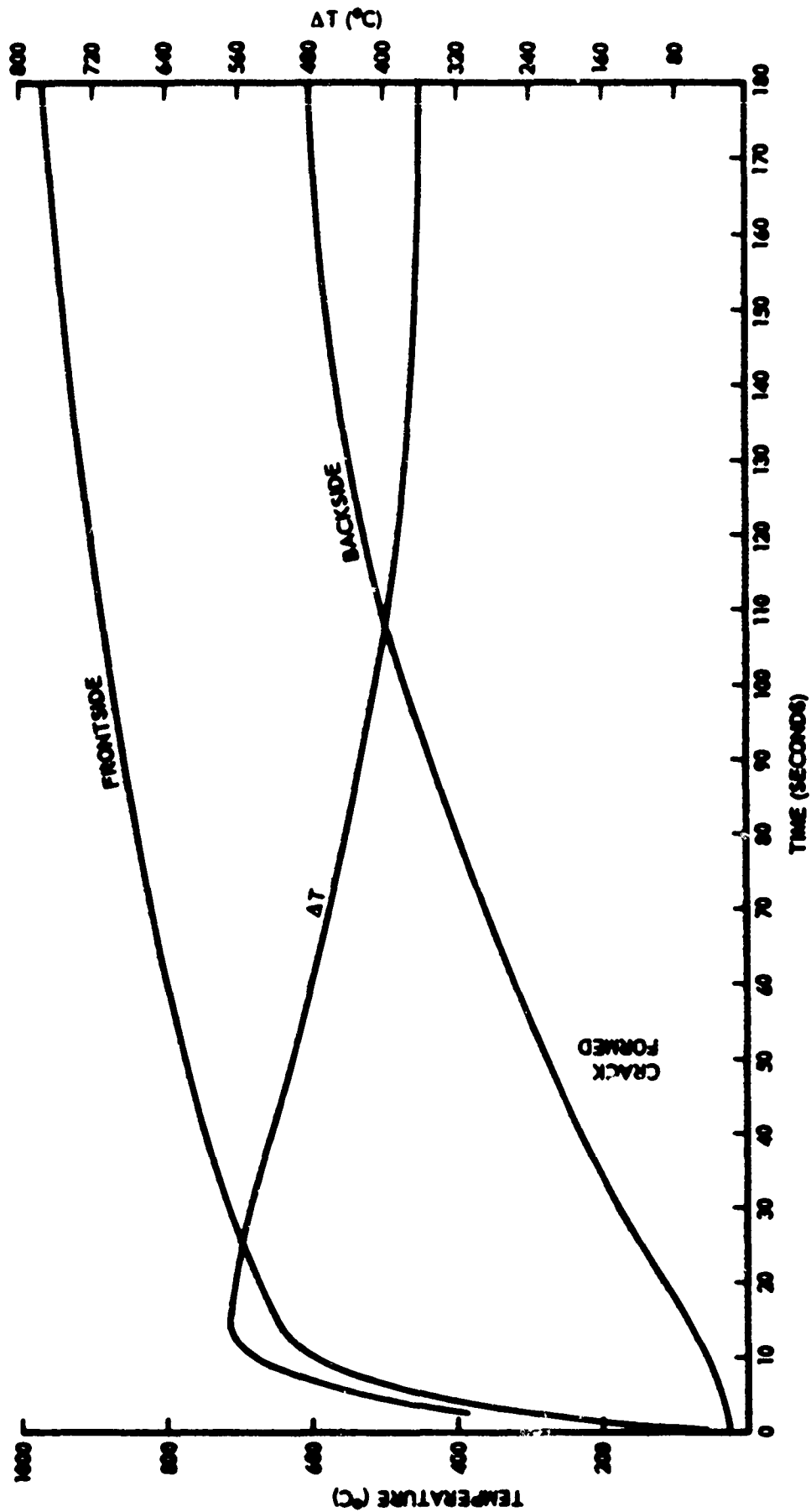


Figure 38. Temperature Measurements on a 1/4-Inch Thick Pyrocera Plate Located 14-Inches from the Exit Plane of the Oxy-Hydrogen Rocket Motor (Ref 8, page 65).

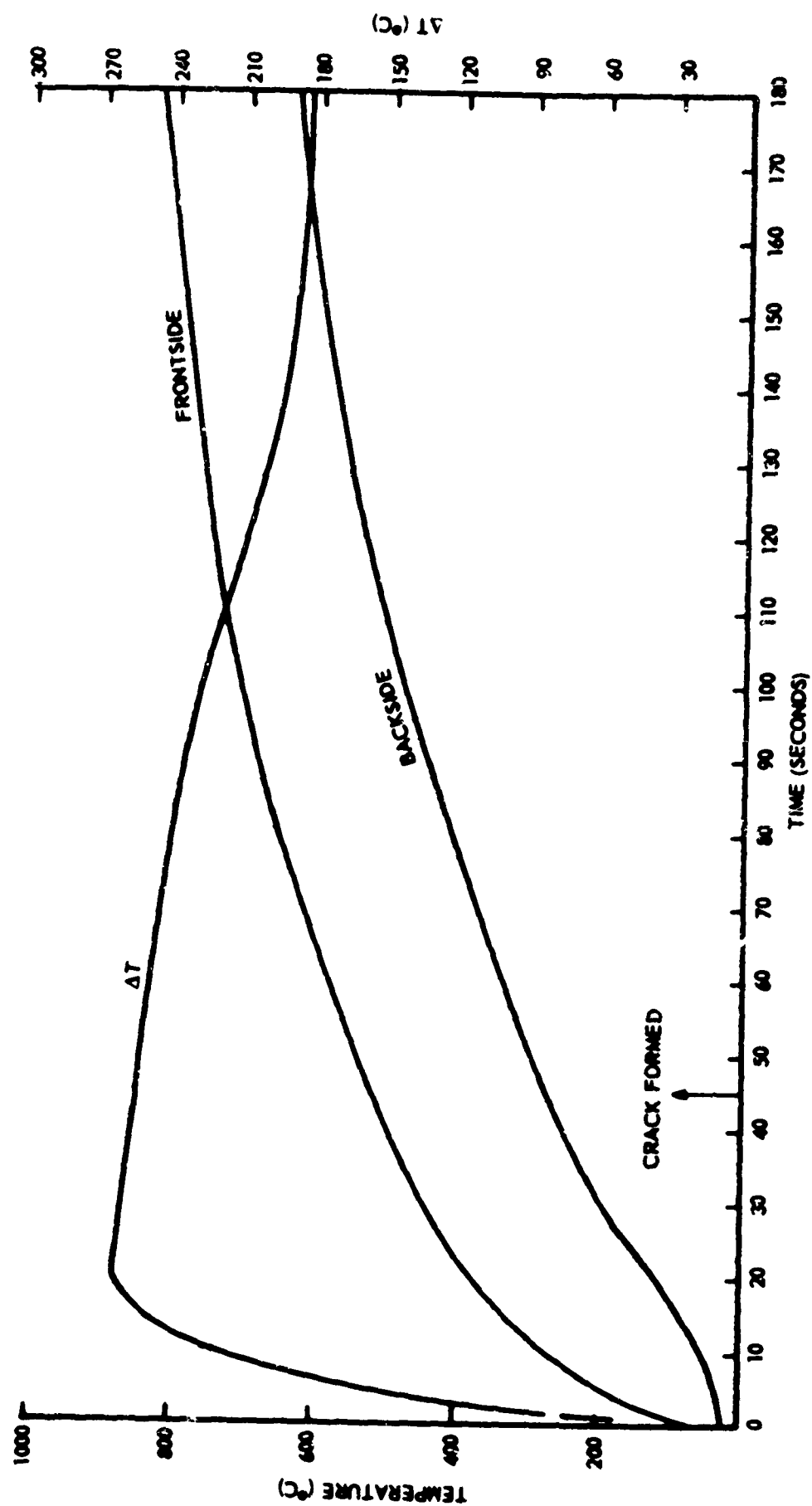


Figure 39. Temperature Measurements on a 1/4-Inch Thick Aluminum Oxide Plate Located 14-Inches from the Exit Plane of the Oxy-Hydrogen Rocket Motor (Ref 8, page 63).

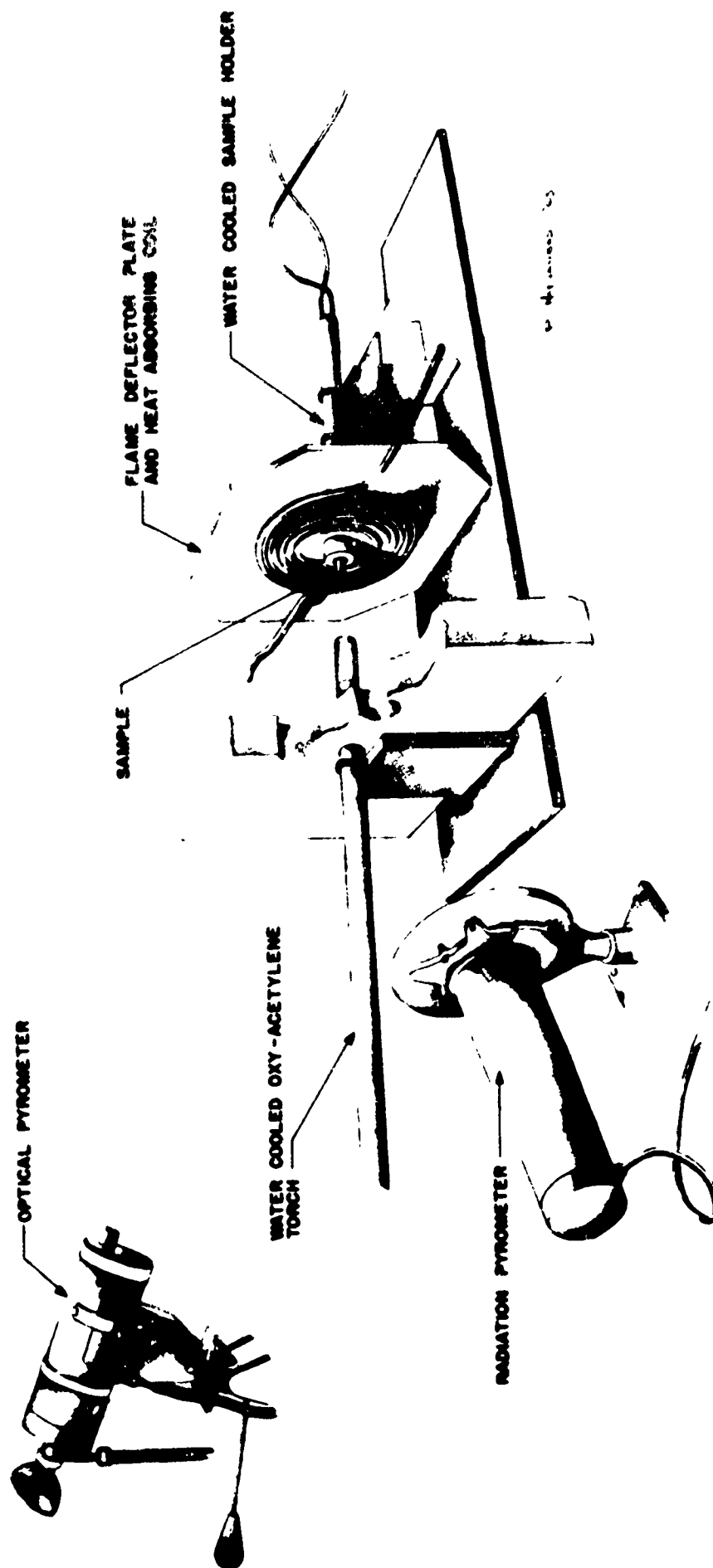


Figure 40. Artist Rendering Oxy-Acetylene Test Facility (Ref 14, page 110).

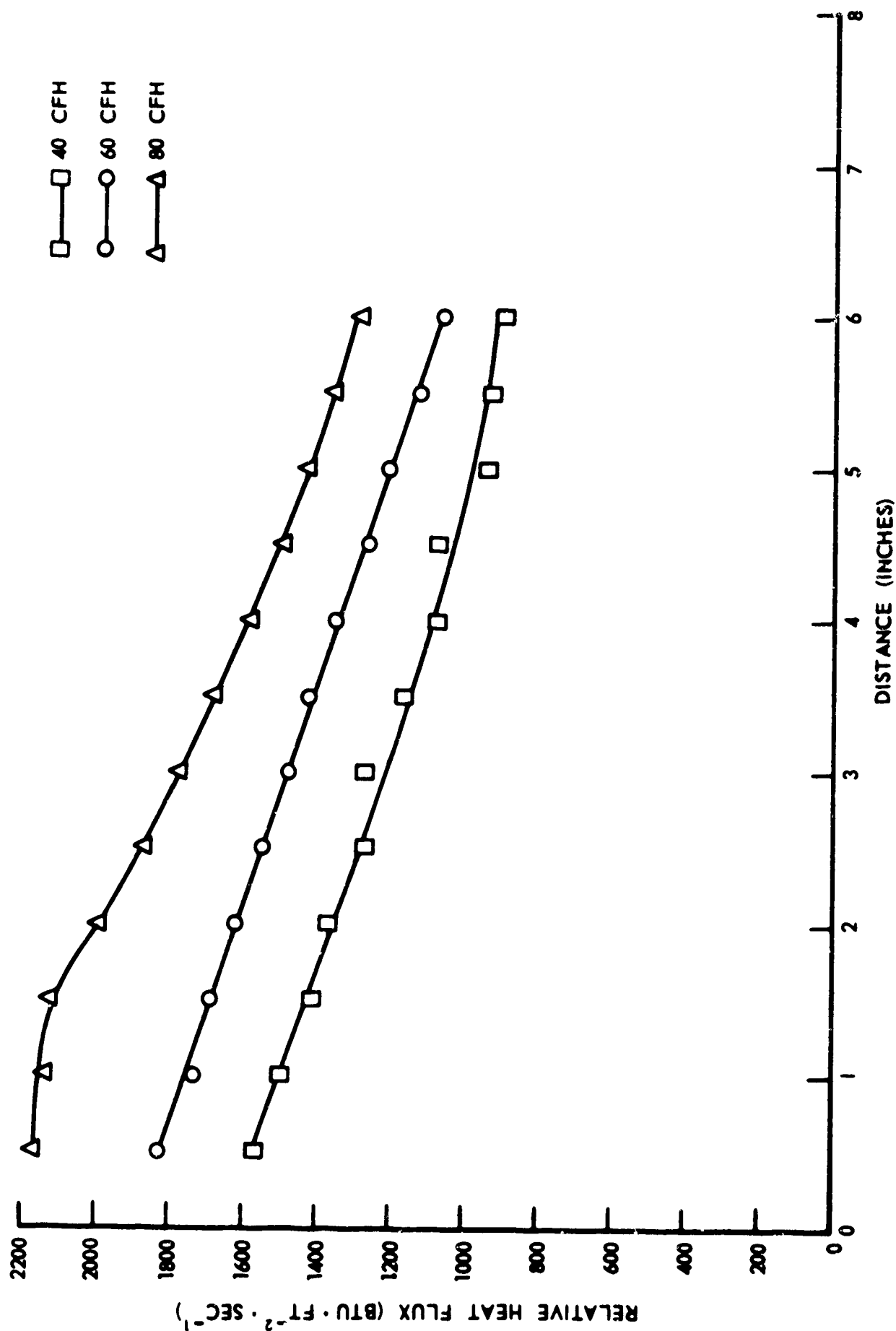


Figure 41. Relative Heat Flux vs. Distance for 40, 60, and 80 CFH Acetylene at Oxygen-to-Acetylene Ratio of 1.5 (Ref 19, page 9).

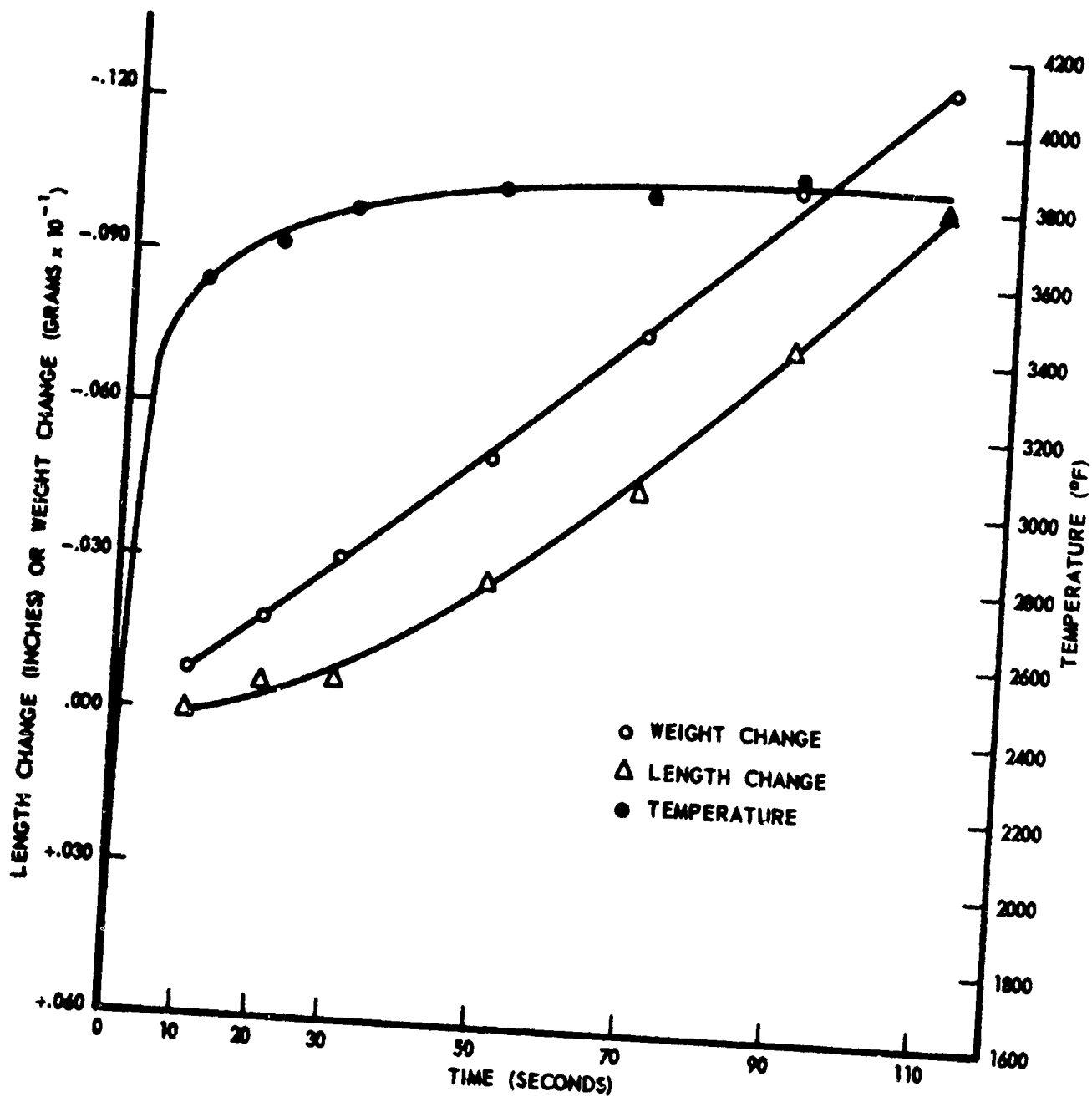


Figure 42. Surface Temperature, Weight Change and Length Change of Slip-Cast Fused Silica as a Function of Time Exposed to Oxy-Acetylene Test Facility (Ref 14, page 46).

TABLE VI
TEST CONDITIONS EMPLOYED FOR MATERIALS TEST WORK

| <u>Test Condition</u> | <u>Subatmospheric Arc</u> | | <u>Atmospheric Arc</u> |
|--|---------------------------|-----------|------------------------|
| | <u>II</u> | <u>VI</u> | |
| Arc Input Power, kw | 400 | 549 | 810 |
| Air Mass Flow, lb/sec | 0.043 | 0.132 | 0.140 |
| Enthalpy, Btu/lb | 5480 | 2570 | 1540 |
| Stagnation Pressure, psia | 2.0 | 5.25 | 15.2 |
| Temperature, °R | 9430 | 6100 | 5040* |
| Approximate Plasma Velocity, ft/sec | 1420 | 1260 | 800 |
| Cold Wall Heat Flux 17/32- inch Nose Radius Calorimeter Btu/ft ² -sec | 271 | 271 | 270 |
| * Estimated. | | | |

TABLE VII
TEST DATA OF SLIP-CAST FUSED SILICA UNDER TEST CONDITIONS
LISTED IN TABLE III

| <u>ARC Exposure Condition</u> | <u>Duration of Exposure</u> (sec) | <u>Duration to Initiation of Melting</u> (sec) | <u>Weight Loss</u> (gms) | <u>Average Mass Ablation Rate</u> (gm/sec) | <u>Stagnation Point Ablation</u> (inch) |
|---------------------------------------|--|---|---------------------------------|---|--|
| Subatmos- pheric II | 120 | 24 | 0.1 | 0.0008 | None |
| Subatmos- pheric VI | 120 | 46 | 0.2 | 0.0017 | None |
| Atmospheric | 120 | 61 | 0.1 | 0.0008 | None |

The simulated altitude and flight velocity for test conditions II, VI, and atmospheric are shown in Figure 43. Also shown is the Manned Recovery Orbit trajectory. Data points for the satellite trajectory as reported by Adams, Powers and Georgiev 21/ under which opaque fused silica should be in radiation equilibrium are seen to be superimposed on the Manned Recovery Orbit Curve.

Rosenbery, Smith and Wurst 22/ also evaluated slip-cast fused silica in an arc facility. The operational parameters for the arc together with test results for fused silica are shown in Table VIII.

It should be evident that under conditions as severe as those shown for the Manned Recovery Orbit trajectory, slip-cast fused silica will survive without significant ablation or surface dimension change. Referring to Figure 43, slip-cast fused silica should operate without ablation in any area above or to the left of the Manned Recovery Orbit curve. Ablation rates below this curve would be expected to be of the order of 0.001-inch/sec.

3. Testing of Full Scale Nose Cone. During one phase of a project to evaluate slip-cast fused silica for nose cone applications 7/, a slip-cast fused silica nose cone 25-inches high, 19-inches in diameter at the base and 3/4-inches thick (See Figure 44) was exposed to the exhaust of an 18,000 pound thrust rocket motor. This nose cone was mounted at a distance of 30-inches from the exit plane 14/ as shown in Figure 45. The conditions provided by this rocket motor were:

| | |
|-------------------|---------------|
| Exit Velocity | 6790 ft/sec |
| Exhaust Gas Temp. | 3920° F |
| Exposure Time | 17.16 seconds |

- SATELLITE TRAJECTORY IN RADIATION EQUILIBRIUM - FROM AVCO DATA
- LAS HIGH TEMPERATURE ARC FACILITY - SLIP CAST
- FUSED SILICA IN RADIATION EQUILIBRIUM

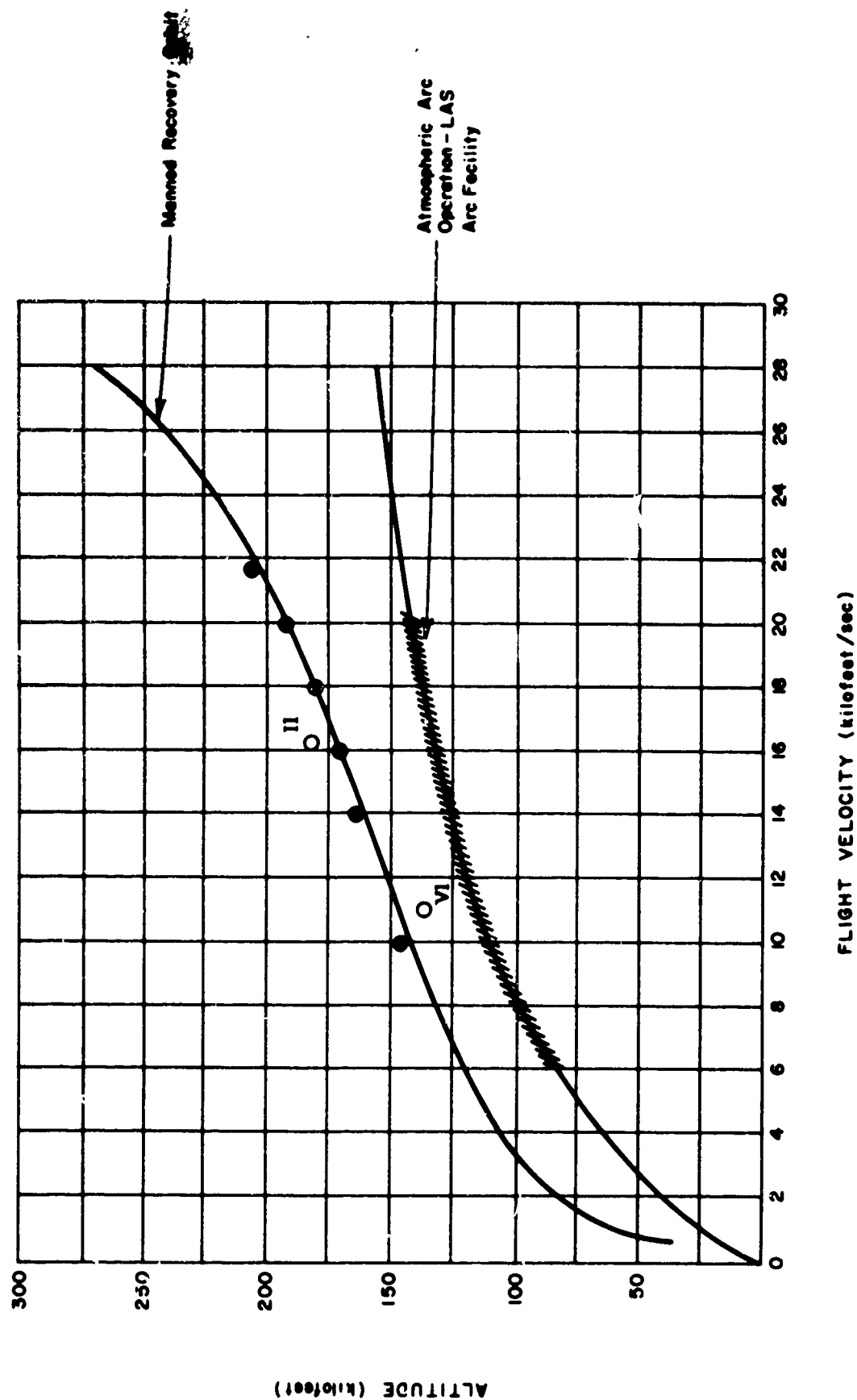


Figure 43. Simulated Capability of LAS Arc-Vacuum Facility, Altitude vs. Velocity Including Radiation Equilibrium Data Points for Fused Silica (Ref 14, page 19).

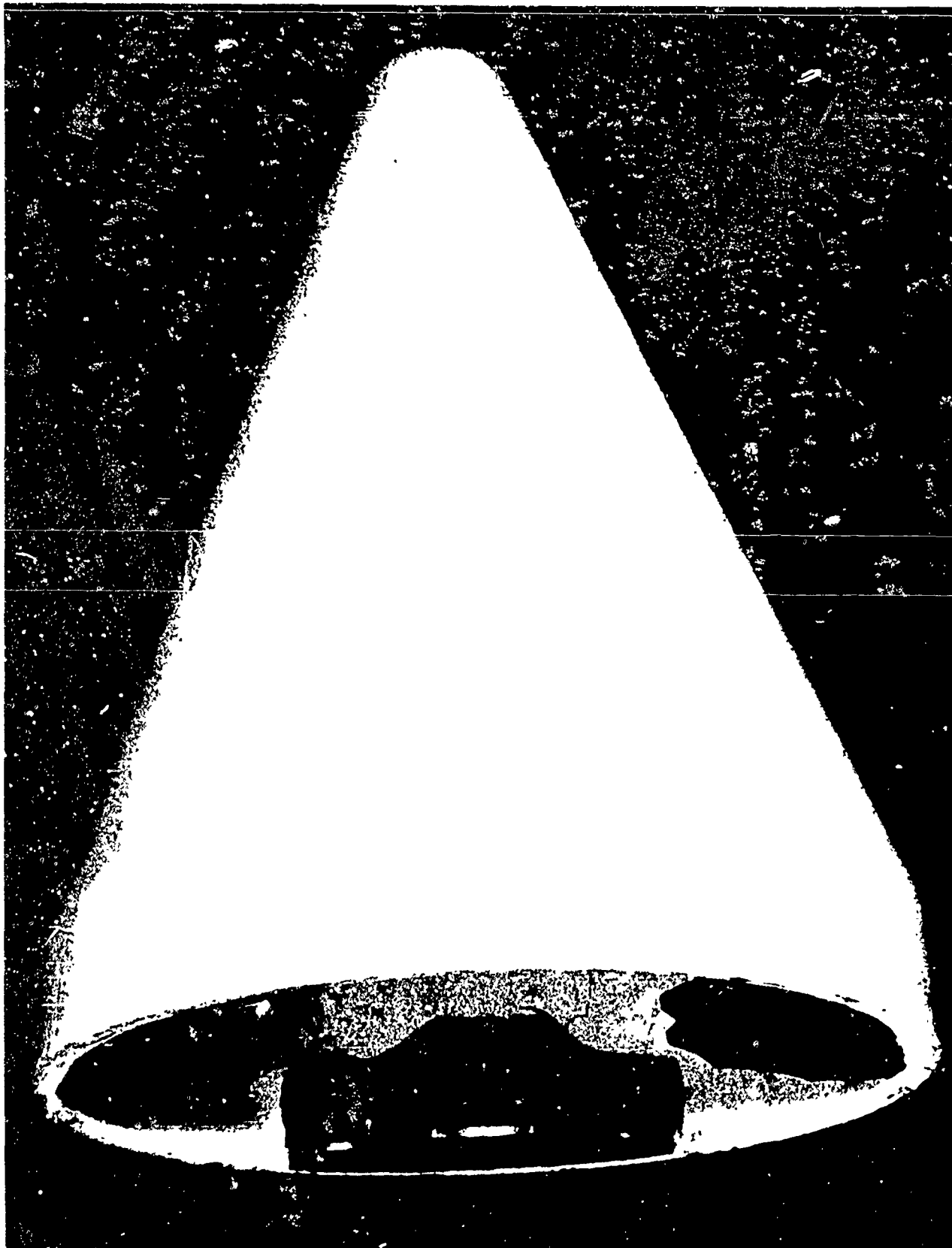


Figure 44. Fused Silica Nose Cone Showing Mounting Brackets Cemented in Place With Adhesive Resin (Ref 7, page 47).



Figure 45. 164 HT Facility (Ref 14, page 14).

TABLE VIII
TEST CONDITIONS AND RESULTS FOR FUSED SILICA SPECIMENS
EXPOSED TO AN ARC-PLASMA JET EFFLUENT

| | | |
|---|---|---|
| Heat Flux (BTU/ft ² -sec) | 109 | 504 |
| Gas Enthalpy (BTU/lb) | 980 | 3750 |
| Gas Velocity (ft/sec) | 600 | 1370 |
| Stagnation Pressure (in. H ₂ O) | --- | 24.1 |
| Gas Temperature (°F) | 3150 | 7200 |
| Test Duration (sec.) | 360 | 72 |
| Depth of Erosion (in.) | 0.003 | 0.029 |
| Final Back Face Temp °F | 330 | 310 |
| Final Front Face Temp °F | --- | --- |
| Remarks | Very little effects were observed, except discoloration of the surface | Volume of specimen increased slightly after test. Evidence of a clear glassy phase on surface. Max. surface temp. >3200° F (optical pyro.) |

(Continued)

TABLE VIII (Continued)

TEST CONDITIONS AND RESULTS FOR FUSED SILICA SPECIMENS
EXPOSED TO AN ARC-PLASMA-JET EFFLUENT

| | | | |
|--|--------------------------------|--------------------------------|--------------------------------|
| Heat Flux (BTU/ft ² -sec) | 300 | 300 | 300 |
| Gas Enthalpy (BTU/lb) | 2340 | 2080 | 4000 |
| Gas Velocity (ft/sec) | 1030 | 750 | 730 |
| Stagnation Pressure (In.H ₂ O) | 18.5 | 0.488 | 6.0 |
| Gas Temperature (°F) | 5670 | 5400 | 7800 |
| Test Duration (sec) | 120 | 40 | 120 |
| Depth of Erosion (in.) | Nil | 0.0100 | Nil |
| Final Back Face Temp °F | 1050 | 160 | 920 |
| Final Front Face Temp °F | 3120 | 2790 | 3600 |
| Remarks | Mass Flow = 0.0082 lbs/sec. | Mass Flow = 0.0082 lbs/sec. | Mass Flow = 0.0037 lbs/sec. |

The slip-cast fused silica nose cone survived this test with only localized melting at the tip. Figures 46 and 47 are photographs of the nose cone after exposure to the rocket exhaust. The ablation rate was difficult to determine precisely, but ranged between 0.0003 and 0.0017-inch/sec maximum. The use of this test motor to evaluate nose cone materials has been described by Lucas and Houston 23/.

D. Improving the Refractoriness of Slip-Cast Fused Silica

1. Ablation Rate. Various coloring oxides have been added to the slip in an effort to raise the emittance of the resulting slip-cast material. Any increase in emittance would lower the surface temperature when exposed to aerodynamic heating and thus have the effect of improving the refractoriness of the material.

Thus far Cr_2O_3 appears to be singular in its ability to improve the performance of slip-cast fused silica when exposed to the oxy-acetylene torch facility 14/ shown in Figure 40.

The optical temperature, change in length and change in weight are shown as a function of time exposed to the oxy-acetylene torch for slip-cast fused silica containing 2-1/2 w/o Cr_2O_3 14/ in Figure 48. The improvement provided by the small addition of Cr_2O_3 can be seen by comparing Figure 48 with Figure 42.

The physical make-up of the ablation testing sample holder was such that only one inch of the 2-1/2-inch long test bar was recessed within the water-cooled holder. When samples were fired for 50 seconds or longer a shrinking or necked effect was noted on the samples. This was due to flame wrap-around. In order to more nearly approximate one dimensional heat flow, guard plates,



Figure 46. Slip-Cast Fused Silica Nose Cone after Test (Elevation)
(Ref 14, page 15).



Figure 47. Slip-Cast Fused Silica Nose Cone after Test (Plan)
(Ref 14, page 16).

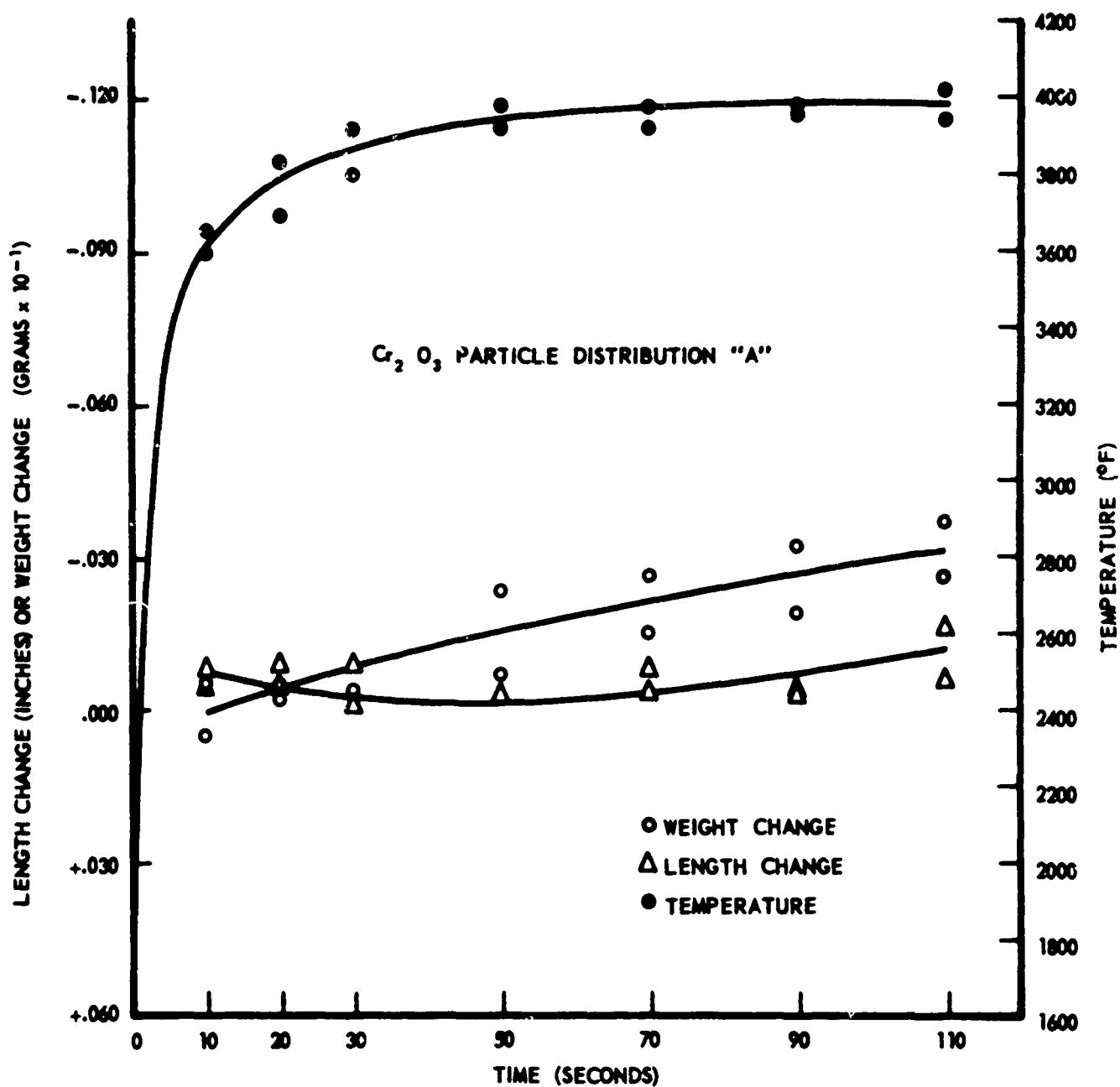


Figure 48. Surface Temperature, Weight Change and Length Change of Slip-Cast 2.5 w/o Chromium Oxide - 97.5 w/o Fused Silica as a Function of Time Exposed to Oxy-Acetylene Test Facility (Ref 14, page 47).

or flame shields were prepared. These shields were 2-inches square and 1-1/2-inch thick and with a 3/4-inch diameter hole drilled in the center face. The blocks were made up of 1-inch thick fused silica foam block substrate and were coated with a 2-1/2 w/o chromium oxide powder - 97.5 w/o fused silica cement approximately 1/2-inch thick. Figure 49 shows this arrangement 14/.

Fusion between the bars and the flame shields occurred during testing and prevented weight measurements, therefore only length change data was taken and is presented in Figures 50 and 51. When fired for 110 seconds the total ablation of the SiO_2 bar when protected was only about 58 per cent of the ablation occurring when unprotected. The protected Cr_2O_3 bar ablated only about 20 per cent of that ablation for the unprotected Cr_2O_3 sample when fired for 110 seconds 14/.

The effective emittance as a function of true temperature, based on a "gray body" assumption, was determined for slip-cast fused silica and 2-1/2 w/o Cr_2O_3 modified slip-cast fused silica 14/. The method consisted of heating the end surface of 3/4-inch diameter bars of each composition in the oxy-acetylene testing facility. After temperature equilibrium had been reached, temperature measurements were made with a Minneapolis Honeywell Small Target Radiometric radiation pyrometer and a Pyrometer Instrument Co. optical pyrometer. These temperatures were used to calculate the effective emittance as shown in Figures 52 and 53. Appendix A 14/ describes the method used to calculate effective emittance.

The fuel gas flow rates and the torch-to-sample surface distance were varied to obtain optical temperatures of approximately 2000°, 2400°, 2800°, 3200°, 3600°, and 4000° F on plain slip-cast fused silica. The fuel gas flow

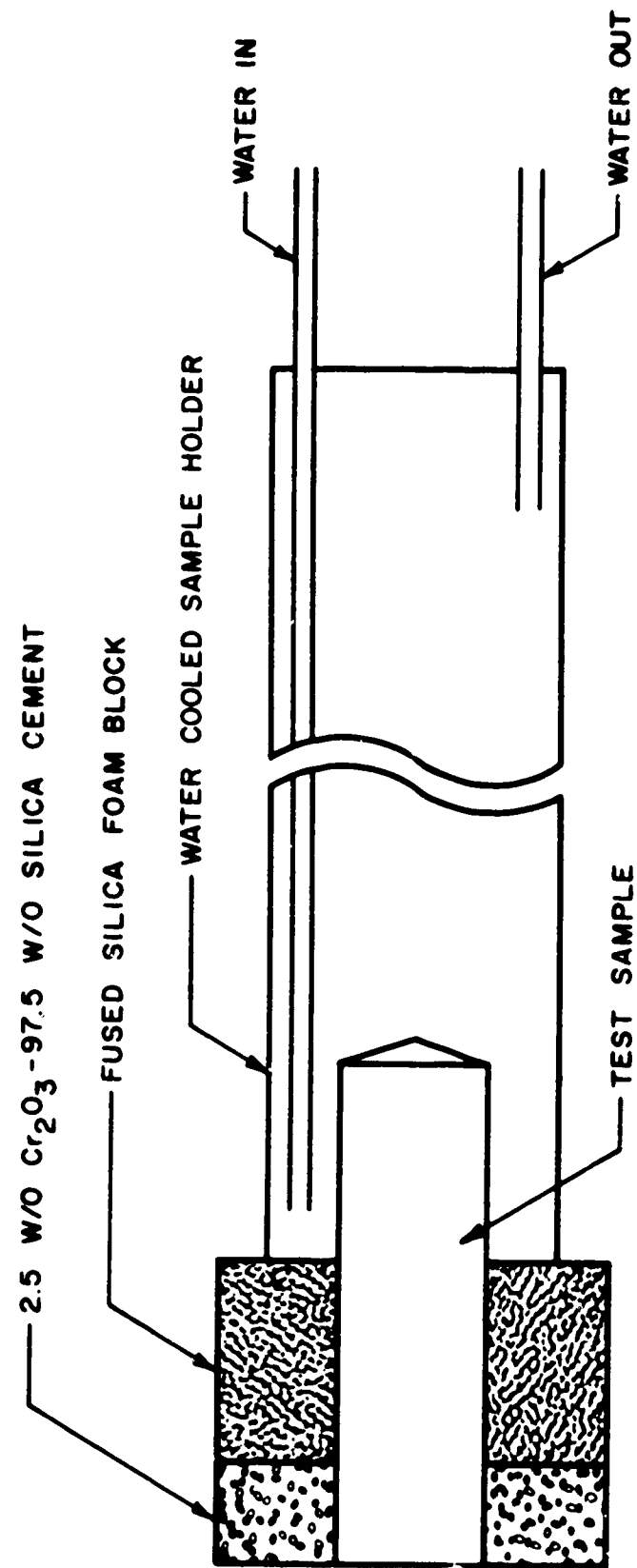


Figure 49. Drawing Illustrating Flame Shield-Test Bar Arrangement
(Ref 14, page 55).

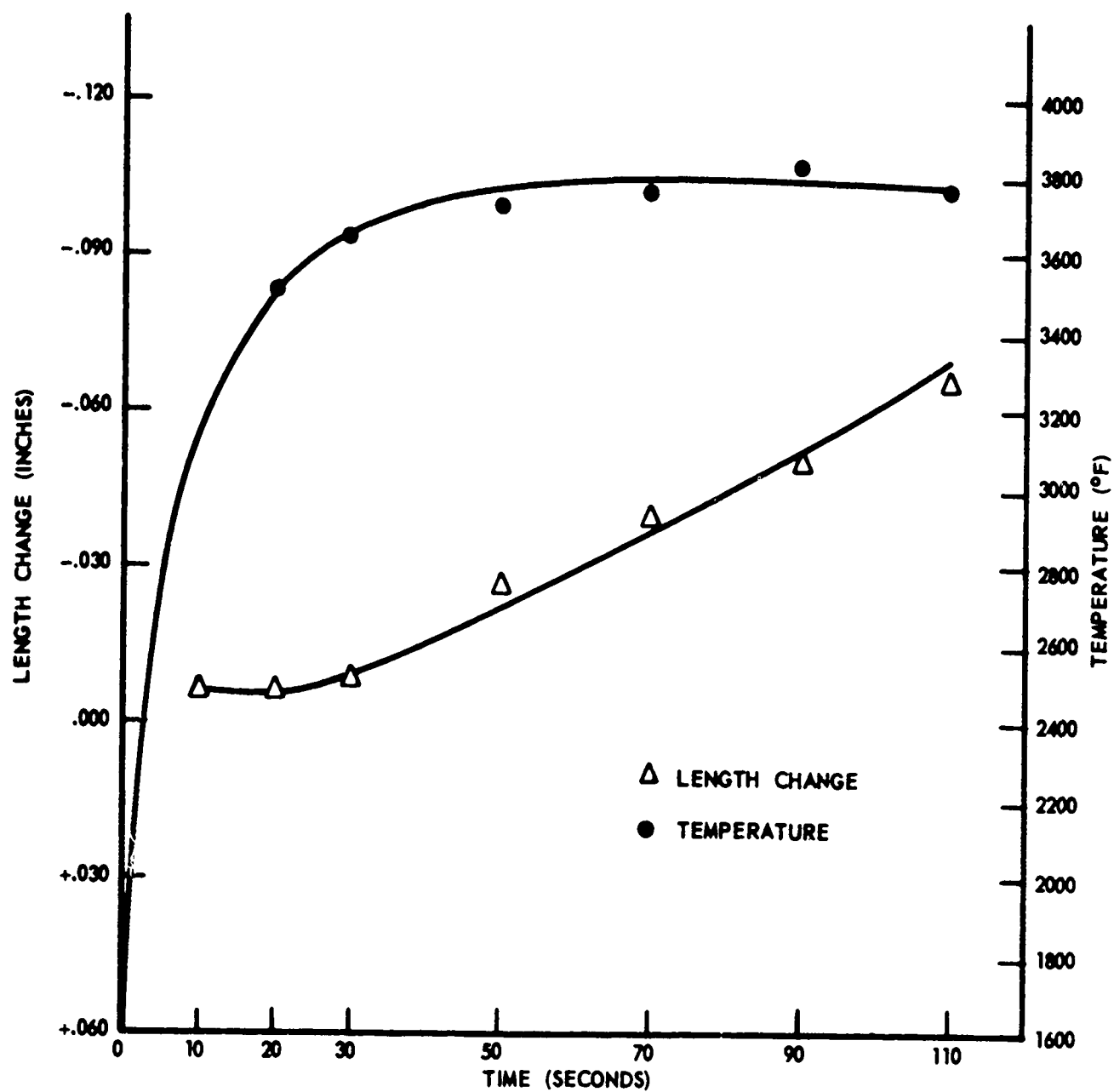


Figure 50. Surface Temperature and Length Change of Slip-Cast Fused Silica with Flame Shield as a Function of Time Exposed to Oxy-Acetylene Test Facility (Ref 14, page 56).

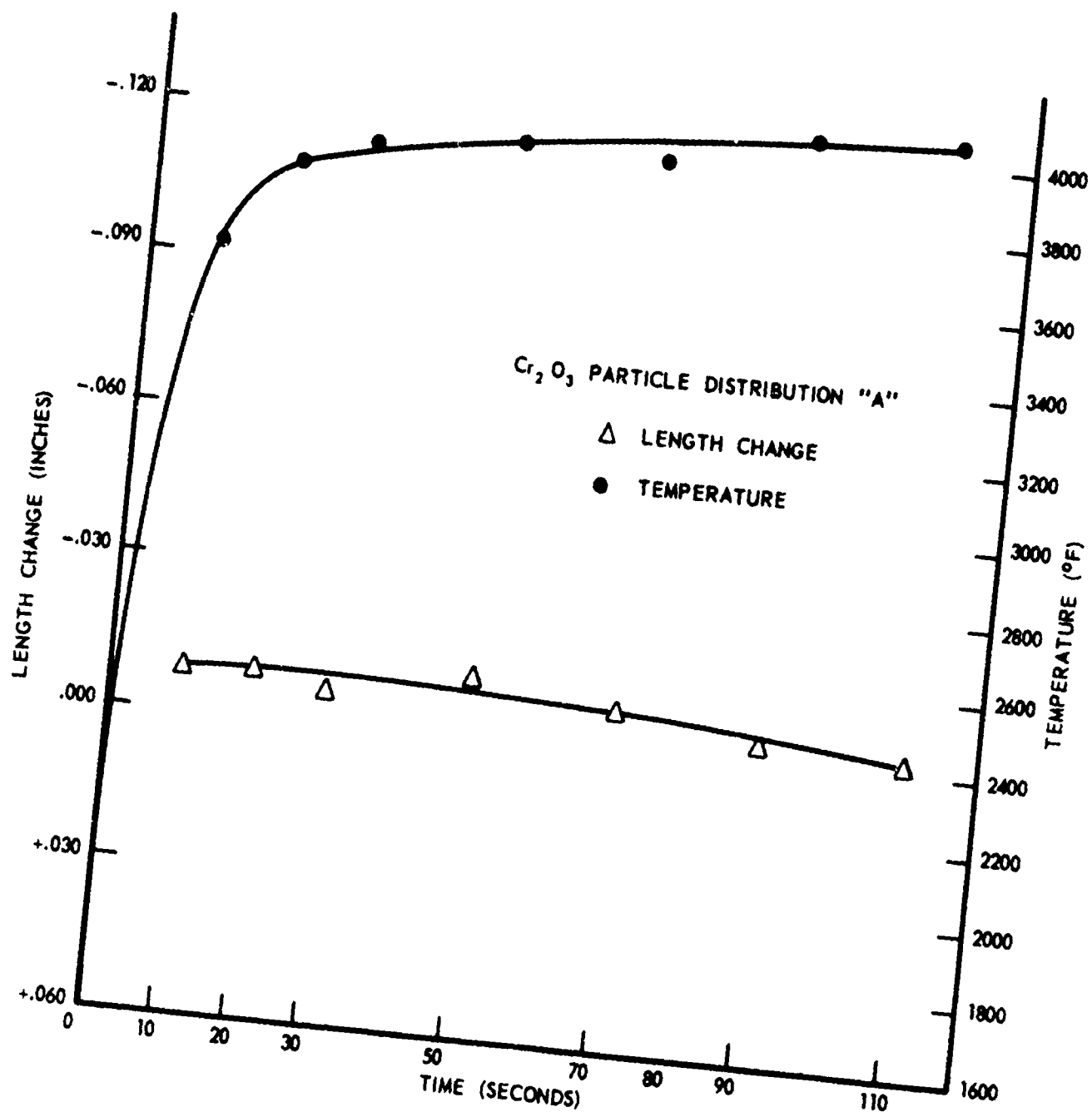


Figure 51. Surface Temperature and Length Change of Slip-Cast 2.5 w/o Chromium Oxide - 97.5 w/o Fused Silica with Flame Shield as a Function of Time Exposed to Oxy-Acetylene Test Facility (Ref 14, page 57).

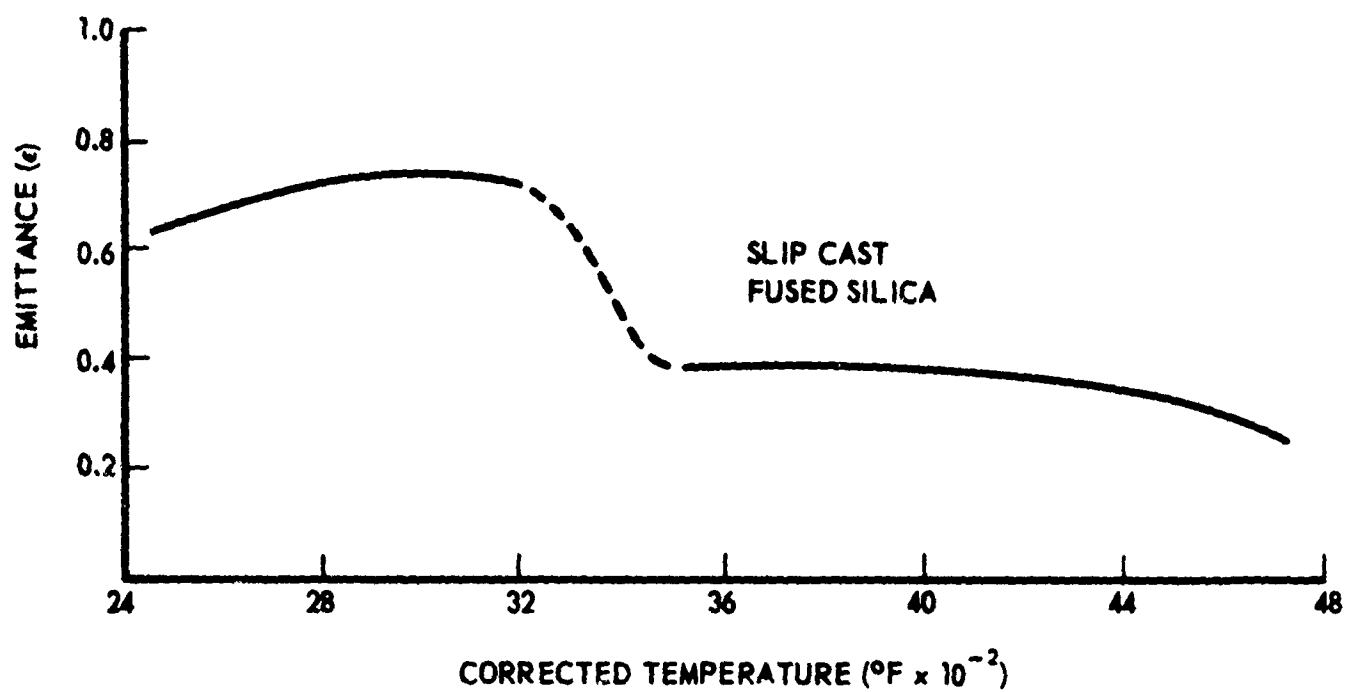


Figure 52. Effective Emittance vs. Corrected Surface Temperature for Slip-Cast Fused Silica (Ref 14, page 70).

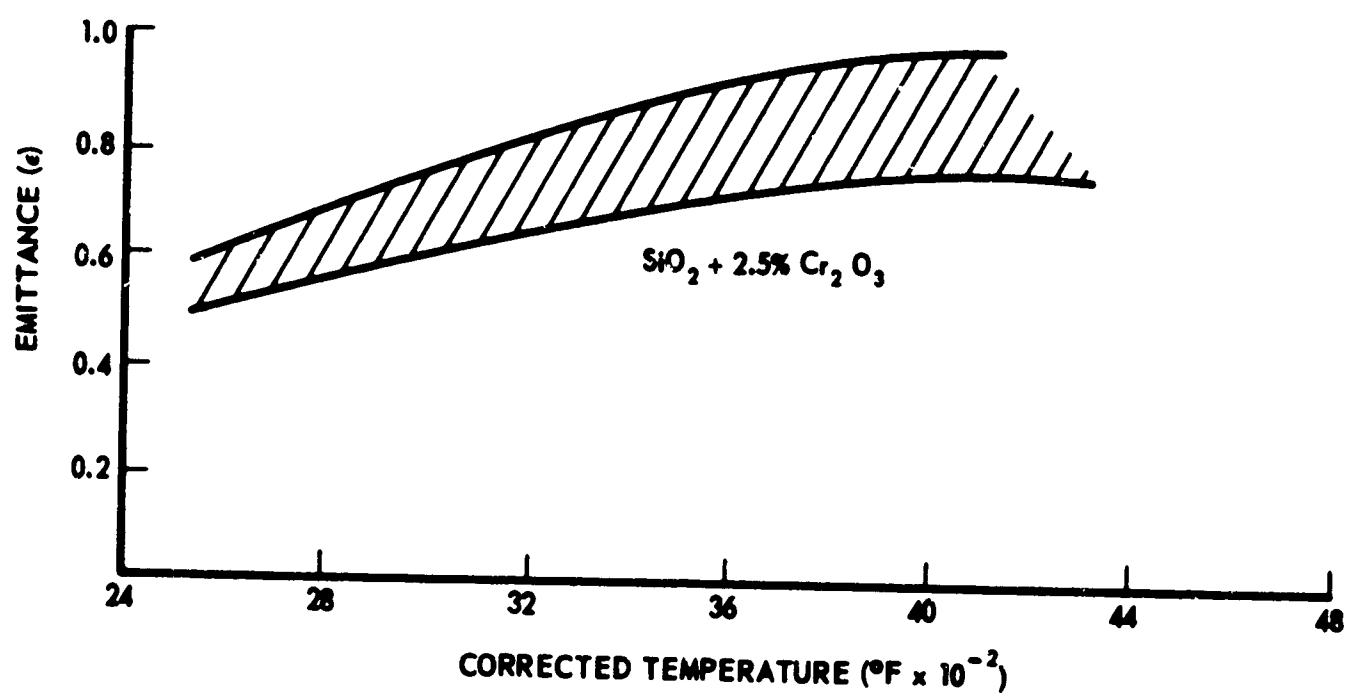


Figure 53. Effective Emittance vs. Corrected Surface Temperature for Slip-Cast 2.5 w/o Chromium Oxide - 97.5 w/o Fused Silica (Ref 14, pages 71-73).

rates and torch-to-sample surface distance established were used to evaluate samples of each of the compositions. These measurements were made with the oxy-acetylene torch at an angle of 25° with the sample surface and with the total radiation pyrometer normal to the sample surface.

The contribution of flame radiation to the measured radiation temperatures was found to be negligible by placing a polished copper plug in the sample holder and observing the radiation pyrometer response with the flame burning. A discernable reading was not obtained with the pyrometer.

The effect of reflected radiation from the sample was not considered in these measurements. It is expected that this effect will also be negligible.

From Figure 54 (Figures 52 and 53 superimposed) it can be seen that the addition of Cr_2O_3 to slip-cast fused silica provides very little improvement in emittance below about 3200°F , or the melting point of silica. However, above this temperature Cr_2O_3 modified silica appears to have a significantly higher emittance than the unmodified silica.

E. Electrical Evaluation of Slip-Cast Fused Silica Radomes

General Dynamics/Pomona is the only known group that has carried out bore-sight error determinations on slip-cast fused silica radomes. They reported that very satisfactory bore-sight data were obtained for an unmachined (as slip-cast) radome. These data were reported to compare favorably with bore-sight data obtained for other ceramic radomes which were machined.

F. Attachment of Slip-Cast Fused Silica Radomes

Slip-cast fused silica has essentially no thermal expansion ($0.54 \times 10^{-6}/^\circ\text{C}$). Rigidly attaching it to almost any material presents problems since thermal expansion mismatch will result. The severity of the

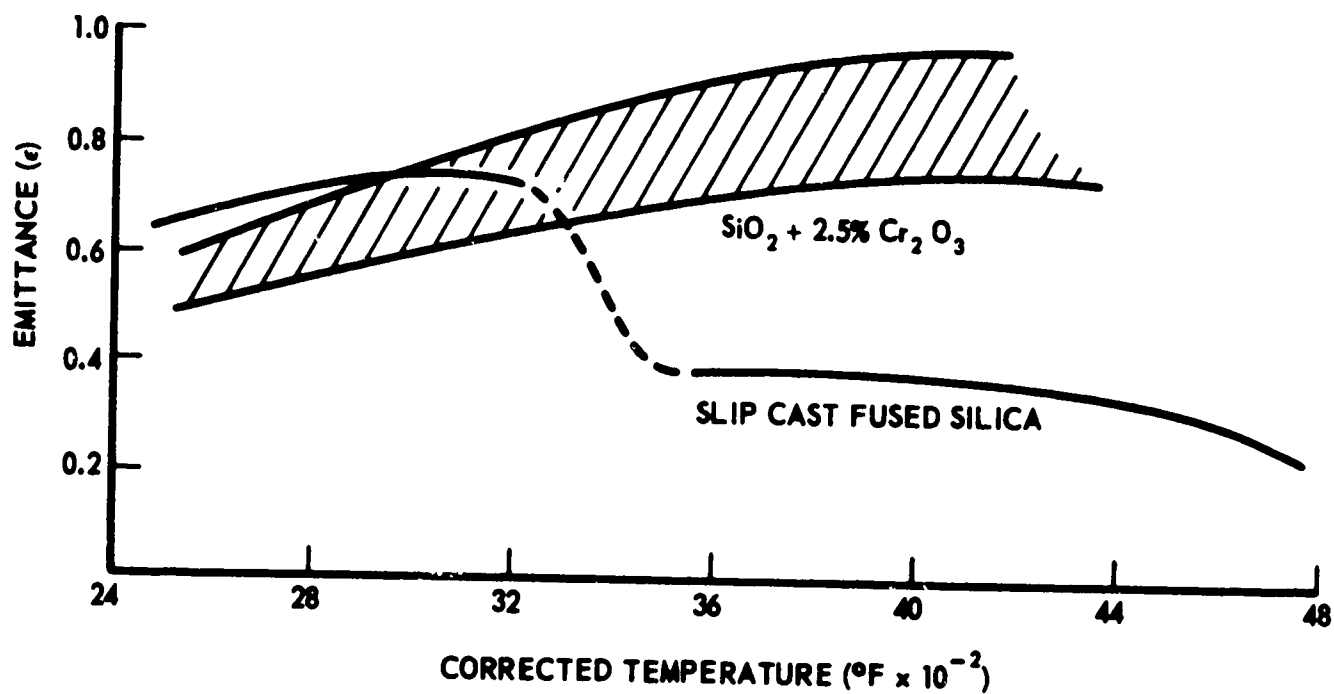


Figure 54. Comparison of Effective Emittance vs. Corrected Surface Temperature of Slip-Cast Fused Silica With and Without Chromium Oxide.

problem depends upon two factors: (1) the difference in expansion and (2) the temperature to which the attachment area will be subjected.

Since the thermal conductivity of slip-cast fused silica is very low, the material itself will delay heating of the attachment area during flight. Therefore, the use of internal attachment systems would be preferred. Also, since it is not recommended that the attachment area be heated, a low temperature curing resin is recommended for bonding the attachment system to the radome.

One attachment system which has proven successful in sled tests was developed by General Dynamics Pomona is shown in Figure 55. The radome for which this system was developed is 13-inches tall and 5-1/2-inches in base diameter.

G. Improving the Strength of Slip-Cast Fused Silica

For large radomes, the strength of slip-cast fused silica would be marginal at best. Since there appeared to be no immediately available method for improving the inherent strength of the slip-cast fused silica, methods for reinforcing the material were considered. The most promising method currently in use was considered to be filament winding. This method is used to reinforce and provide attachment systems for certain radomes. One of the advantages of such a system lies in the fact that the ceramic is prestressed by the tension provided from the tensile stress imposed in the filament during winding. Such a system makes use of the compressive strength of the ceramic and the tensile strength of the filament.

In order to extend the mechanical performance of slip-cast fused silica it was decided that filament winding would be considered as a means of prestressing slip-cast fused silica radomes 24/.

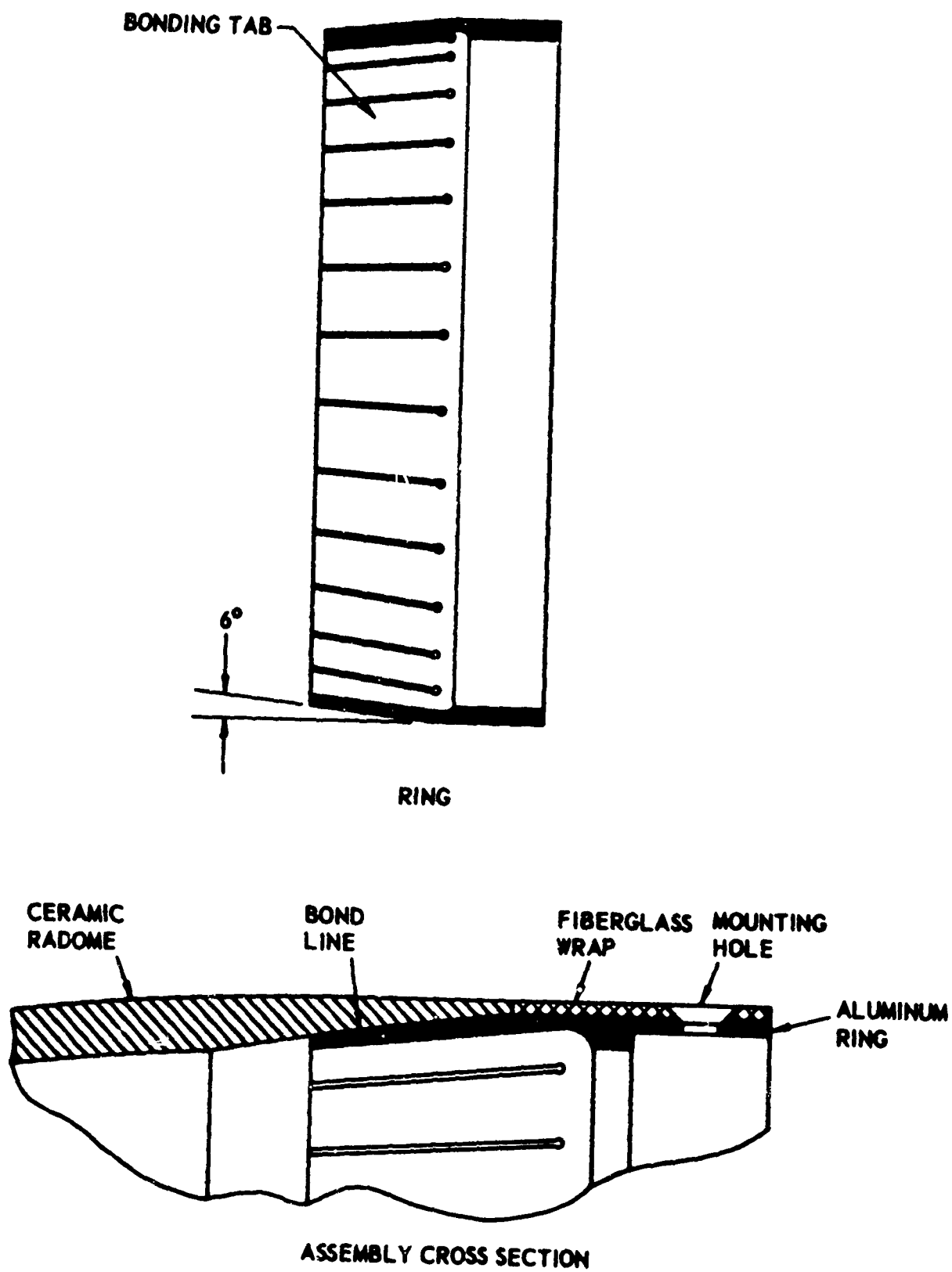


Figure 55. Experimental Ring Configuration for Mounting Slip-Cast Fused Silica Radome.

Slip-cast fused silica cylinders were fabricated for filament winding in the preliminary study of prestressing. These cylinders were 10-inches in length by 3-inches in outside diameter. The wall thickness was approximately 1/2-inch. These cylinders were fired at 2200° F for three and one-third hours. They were then wrapped with Owens-Corning "Fiberglas" continuous yarn No. ECD 450-4/3. A metal lathe was used as the rotating device and the automatic feed as a traveling guide for positioning the yarn as it was fed onto the cylinder.

The wrapping tension in the yarn was controlled by a precision tension control device. This device is capable of maintaining a constant tension on glass filament during the winding operation regardless of speed of winding. Tension can be set at any point from 0 to 15 pounds.

Two cylinders were wrapped with the above yarn at a feed rate of 0.0129-inches per revolution. This feed rate gave a smooth, close wrap with no overlapping. The yarn was held in place with a conventional resin. Each cylinder was wrapped so that 1/4 of the length of the cylinder received two layers of yarn; 1/4, four layers; and 1/4, five layers. One quarter of the cylinder was left unwrapped. One cylinder was wrapped with a yarn tension of 4.5 pounds and the other at 9 pounds. The yarn was found to break at a load of 10-11 pounds.

After wrapping, the resin was cured for 48 hours at 130° F and 2 hours at 200° F. Rings approximately 1-inch in thickness were cut from the unwrapped portion of the cylinder, and from each of the sections with different layers of yarn. Each ring was then broken at room temperature using diametral compressive loading. It has been shown by Bortz and Lund 25/ that compressive loading of this type can be used in the measurement of tensile properties. Tensile strength can be calculated using the formula

$$\delta_{app} = K \frac{P}{(O.D.-I.D.)t}$$

Where

δ_{app} = apparent tensile strength

P = load in pounds

t = thickness in inches

O.D. = outside diameter

I.D. = inside diameter

K = constant depending on the ratio $\frac{I.D.}{O.D.}$

(in each case K was taken from a curve by Frocht)

The brittle ring test was designed for homogenous materials but was used here to obtain relative or apparent tensile strength values.

Two specimens of each type were broken. The apparent tensile strength was calculated for each wrapped ring at the first sign of a crack in the ceramic, and at the point of ultimate failure. The results of these tests are shown in Figure 56.

H. Rain Erosion Testing of Slip-Cast Fused Silica

Under Naval Bureau of Weapons Contract No. N0w 62-1087 #35 TOC, General Dynamics/Pomona supervised supersonic sled tests to determine the rain erosion resistance of slip-cast fused silica at Naval Ordnance Test Station (NOTS), China Lake, California. Appendix C contains the text of their report on this work.

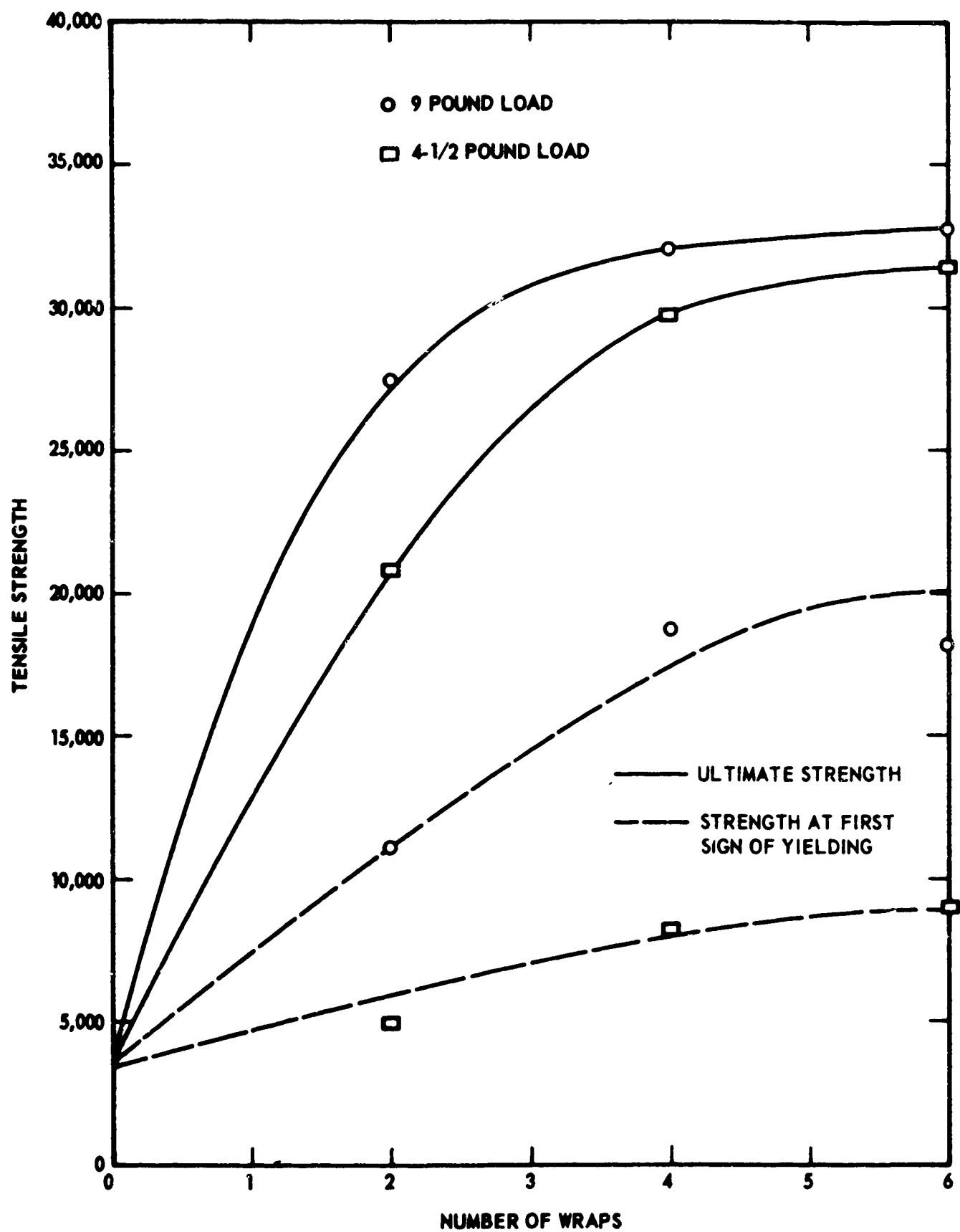


Figure 56. Apparent Tensile Strength of Fused Silica Cylinders Wrapped with Fiberglass Yarn Using Constant Tension Device.

VIII. BIBLIOGRAPHY

1. Sosman, R. B., The Properties of Silica, American Chemical Society Monograph Series, The Chemical Catalog Co., Inc., New York, 1st ed. 1927.
2. Fleming, J. D., Johnson, J. W., Boland, Paul, Bomar, S. H., and Colcord, A. R., "Materials for High Temperature Nuclear Applications," Summary Report No. 1, Georgia Tech Project No. B-153, USAEC Contract No. AT-(40-1)-2483 (June 1962).
3. Walton, J. D., "Fused Silica Ceramics," Part I, Ceramic Age, May 1961.
4. Fleming, J. D., and Johnson, J. W., "Fused Silica For Reactor Applications," Progress Report No. 1, Georgia Tech Project No. B-153, USAEC Contract No. AT-(40-1)-2483 (15 August 1959).
5. Poulos, N. E., Elkins, S. R., Murphy, C. A., and Walton, J. D., "High Temperature Ceramic Structures," Final Summary Report, Georgia Tech Project No. A-212, BuWeaps Contract No. NOrd - 15701, 31 October 1962.
6. Fleming, J. D., Johnson, J. W., Boland, Paul, and Bomar, S. H. "Materials for High Temperature Nuclear Applications," Summary Report No. 2, Georgia Tech Project No. B-153, USAEC Contract No. AT-(40-1)-2483 (June 1963).
7. Poulos, N. E., Walton, J. D., Teague, W. T., and Bowen, M. D., "Development of Monolithic Ceramics and Heterogeneous Ceramic-Metal Bodies for Aerodynamic Applications at High Velocities and Temperatures," Final Report, Georgia Tech Project No. A-330, U. S. Army Ordnance ABMA Contract No. DA-01-009-ORD-548 31 March 1959.
8. Mason, C. R., Walton, J. D., Bowen, M. D., and Teague, W. T., "Investigation of High Temperature Resistant Materials," Summary Report No. 3, Georgia Tech Project No. A-212, BuOrd Contract No. NOrd-15701, 31 October 1959.
9. Fleming, J. D., Johnson, J. W., Boland, Paul, and Bomar, S. H., "Materials for High Temperature Nuclear Engineering Applications," Quarterly Report No. 4, Georgia Tech Project No. B-153, USAEC Contract No. AT-(40-1)-2483, 1 April 1963.
10. Fleming, J. D., Johnson, J. W., Boland, Paul, and Bomar, S. H., "Materials for High Temperature Nuclear Engineering Applications," Quarterly Report No. 5, Georgia Tech Project No. B-153, USAEC Contract No. AT-(40-1)-2483, 1 October 1963.
11. Walton, J. D., and Harris, J. N., "Ceramics for High Temperature Electrical Applications," AIEE CP #5058 National Conference on the Application of Electrical Insulation, December 8-11, 1959, Washington, D. C. pp. 187-193.

BIBLIOGRAPHY (Continued)

12. Von Hippel, A., and Maurer, R. J., "Electrical Breakdown of Glasses and Crystals as a Function of Temperature," *Physical Review*, Vol. 59, pp. 820, (1941).
13. Fleming, J. D., and Johnson, J. W., "Materials for High Temperature Nuclear Engineering Applications," Progress Report No. 3, Georgia Tech Project No. B-153, USAEC Contract No. AT-(40-1)-2483, 15 August 1961.
14. Walton, J. D., Poulos, N. E., Murphy, C. A., Harris, J. N., and Wolf, J. M., "Design and Development of an E-M Window for Air Lift Reentry Vehicles," Interim Engineering Report No. 1, Georgia Tech Project No. A-694, Air Force Contract No. AF 33(657)-11504, 31 July 1963.
15. Hallse, R. L., and Walton, J. D., "Slip-Cast Fused Silica Radomes," Presented at the OSU - ASD Symposium on Electromagnetic Windows, Columbus, Ohio, June 4-6, 1962.
16. Walton, J. D., and Bowen, M. D., "The Evaluation of Ceramic Materials Under Thermal Shock Conditions," Mechanical Properties of Engineering Ceramics, Interscience Publishers, New York, 1963 pp. 149-171.
17. Poulos, N. E., Elkins, S. R., and Walton, J. D., "Development of Monolithic Ceramics and Heterogeneous Ceramic-Metal Bodies for Aerodynamic Applications at High Velocities and Temperatures," Final Report, Georgia Tech Project No. A-512, NASA Contract No. NASA8-8, 31 October 1960.
18. Mason, C. R., Murphy, C. A., Sales, A. T., and Walton, J. D., "Investigation of High Temperature Resistant Materials," Summary Report No. 4, Georgia Tech Project No. A-212, BuOrd Contract No. NOrd - 15701, 31 October 1960.
19. Poulos, N. E., Murphy, C. A., and Walton, J. D., "Ceramic Systems for Missile Structural Applications," Quarterly Report No. 2, Georgia Tech Project No. A-651, BuWeaps Contract No. NOW 63-0143-d, 30 April 1963.
20. "Characterization and Extension of Simulation Capabilities of the LAS High Temperature Arc Facility," Technical Documentary Report No. ASD- TDR - 62-461, August 1962.
21. Adams, Mac C., Powers, W. E., and Georgiev, S., "An Experimental and Theoretical Study of Quartz Ablation at the Stagnation Point," Research Report 57 Avco Everett Research Laboratory, June 1959.
22. Rosenberry, J. W., Smith, H. E., and Wurst, J. C., "Evaluation of Materials Systems for Use in Extreme Thermal Environments Utilizing an Arc Plasma-Jet," WADD Technical Report 60-926, March 1961.
23. Lucas, W. R., and Houston, M. E., "Planning a Reentry and Recovery Test Program," Astronautics, March 1959, p. 30-31, 88.

BIBLIOGRAPHY (Concluded)

24. Walton, J. D., Poulos, N. E., Murphy, C. A., Harris, J. N., and Wolf, J. M., "Design and Development of an E-M Window for Air Lift Re-entry Vehicles," Interim Engineering Report No. 3, Georgia Tech Project No. A-694, Air Force Contract No. AF-33(657)-11504, 31 January 1964.
25. Bortz, S. A., and Lund, H. H., "The Brittle Ring Test," Mechanical Properties of Engineering Ceramics, Interscience Publishers, Inc., New York, 1961.

IX. APPENDIXES

- Appendix A. Effective Emittance Calculation.
- Appendix B. Thermal Shock Considerations
- Appendix C. General Dynamics/Pomona
Technical Memorandum No. 6-223-571
on Results of Testing Slip-Cast
Fused Silica Radomes Under
Rain Environment.

APPENDIX A

EFFECTIVE EMITTANCE CALCULATION

Nomenclature

ϵ = Effective Emittance

R_N = Total Normal Radiation

σ = Stefan-Boltzmann Factor

T_O = Brightness Temperature

T_r = Radiation Temperature

T_s = True Temperature

The effective emittance of a material can be determined from two temperature measurements, total radiation temperature and optical temperature. For the preliminary data presented herein the assumption is made that the spectral emittance at 6500 A° is equal to the effective emittance. This assumption simplifies the analysis and provides for rapid numerical solutions.

Consider a surface at some true temperature, T_s with a radiation temperature, T_r , and an optical temperature, T_O . The measured radiation temperature, T_r , suggests the surface to be "black" in nature and having a unit area radiant flux of,

$$R_N = \sigma T_r^4 \quad (1)$$

However, if the surface is not "black" the radiant flux will be,

$$R_N = \epsilon \sigma T_s^4 \quad (2)$$

From equations (1) and (2),

$$\sigma T_r^4 = \epsilon \sigma T_s^4$$

or,

$$\epsilon = \left[\frac{T_r}{T_s} \right]^4 \quad (3)$$

The true temperature, T_s , is tabulated as a function of optical temperature, T_o , for 49 effective spectral emissivities in a National Bureau of Standards Monograph.*

Thus (3) can be written as,

$$\epsilon = \left[\frac{T_r}{T_s(T_o, \epsilon)} \right]^4 \quad (4)$$

Solutions are obtained by "trial and error" and are accomplished by assuming an effective emittance, determining the true temperature, T_s , associated with this particular emittance and optical temperature, T_o , and evaluating the expression until equality is reached between the right and left hand portions of equation (4).

*Poland, D. E., Green, J. W., and Margrave, J. L., "Corrected Optical Pyrometer Readings," U. S. Department of Commerce, National Bureau of Standards, NBS Monograph 30, April 21, 1961.

APPENDIX B

THERMAL SHOCK CONSIDERATIONS

It is not always appreciated that the thermal shock resistance of a material is not only dependent upon the physical and mechanical properties of the material but also upon the severity of the thermal shock environment. Further, the severity of the environment is not necessarily associated with temperature, but rather with the heat transfer rate to the material. This relationship can be illustrated by considering air and water, both at 200° F. It is easy to imagine that the heat transfer rate is much higher in the water than in the air. This difference would be evidenced by one if he put his hand into each environment.

It is often desirable to compare two or three materials as to their relative thermal shock resistance. To do this it is not uncommon to use the expression

$$M = \frac{K\delta}{E\alpha} \quad (1)$$

where

M = merit index

K = thermal conductivity

δ = tensile strength

E = elastic modulus

α = coefficient of thermal expansion

What is overlooked in using this expression is that this relationship holds only for low heat transfer rates, or a very mild thermal shock environment.

Manson 1/ and Kingery 2/ have developed expressions which take into account the thermal shock environment. These expressions relate the maximum temperature from which a material can be quenched (to room temperature) to the severity of the quench. The term ah has been used to denote this severity, where:

$a = 1/2$ the thickness of the plate

$h =$ heat transfer coefficient

If the term $T_{O \text{ max}}$ is the maximum temperature from which the material can be quenched, then

$$T_{O \text{ max}} \propto \frac{K\delta}{E\alpha} \quad (2)$$

but for severe conditions (high values of ah)

$$T_{O \text{ max}} \propto \frac{\delta}{E\alpha}$$

These expressions emphasize the fact that a material may have satisfactory thermal shock resistance under mild thermal shock conditions by possessing a high thermal conductivity. However, it will receive essentially no benefit from this property under very severe conditions. Manson determined the maximum temperature from which Al_2O_3 and BeO could be quenched as a function of the thermal shock environment. The data are shown in Figure 1. According

1/Manson, S. S., "Behavior of Materials Under Conditions of Thermal Stress," NACA Report 1170, Lewis Flight Propulsion Laboratory, Cleveland, Ohio, 34 pages (1954); "Thermal Stress in Design," Part 1, Machine Design 30 (12) 114-120 June 12, 1958; "Thermal Stress in Design," Part 2, Machine Design 30 (13) 19-103, June 26, 1958.

2/Kingery, W. D., "Factors Affecting Thermal Stress Resistance of Ceramic Materials," Jour. Amer. Ceramic Soc. Vol. 38, No. 1, 3-15 (1955).

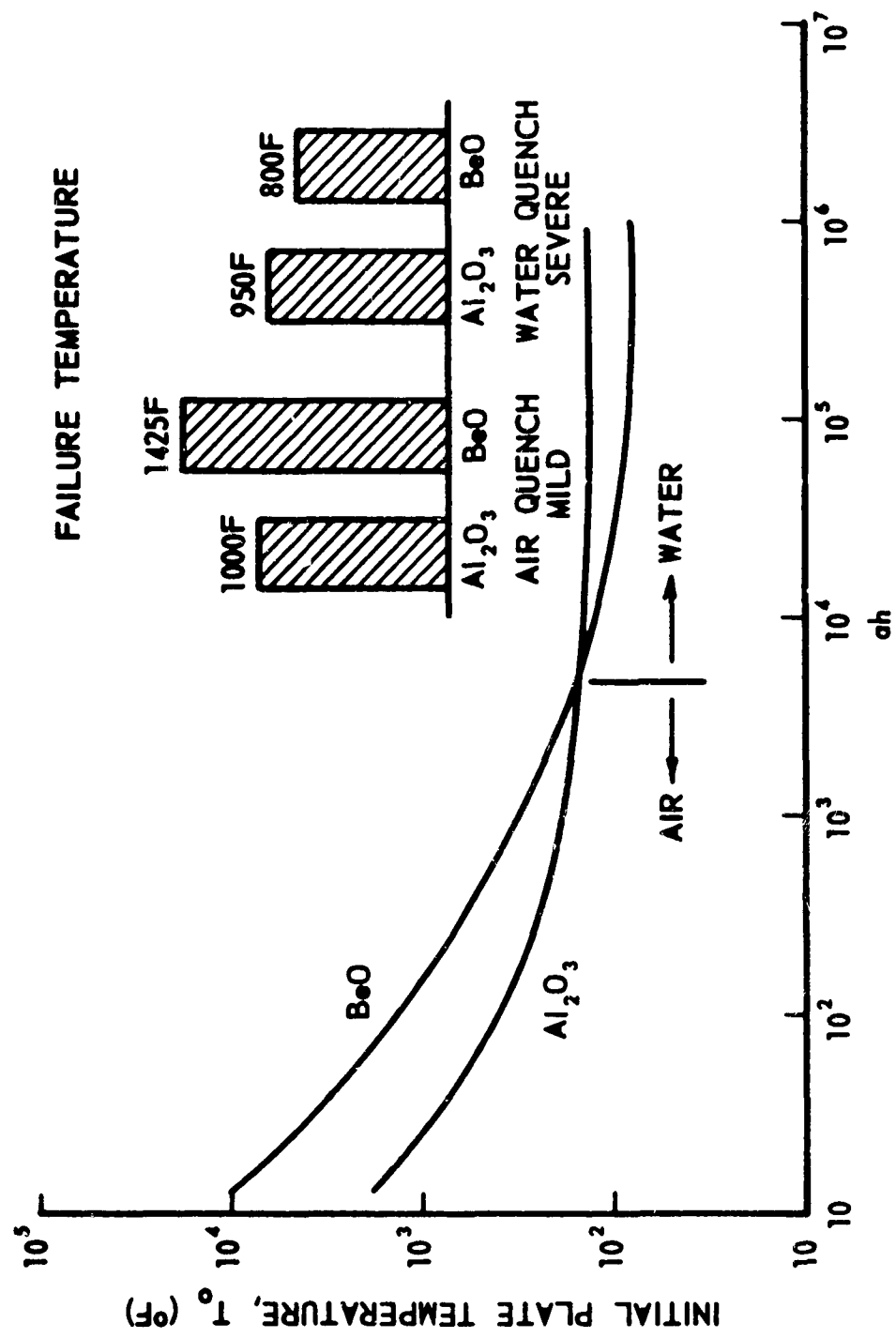


Figure 1. Relative Thermal Shock Resistance of Al_2O_3 and BeO as Function of Thermal Shock Environment (ah).

to these data BeO should be superior to Al_2O_3 in a mild thermal shock environment while the reverse should be true under more severe thermal shock conditions. Also in Figure 1 are experimental data showing the maximum temperature from which BeO and Al_2O_3 withstood quenching into room temperature air and water. The air represented a mild thermal shock environment and water a severe environment. The predicted reversal in the order of merit of these materials was observed experimentally.

The thermal shock resistance of radome materials is stressed here because of the importance, from the standpoint of material selection, of specifying the thermal environment in which the material is to be used. So often it has been the practice to give a single number, or merit index, to indicate the thermal shock resistance of materials using formula (1). However, as pointed out above, such a number is of value only under conditions of rather mild thermal shock; and, under conditions of severe thermal shock, such as re-entry these numbers may not only provide meaningless data, but may be seriously misleading.

This situation was observed when a number of candidate radome materials were evaluated with respect to their thermal shock resistance. The physical, mechanical and thermal properties of the materials shown in Table I were used to calculate the maximum temperature from which each material could be quenched. These data are shown plotted as a function of the thermal shock environment (Δh) in Figure 2. It can be seen that the thermal shock resistance order of merit among these materials is almost entirely dependent upon the severity of the thermal shock environment. For example, BeO should have the highest thermal shock resistance under mild thermal shock conditions, but will be next to the poorest under severe conditions. It is interesting to note that

TABLE I
MECHANICAL AND THERMAL PROPERTIES OF CERAMIC RADOME MATERIALS

| | Thermal Conductivity (btu/hr-ft-°F) | Transverse Strength (psi x 10 ³) | Young's Modulus (psi x 10 ⁶) | Thermal Expansion ($\alpha \times 10^{-6}/^{\circ}\text{F}$) | Specific Gravity (gm/cc) | Melting Temperature (°F) |
|------------------------------|---|--|---|---|--------------------------------|--------------------------------|
| Aluminum Oxide | 20 | 47 | 52.4 | 4.35 | 3.97 | 3720 |
| Beryllium Oxide | 125 | 35 | 42.8 | 5.1 | 3.0 | 4660 |
| Boron Nitride | 18 | 15.9 | 12.4 | 4.2 | 2.1 | 4950 |
| Forsterite | 1.94 | 20 | | 5.4 | 2.90 | 3430 |
| Magnesium Oxide | 27 | 23 | 40.0 | 7.7 | 3.57 | 5072 |
| Pyroceram 9606 | 2.1 | 20 | 17.3 | 2.7 | 2.6 | 2280 Softens |
| Slip-Cast Fused Silica | 0.4 | 4.5 | 3.8 | 0.3 | 1.90 | 3038 |
| Spinel | 6.8 | 24.1 | 31.7 | 3.6 | 3.7 | 3860 |
| Steatite | 2.5 | 15 | 14.5 | 4.6 | 2.65 | 3430 |
| Zircon | 3.15 | 22 | 24 | 2.7 | 3.68 | 2800 Softens |

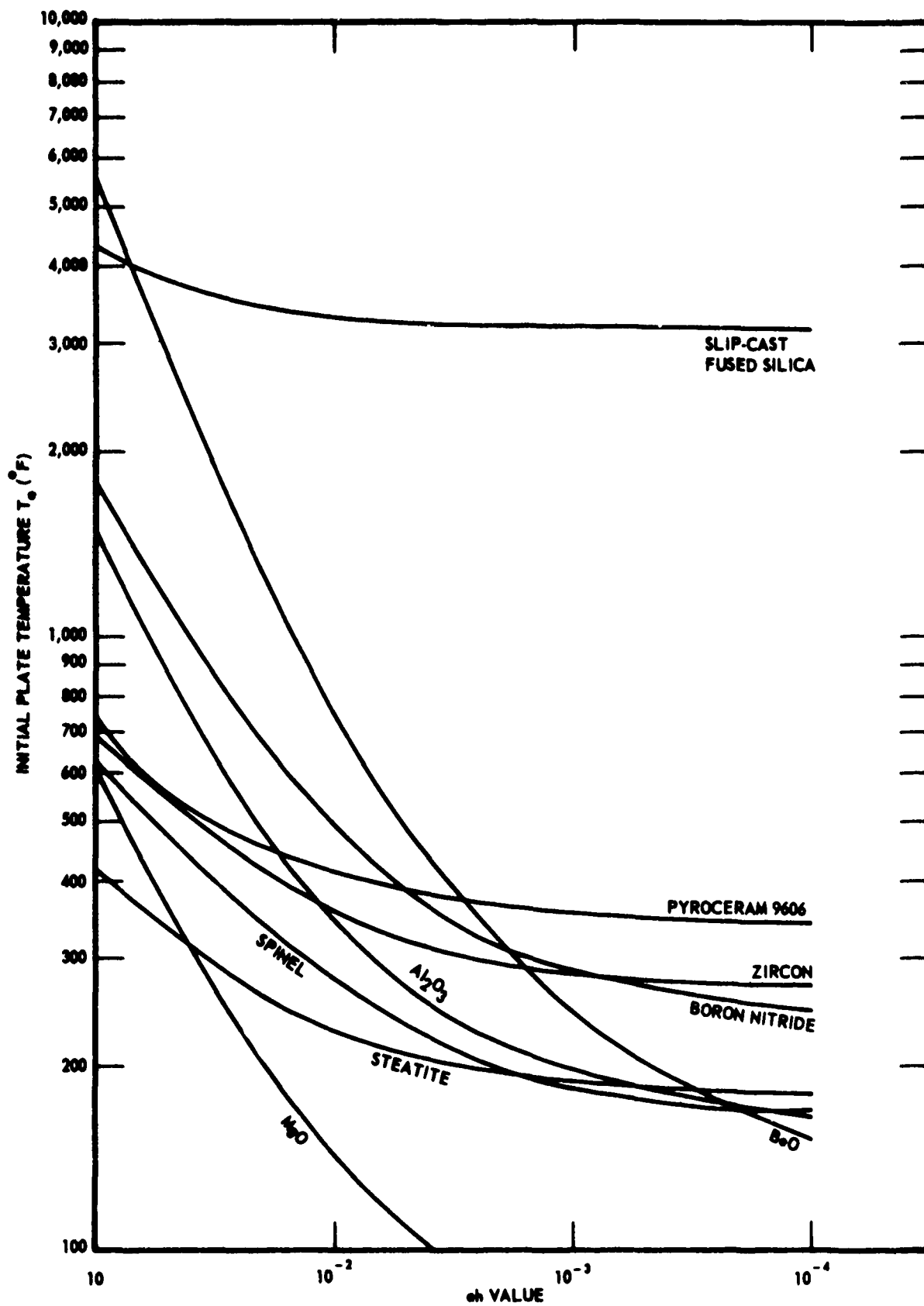


Figure 2. Relative Thermal Shock Resistance of Candidate Reentry Radome Materials as a Function of Thermal Shock Environment (ah).

the maximum quench temperature for slip-cast fused silica is above its melting point for all conditions of thermal shock. Therefore, it should not be possible to thermal shock slip-cast fused silica under any conditions.

The αh values associated with re-entry is not known. However, Kingery 2/ has reported that the αh value provided by water quench is of the order of 10^3 to 10^4 . From the high heat flux associated with re-entry it might be expected that this environment would provide an αh value in the same range as water quench.

From the data thus presented it can be seen that the very low coefficient of thermal expansion of fused silica more than offsets its low strength and low thermal conductivity in providing excellent thermal shock resistance under all thermal shock environments. This was the primary factor in selecting slip-cast fused silica for a re-entry radome.

APPENDIX C

General Dynamics/Pomona
Technical Memorandum No. 6-223-571
on Results of Testing Slip-Cast
Fused Silica Radomes Under
Rain Environment

The following is an excerpt from a report prepared by General Dynamics/
Pomona, and only the rocket sled test results of slip-cast fused silica
are reprinted here.

INTRODUCTION

Slip cast fused silica (SCFS) is being considered for missile radome applications. For this reason rain erosion tests were conducted at the Naval Ordnance Test Station (NOTS), China Lake to determine the capability of the material to withstand rain environment on a missile in flight at Mach 3. The test conditions were (1) Rain drop size of 2.0 MM, (2) Rain rate of 2-in/hr., (3) Max. sled velocity of 3,000 Ft/sec or Mach 2.7.

HISTORY

General Dynamics/Pomona (GD/P) has been actively engaged in the development of SCFS as a radome material since September of 1961. During this time interval, GD/P has manufactured a large number of SCFS radomes of various sizes and shapes from 5.5 inch diameter base and 6 inches long to 13.5 inch diameter base and 30 inches long.

In order to assure that SCFS radomes have all weather flight capability, rain erosion testing was funded under Contract No. NOW 62-1087 #35 TOC.

PURPOSE

Rain erosion resistance of a material is an acute problem in the design of an all weather supersonic missile. There are a number of factors that influence erosion damage. They are:

(1) Type of material, (2) Surface finish, (3) Shape of radome, (4) Missile velocity, (5) Drop size, (6) Rain rate and (7) Length of rain field.

The objectives of this series of tests were (1) to compare the rain erosion data of SCFS with that of other known radome materials, (2) to determine the effectiveness of a glazed surface as a protective coating on SCFS and (3) to compare the effectiveness of a pointed nose vs. a rounded nose radome.

TEST INSTALLATION

There are several methods of testing radome materials for rain erosion. Among these are (1) whirling arms, (2) 20-mm ballistics, (3) actual flights and (4) single drop.

The most realistic and best controlled method however, is a high speed rocket sled test.

The Supersonic Naval Ordnance Research Track (SNORT) at NOTS runs in a northerly direction for 21,500 feet. The first 2,000 feet is used for the sled acceleration phase; next 2,500 feet is exposed to simulated rain fall while the remaining 17,000 feet are required to slow the vehicle to a stop. Plastic water bags are taped on the last 1,500 feet of the track to provide the necessary energy exchange to stop the sled completely. The curvature of the earth is taken into consideration by raising the track at one

and by several inches. Earth's rotational effect is negligible and therefore omitted.

Artificial rain is created by sprinkler heads located five feet above and on the west side of the track. Sampling of the rain field area showed that the drop distribution was the same over the samples area and corresponded to that occurring in a two inch per hour of natural rainfall (See Figure 1). Since the track area is exposed to wind, tests are cancelled if there is a crosswind of five knots or more. Sandia Corporation has concluded that the average drop size in an average rain storm is 1.5 millimeters with a rate of fall of half inch per hour (227 drops per cubic foot). The artificial rainfall for these tests was 2.0 millimeters with a rate of 2 inches per hour.

The sled mounts two radomes and consists of streamlined fairings back of the radomes. This provides aerodynamic stability and mounts a telemetering pack and stub antenna. The sled is powered by two Cajun Rockets, each delivering 8,000 pounds of thrust. The test specimens are mounted at a zero angle of attack as shown in Figure 2.

A dummy run was made on March 5, 1963 to obtain velocity curves for this series of tests (see Figure 3).

TEST SAMPLES

Of the 20 radomes tested thru the rain field, 18 were of the Mauler configuration (13 inches long and 5.5 inch diameter base). The other two were fiberglass hemispheres of about 6 inch diameter having a base of 5.5 inches.

The test runs included rounded and pointed nose SCFS radomes having (1) external surface as cast, (2) external tip region glazed and (3) external surface glazed. The glazed radomes were glazed at Georgia Tech, by means of an Arc Plasma Jet.

PRE-SLED TEST

On January 31, 1963 a rain erosion sled built by NADC was destroyed during a dummy dry run with steel radomes. The object of the firing was to (1) obtain a velocity curve, (2) obtain vibration data in all three planes and (3) test telemetry, arresting system, etc. The sled was held at the breech for one second after ignition and then released. It is surmised that the arresting parachute deployed prematurely at 1,200 feet due to the high acceleration of the sled. The opened parachute produced forces and/or vibrations severe enough to pull the rivets out of the telemetry cover at 2,900 feet. One of the two steel radomes was found at 4,000 feet while the other was located at 4,500 feet. Both had sheared off. Water bags stopped the sled at 20,850 feet. Peak velocity of sled was M 2.3. The vibration in the roll and yaw axis was 80 to 100 g's. The pitch axis recorded over 100 g's. Due to the sled failure it was decided to perform vibration and static tests on three SCFS radomes.

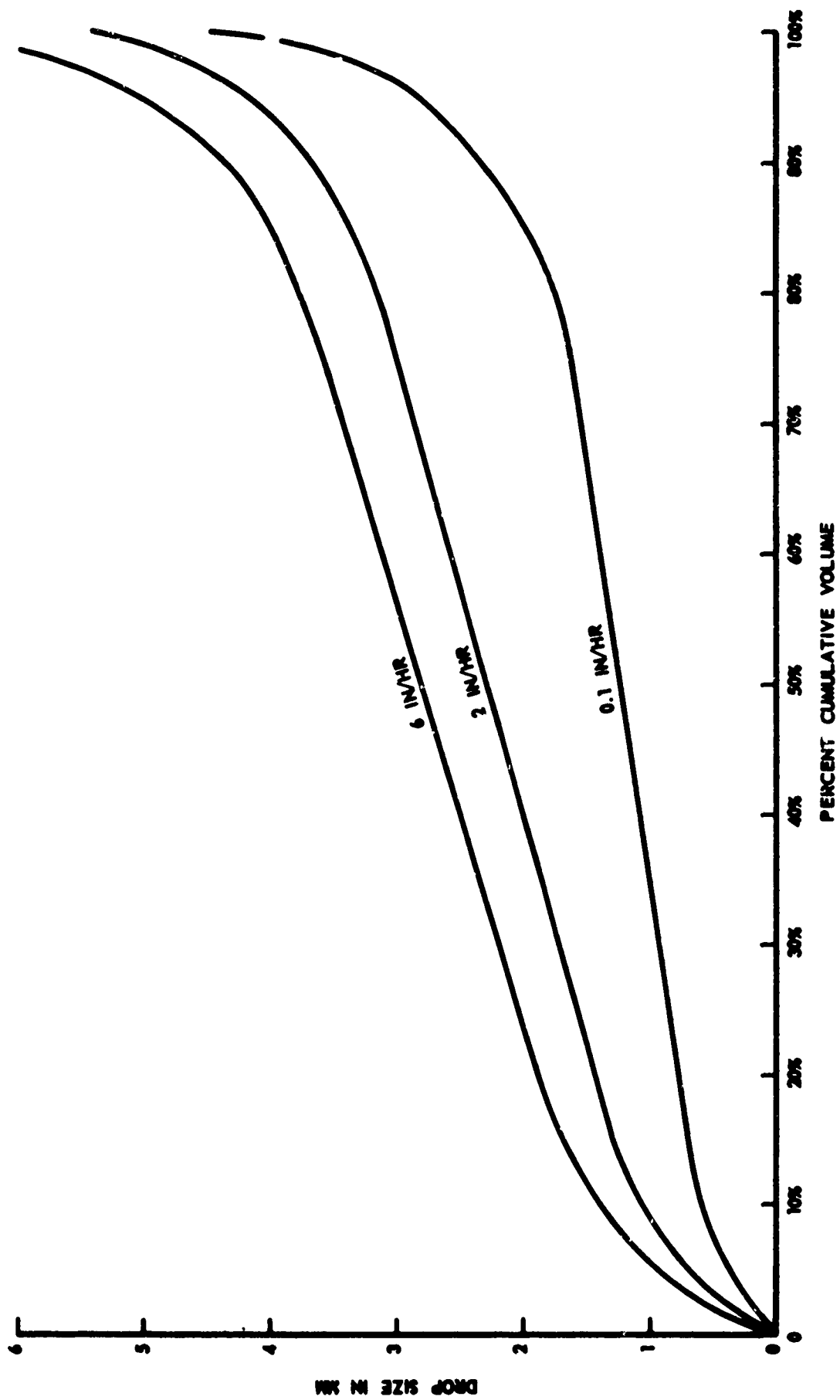


Figure 1. Natural Rainfall Distribution.

end by several inches. Earth's rotational effect is negligible and therefore omitted.

Artificial rain is created by sprinkler heads located five feet above and on the west side of the track. Sampling of the rain field area showed that the drop distribution was the same over the samples area and corresponded to that occurring in a two inch per hour of natural rainfall (See Figure 1). Since the track area is exposed to wind, tests are cancelled if there is a crosswind of five knots or more. Sandia Corporation has concluded that the average drop size in an average rain storm is 1.5 millimeters with a rate of fall of half inch per hour (227 drops per cubic foot). The artificial rainfall for these tests was 2.0 millimeters with a rate of 2 inches per hour.

The sled mounts two radomes and consists of streamlined fairings back of the radomes. This provides aerodynamic stability and mounts a telemetering pack and stub antenna. The sled is powered by two Cajun Rockets, each delivering 8,000 pounds of thrust. The test specimens are mounted at a zero angle of attack as shown in Figure 2.

A dummy run was made on March 5, 1963 to obtain velocity curves for this series of tests (see Figure 3).

TEST SAMPLES

Of the 20 radomes tested thru the rain field, 18 were of the Mauler configuration (13 inches long and 5.5 inch diameter base). The other two were fiberglass hemispheres of about 6 inch diameter having a base of 5.5 inches.

The test runs included rounded and pointed nose SCFS radomes having (1) external surface as cast, (2) external tip region glazed and (3) external surface glazed. The glazed radomes were glazed at Georgia Tech, by means of an Arc Plasma Jet.

PRE-SLED TEST

On January 31, 1963 a rain erosion sled built by NADC was destroyed during a dummy dry run with steel radomes. The object of the firing was to (1) obtain a velocity curve, (2) obtain vibration data in all three planes and (3) test telemetry, arresting system, etc. The sled was held at the breech for one second after ignition and then released. It is surmised that the arresting parachute deployed prematurely at 1,200 feet due to the high acceleration of the sled. The opened parachute produced forces and/or vibrations severe enough to pull the rivets out of the telemetry cover at 2,900 feet. One of the two steel radomes was found at 4,000 feet while the other was located at 4,500 feet. Both had sheared off. Water bags stopped the sled at 20,850 feet. Peak velocity of sled was M 2.3. The vibration in the roll and yaw axis was 80 to 100 g's. The pitch axis recorded over 100 g's. Due to the sled failure it was decided to perform vibration and static tests on three SCFS radomes.

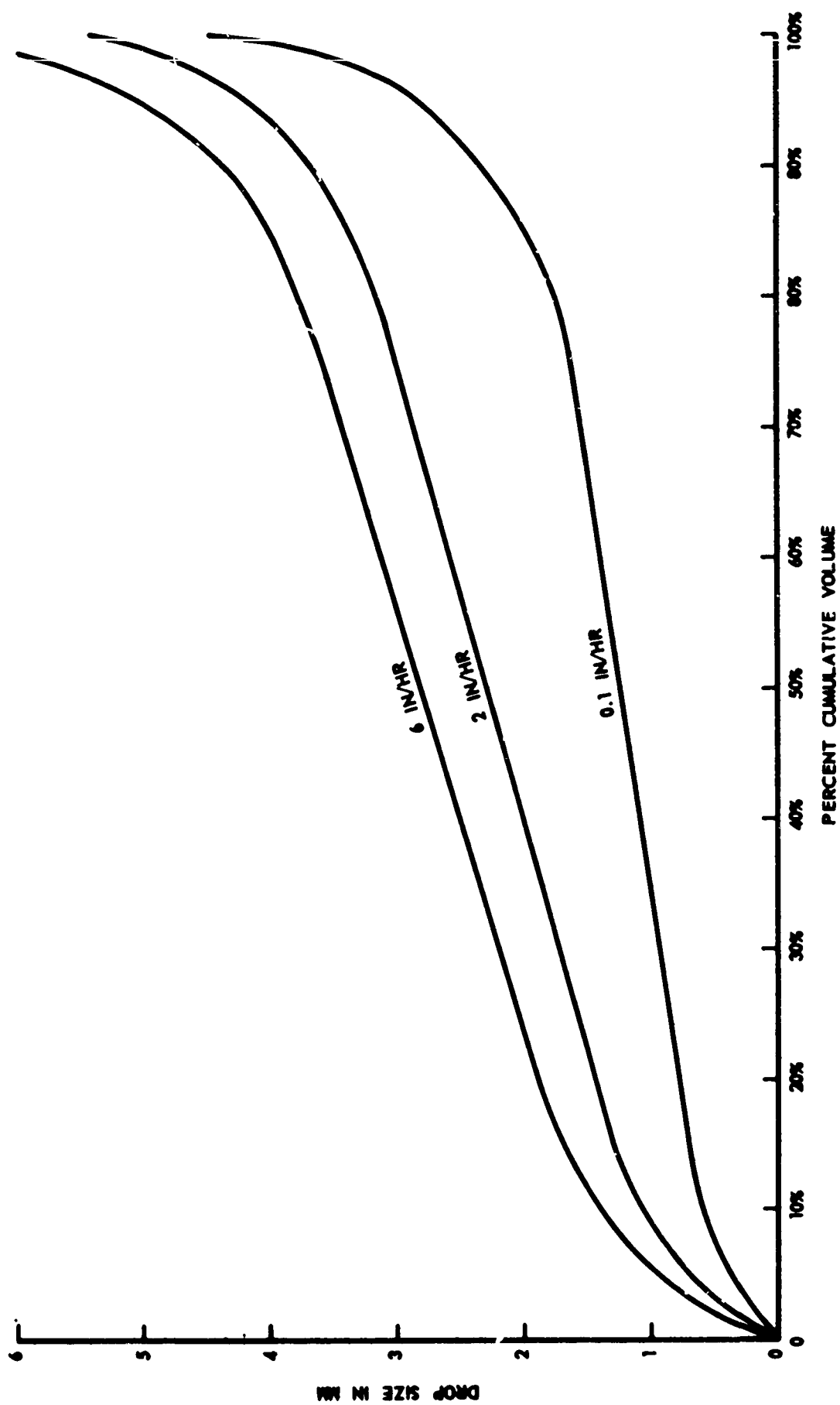


Figure 1. Natural Rainfall Distribution.

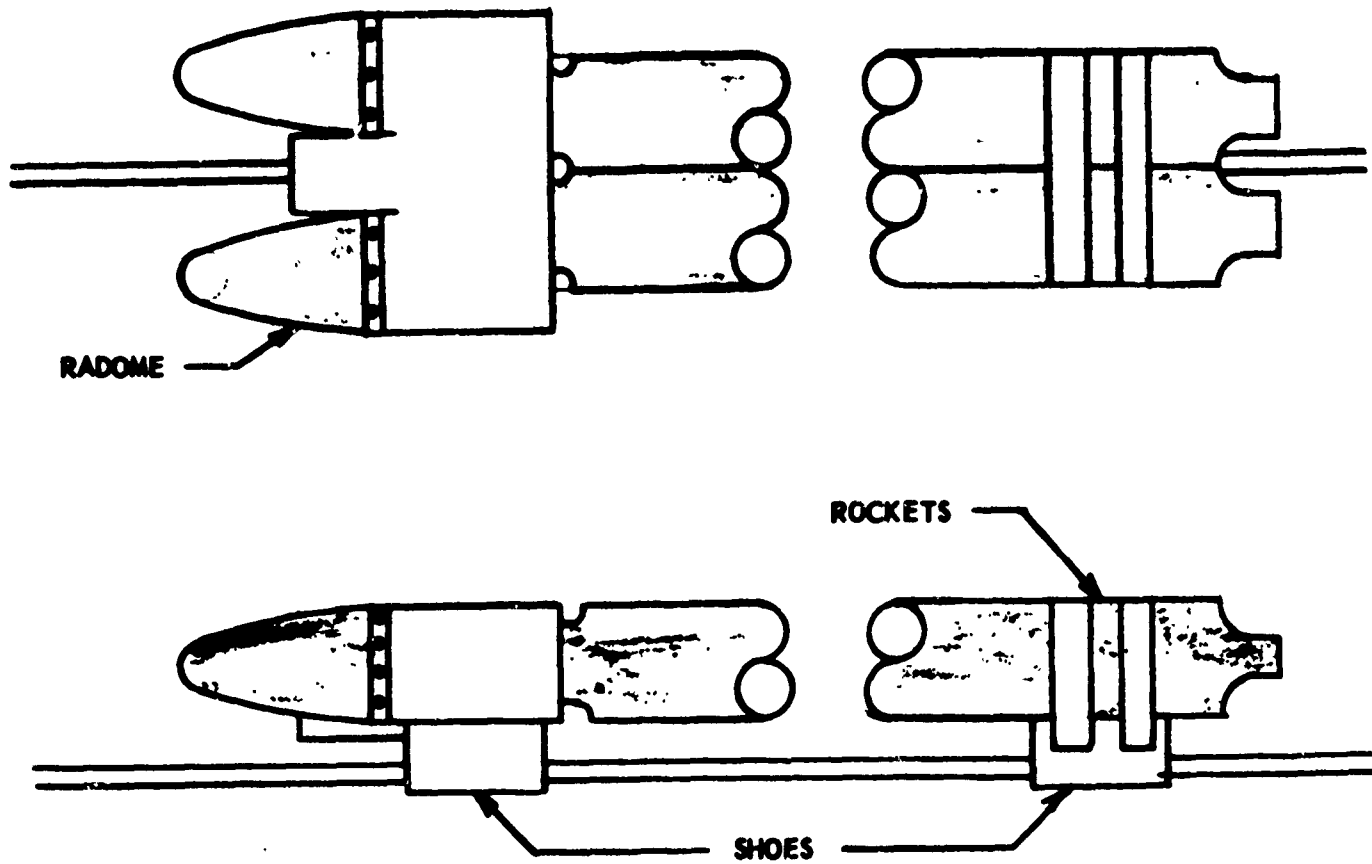


Figure 2.

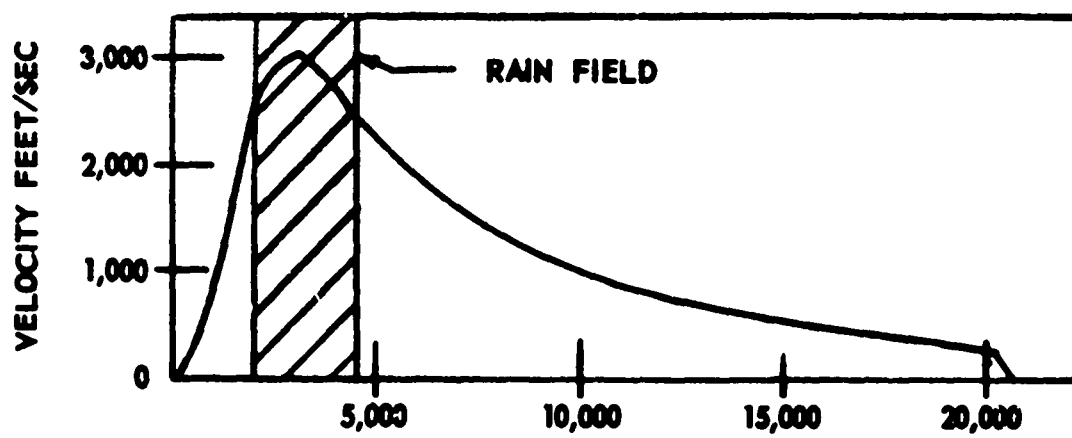


Figure 3.

The three radomes were vibrated in the three major planes at 60 g's from 90 - 2,000 cycles. There was no visual degradation. Next, the items were subjected to a static cantilevered pull test. The radome assemblies did not fail until after exceeding 220 per cent, 160 per cent and 219 per cent of maximum Mauler Flight loads.

TEST RESULTS OF SCFS

It must be noted that length of erosion was measured along the longitudinal axis of the radome from the original nose tip to the eroded nose tip.

Method of attaching radomes to ring is shown in Figure 4.

Run 5 - 3/26/63

- (EAST) The test specimen was a rounded nose (1.12 inch diameter) radome in the "as cast" condition with a 0.350 inch wall. The thickness through the nose was 1.31 inches before run. Approximately 0.40 inch of material was removed from the tip by the rain drops.
- (WEST) This rounded nose with a 0.350 inch wall had been "plasma glazed". Thickness through nose was 1.87 inches before a test. The tip eroded 0.45 inch.

Run 6 - 3/26/63

- (EAST) Next, a pointed nose radome of 0.350 inch wall and "Plasma Glazed" was run. The item failed in the rain field. Small pieces were found at a distance of 200 feet (station 2,200) in the rain field with larger ones at 575 feet (station 2,575).
- (WEST) A pointed--"as cast"--.350 inch wall radome with a nose thickness of 1.67 inches was tested. Tip was eroded by 0.60 inch, area aft of tip showed signs of erosion for 4.5 inches.

The radome was returned to GD/P where 0.90 inch of the tip was removed (0.70 inch diameter) and a steel cone tip was bonded in place.

Run 8 - 4/11/63

- (EAST) The reworked radome from Run #6 with the steel tip was re-run. The only visual damage was a very small increase in erosion aft of steel tip.
- (WEST) A pointed radome that had its forward end plasma glazed was run. This item was 0.350 inch thick and had a 1.67 inch nose. There was no significant erosion on the test piece. Tip had eroded 0.25 inches with a few pits from 3 to 6 inches aft.

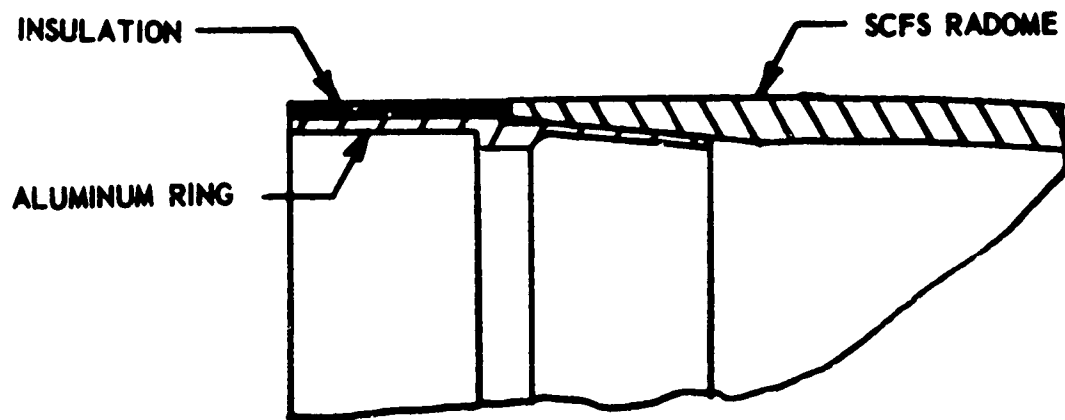


Figure 4. (SCFS).

Run 9 - 4/11/63

(WEST) The pointed - part glazed radome from Run #8, was retested. Erosion was increased by 0.20 inch for a total of 0.45 inch for the two runs.

SCFS CONCLUSION

Under the test environment, and at high incidence angles, SCFS undergoes an erosion process as evidenced by pits and roughened areas of material after exposure. Materials with higher hardness numbers behave quite differently. Their failure is due to inadequate impact resistant and could be indicated as a tensile failure beginning on inner surface.

On the rounded radomes, glazing did not appear to provide a protective coating (0.45 inch vs. 0.40 inch) while on the pointed radomes glazing seemed to be of value (0.25 inch vs. 0.60 inch).

Pointed radomes faired better than rounded noses in relationship to the volume of material eroded (Table I). The removal of a half inch of material on the rounded radomes in the nose area may be a serious degradation to the missile's electrical characteristics. As a solution, it is suggested that a spherical ceramic or steel cap be placed on the nose which would eliminate rain erosion of the rounded nose but still allow the radome to meet its electrical criteria.

TABLE I
VOLUME OF MATERIAL ERODED FROM
NOSE AREA OF SLIP CAST FUSED SILICA (SCFS) RADOMES

| <u>Radome Surface</u> | <u>Pointed</u> (in ³) | <u>Rounded</u> (in ³) |
|-----------------------|--------------------------------------|--------------------------------------|
| Glazed | 0.01 | 0.5 |
| Unglazed | 0.06 | 0.5 |

In summary it may be stated that:

- (1) A pointed SCFS radome will successfully pass rain erosion requirements
- (2) Glazing is an advantage on pointed SCFS radomes
- (3) Rounded SCFS radomes require a protective cap of ceramic or metal
- (4) A SCFS radome is able to experience the vibration, acceleration and acoustics of a missile launch and flight.

TABLE II
RAIN EROSION TEST RESULTS

| Run No. and Date | Radome Position | Radome Description | Results of Exposure | Radome Velocity (ft/sec) at | | |
|------------------------|--------------------|--|---|-----------------------------|---------|---------|
| | | | | Station | Station | Station |
| #5 3/26/63 | EAST | General Dynamics/ Pomona (GD/P) furnish- ed 0.350 wall of SCFS with a rounded nose in the "as cast" condition. | Approximately 0.40 inch of nose eroded. | 1,975 | 3,175 | 4,500 |
| | | | | 2,320 | 2,950 | 2,460 |
| #6 3/26/63 | WEST | GD/P 0.350 inch wall of SCFS with a rounded nose in the "Plasma Glazed" condition. | Approximately 0.45 inch of nose eroded. | | | |
| | | | | | | |
| #6 3/26/63 | EAST | GD/P 0.350 inch wall of SCFS with a pointed nose and "Plasma Glazed". | Item failed in 200 feet of rain. | 2,395 | 2,930 | 2,360 |
| | | | | | | |
| #6 3/26/63 | WEST | GD/P 0.350 inch wall of SCFS with a pointed nose and "as cast". | Tip eroded 0.60 inch with area AFT of tip showing some signs of erosion. | | | |
| | | | | | | |

(Continued)

TABLE II (Continued)
RAIN EROSION TEST RESULTS

| Run No. and Date | Radome Position | Radome Description | Results of Exposure | Radome Velocity (ft/sec) at | | |
|------------------------|--------------------|--|--|-----------------------------|---------|---------|
| | | | | Station | Station | Station |
| #8 4/11/63 | EAST | GD/P Radome of Run #6 with a cone shaped steel tip. | Only damage was a small increase aft of tip. | 1,975 | 3,175 | 4,500 |
| | WEST | GD/P 0.350 inch wall of SCFS with a pointed nose and front half "Plasma Glazed" | Tip eroded by 0.25 inch with a few other pits. | 2,480 | 2,930 | 2,310 |
| #9 4/11/63 | WEST | GD/P pointed part glazed from Run #8. | Erosion in tip was increased from 0.25 to 0.45 inch. | 2,440 | 2,880 | 2,110 |

Note: Station numbers are feet from the point of ignition of the rocket sled.

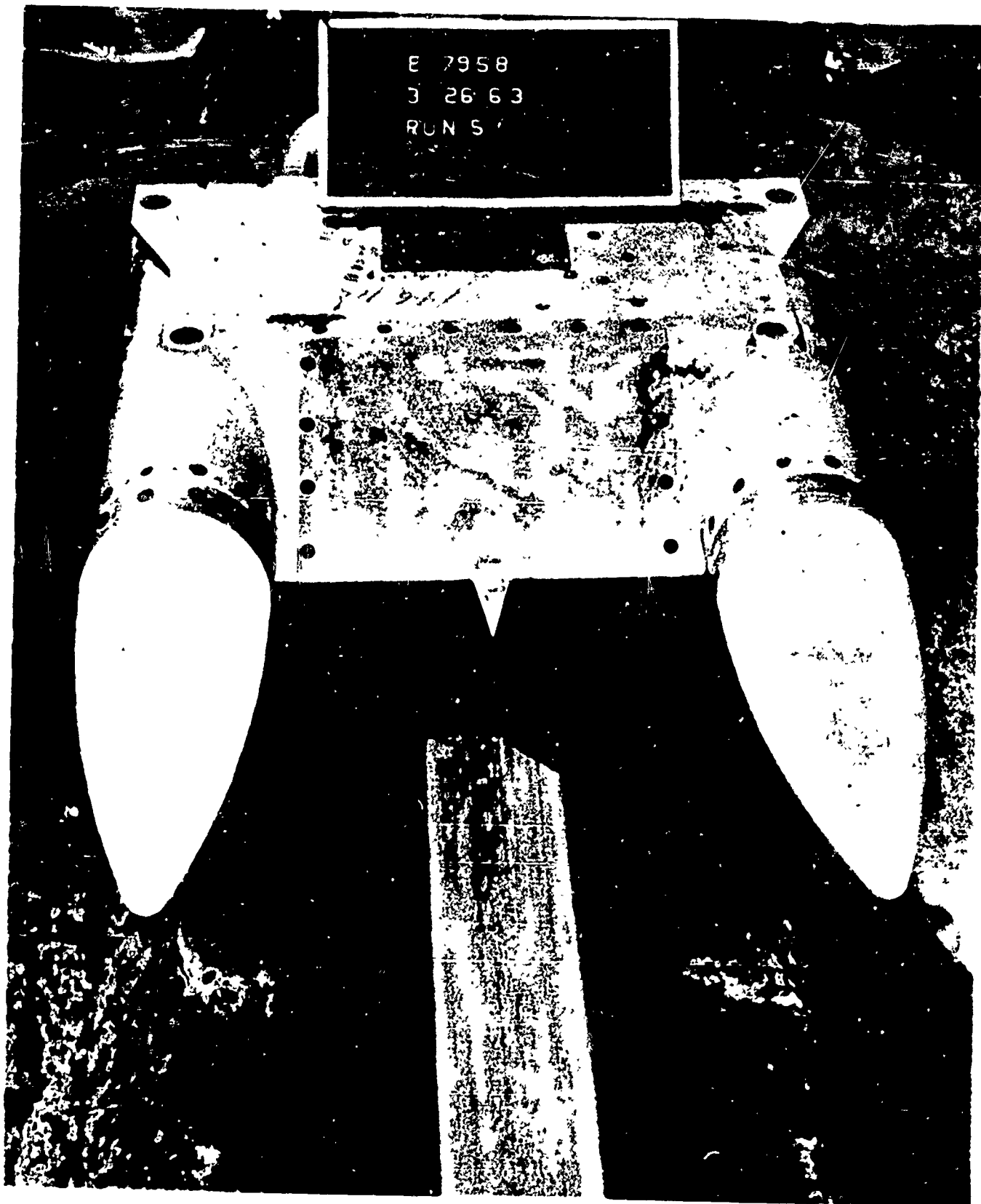


Figure 5. Blunt Glazed and Unglazed SCFS Domes Before Run #5.

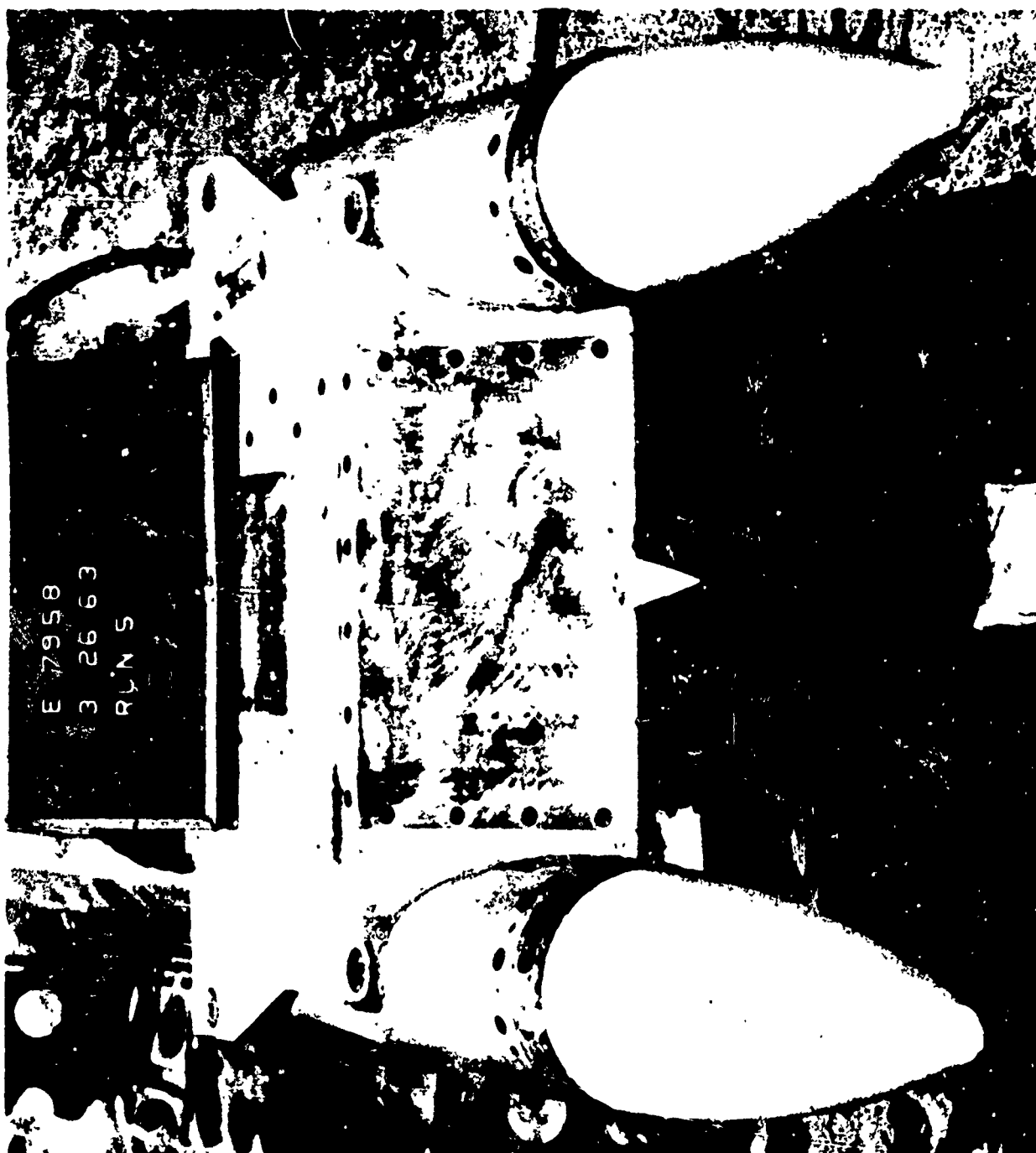


Figure 6. Blunt Domes After Run #5.

0054-S
263
50
79585218-5
26MAR63
3175X0
RD5
5
SAF ILM
5-1975

Figure 7. Synchroballistic Camera Shots of Run #5.

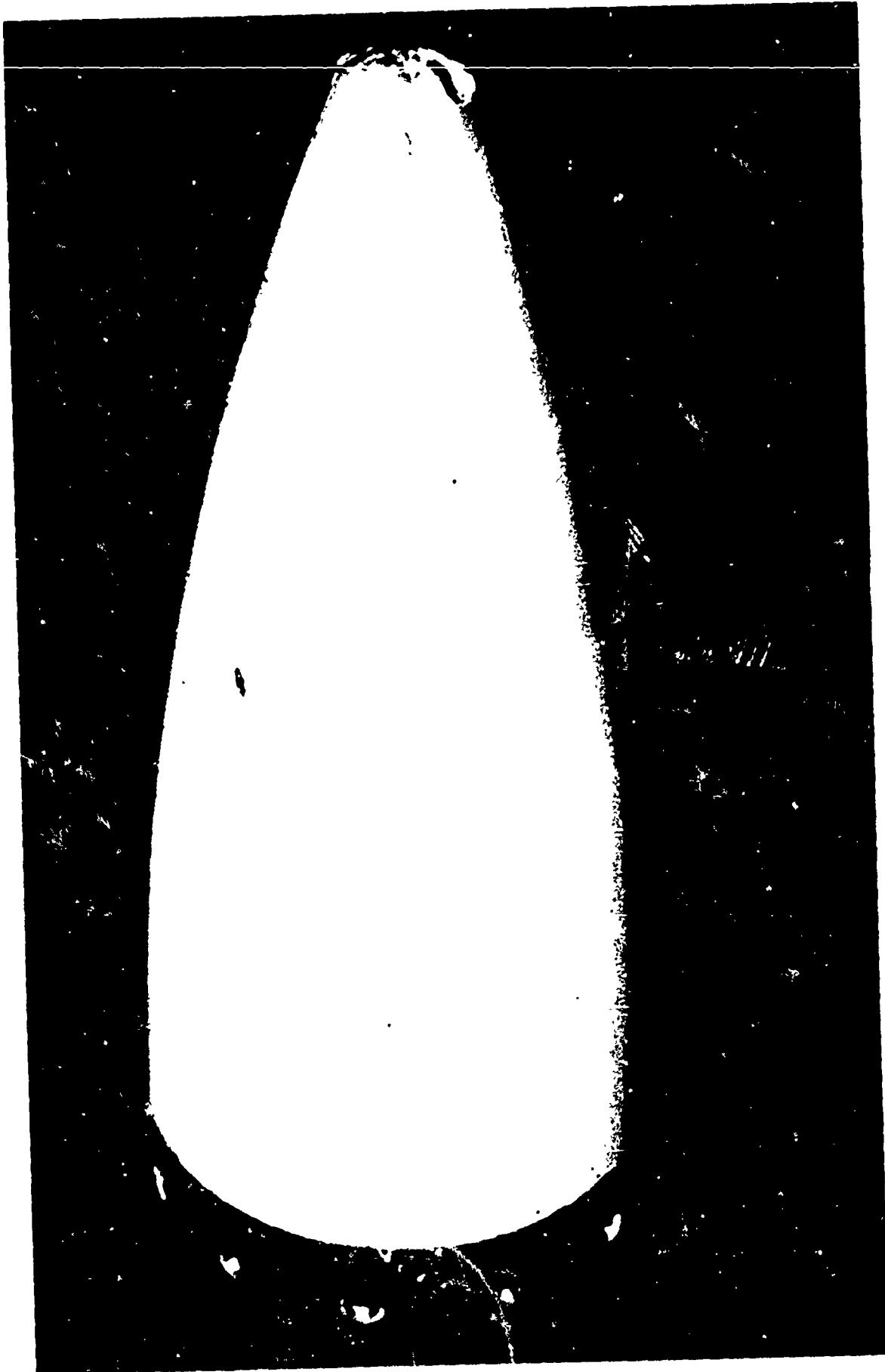


Figure 8. Glazed Dome After Run #5.



Figure 9. Closeup of Glazed Dome After Run #5.

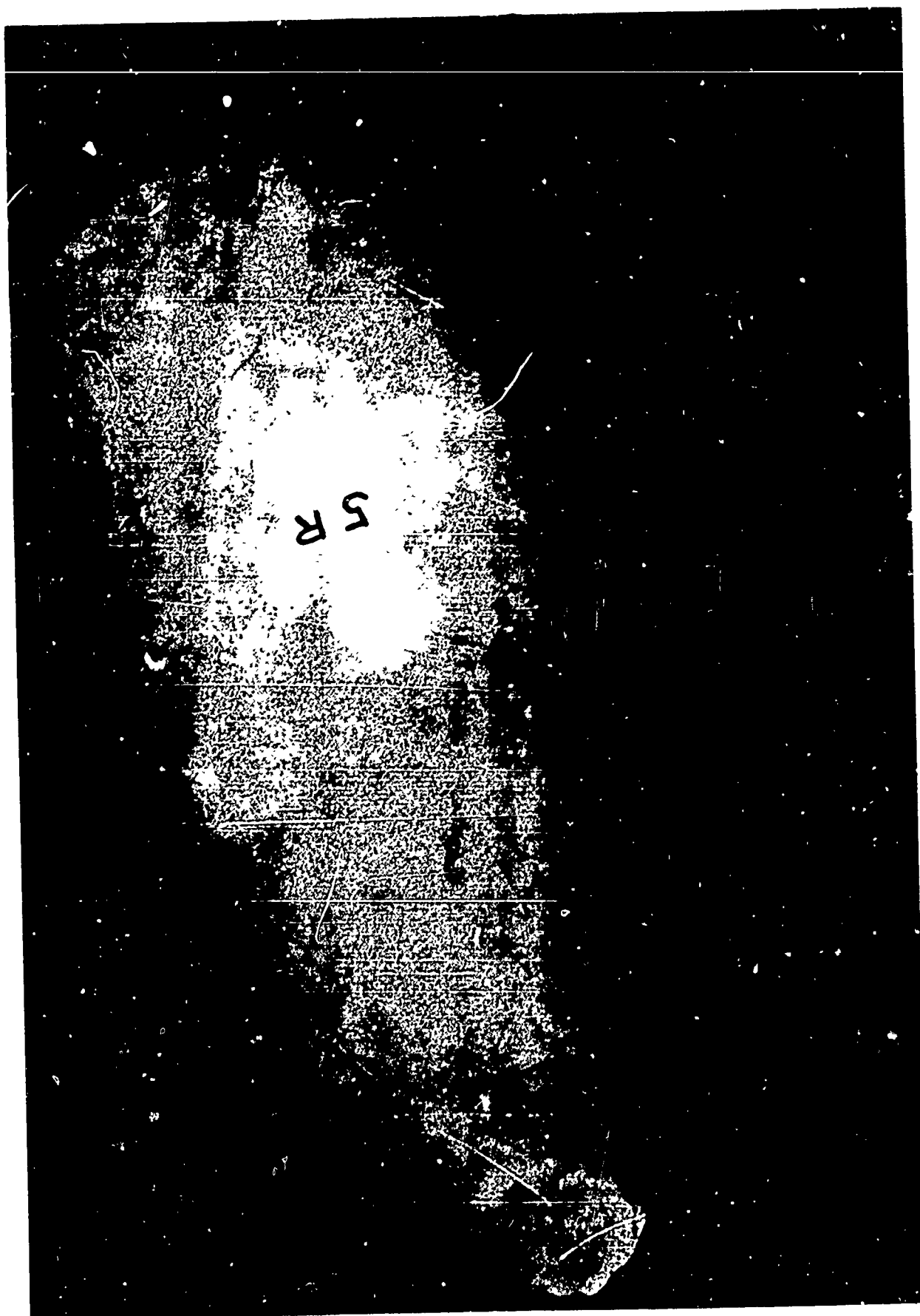


Figure 10. Unglazed Dome After Run #5.



Figure 11. Closeup of Unglazed Dome After Run #5.

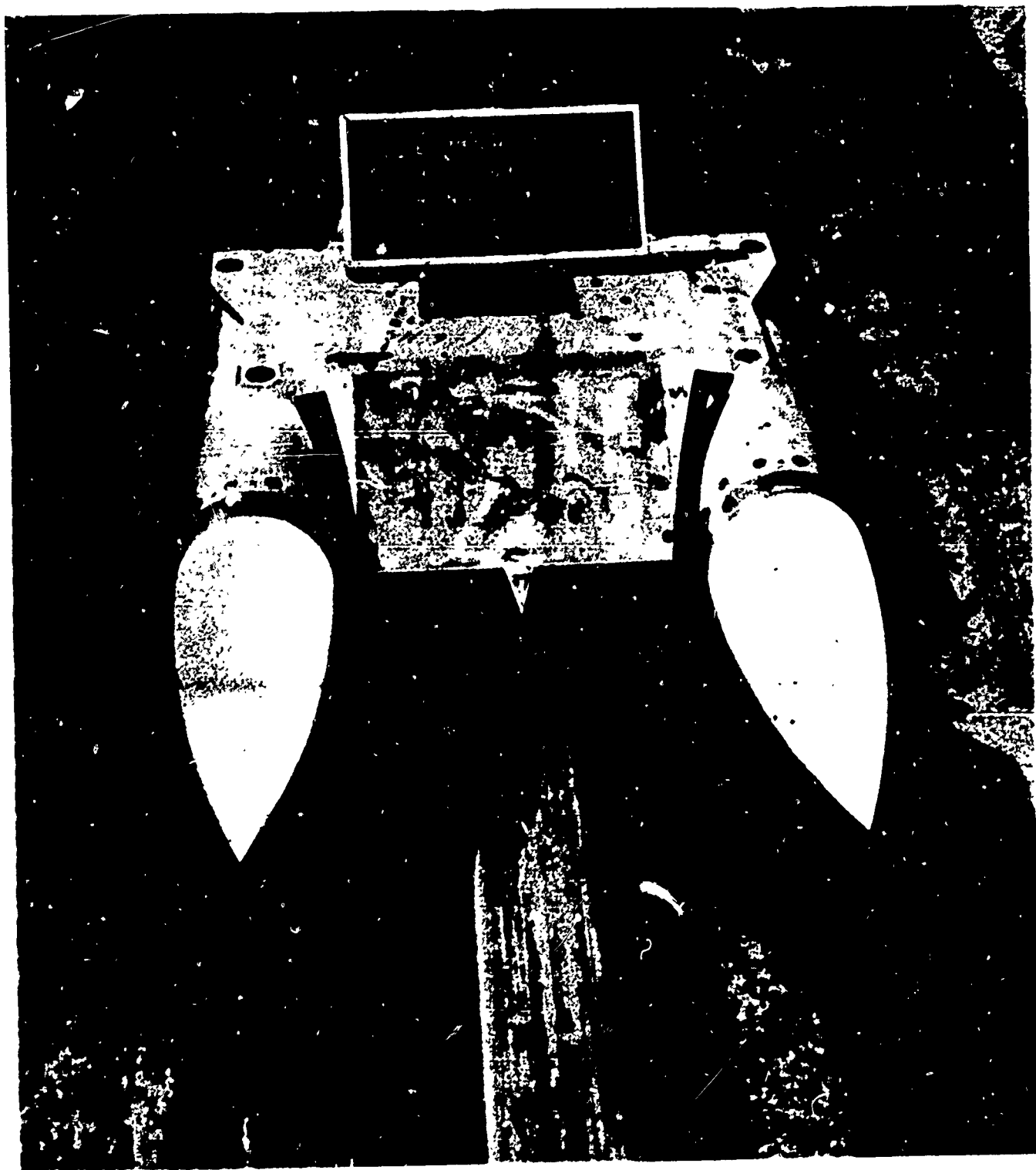


Figure 12. Pointed SCFS Domes Before Run #6.

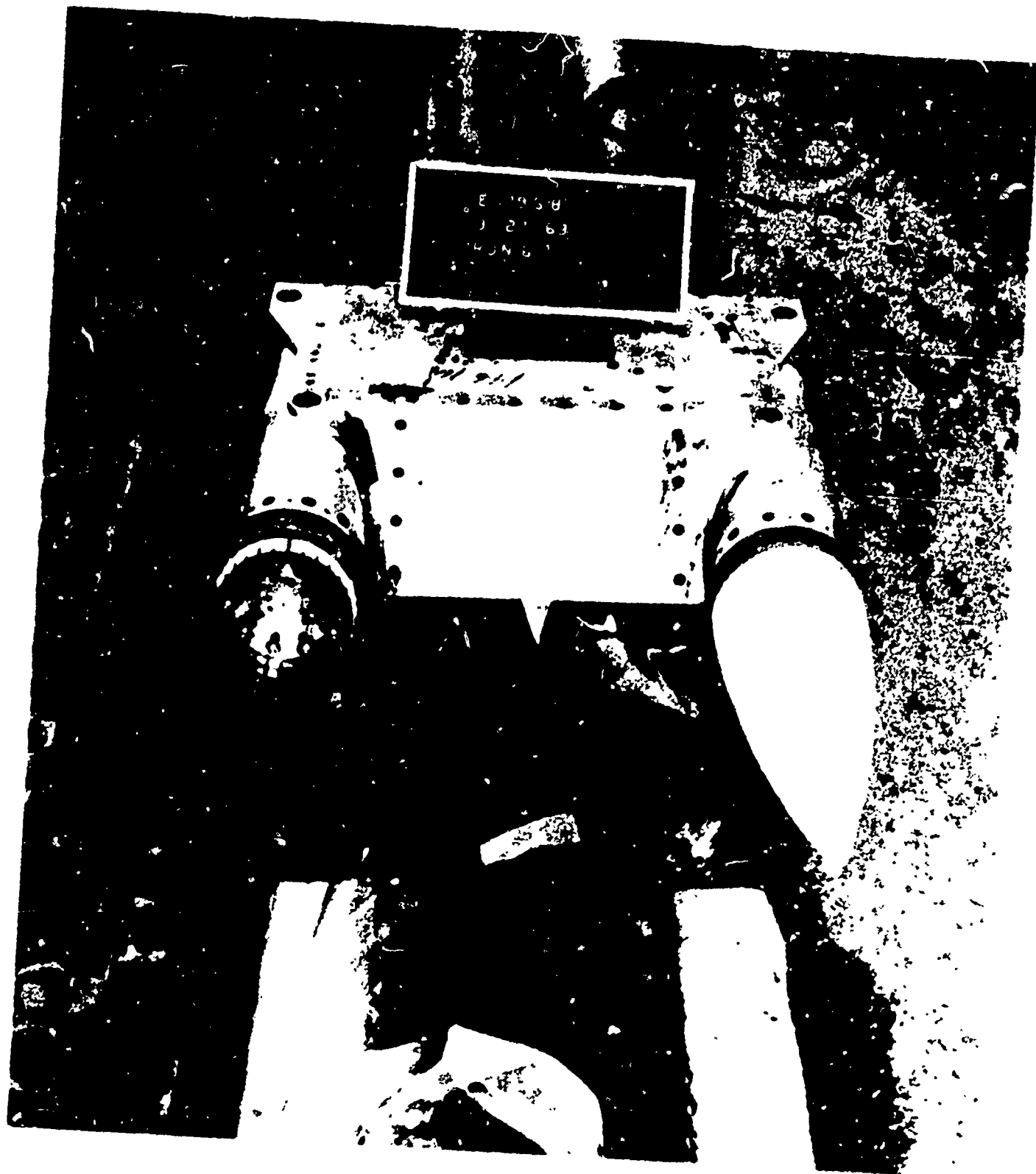


Figure 13. Pointed Unglazed Dome and Ring Attachment of Glazed Dome After Run #6.



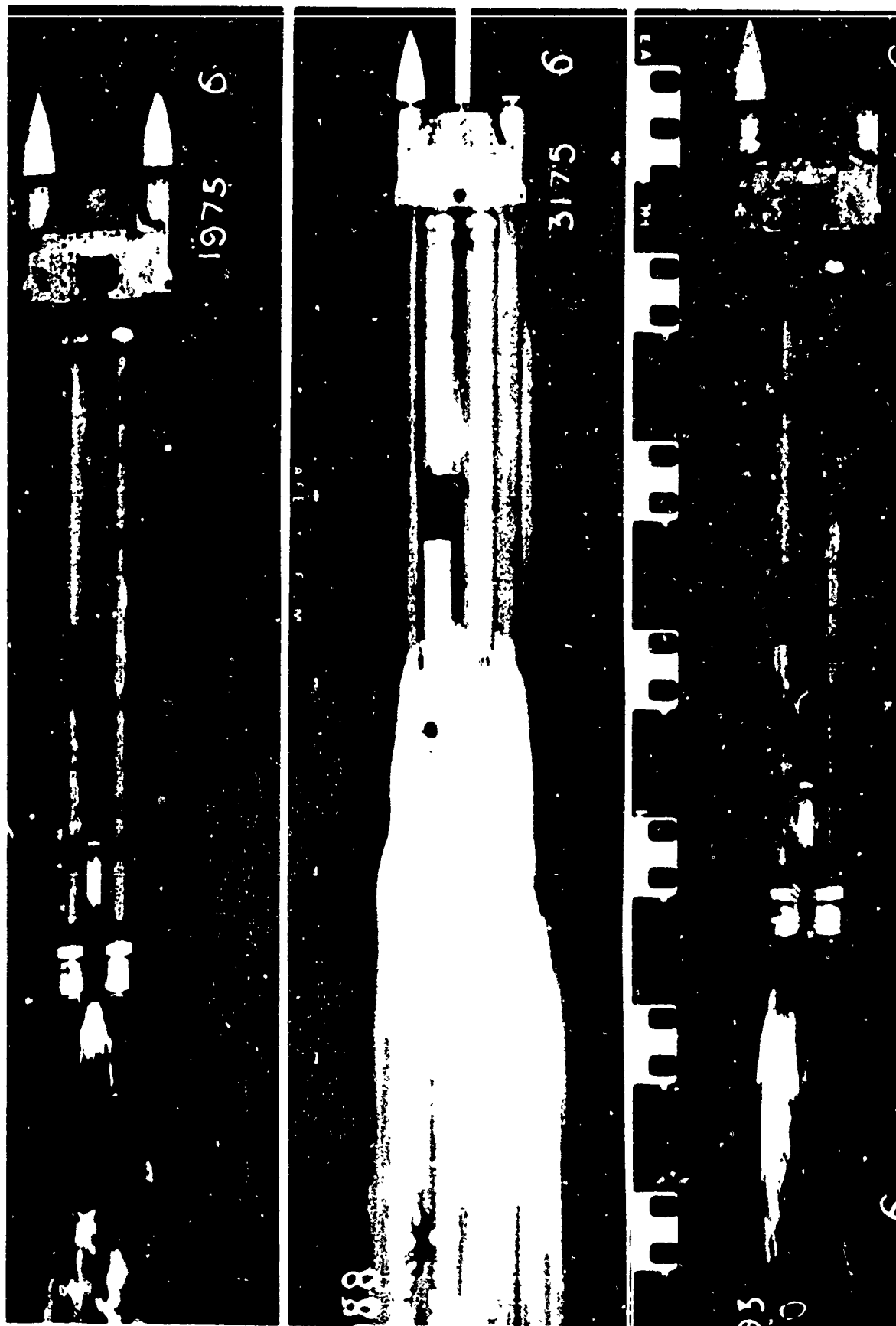


Figure 14. Synchronballistic Camera Shots of Run #6.

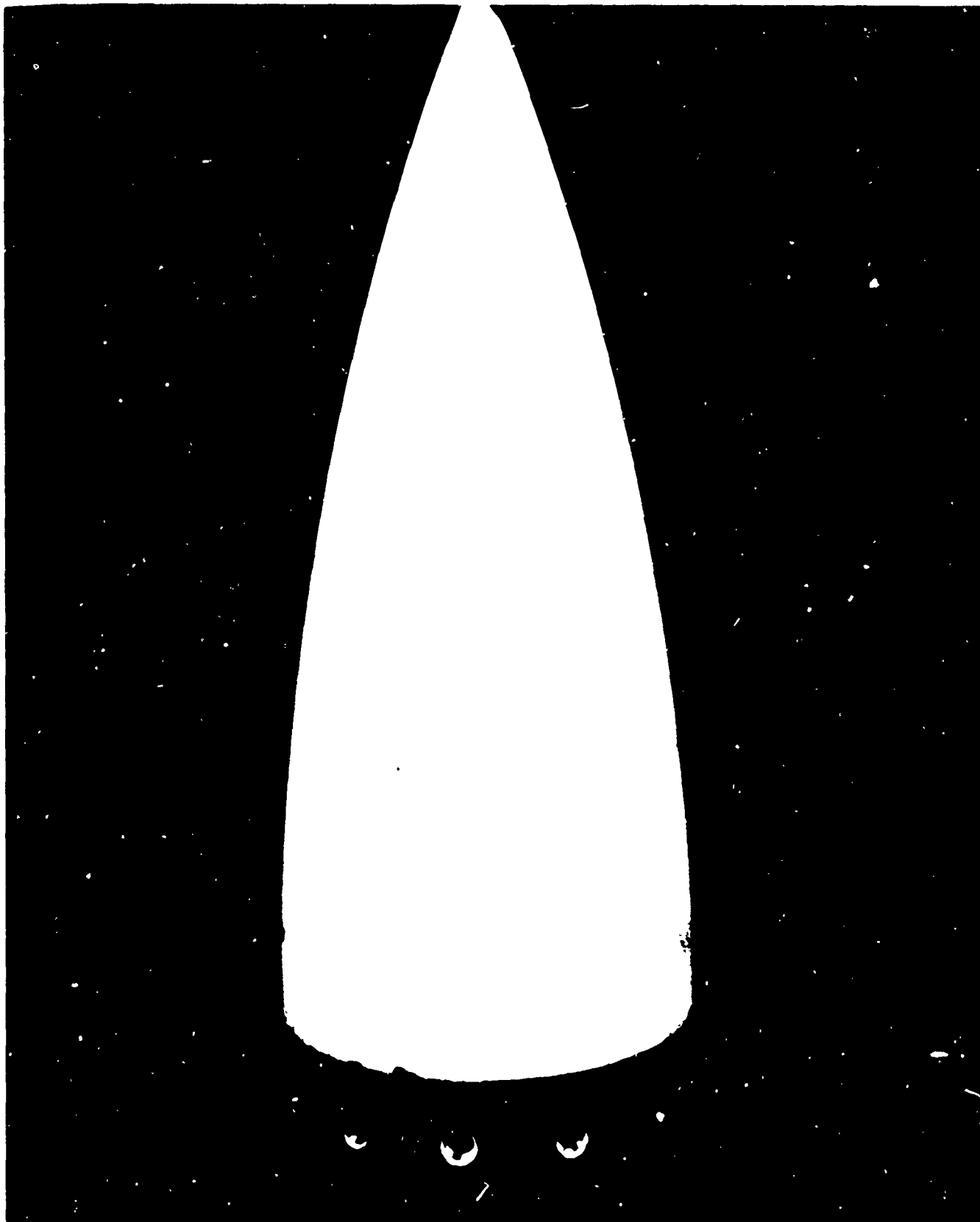


Figure 15. Unglazed Dome After Run #6.



Figure 16. Closeup of Unglazed Dome After Run #6.

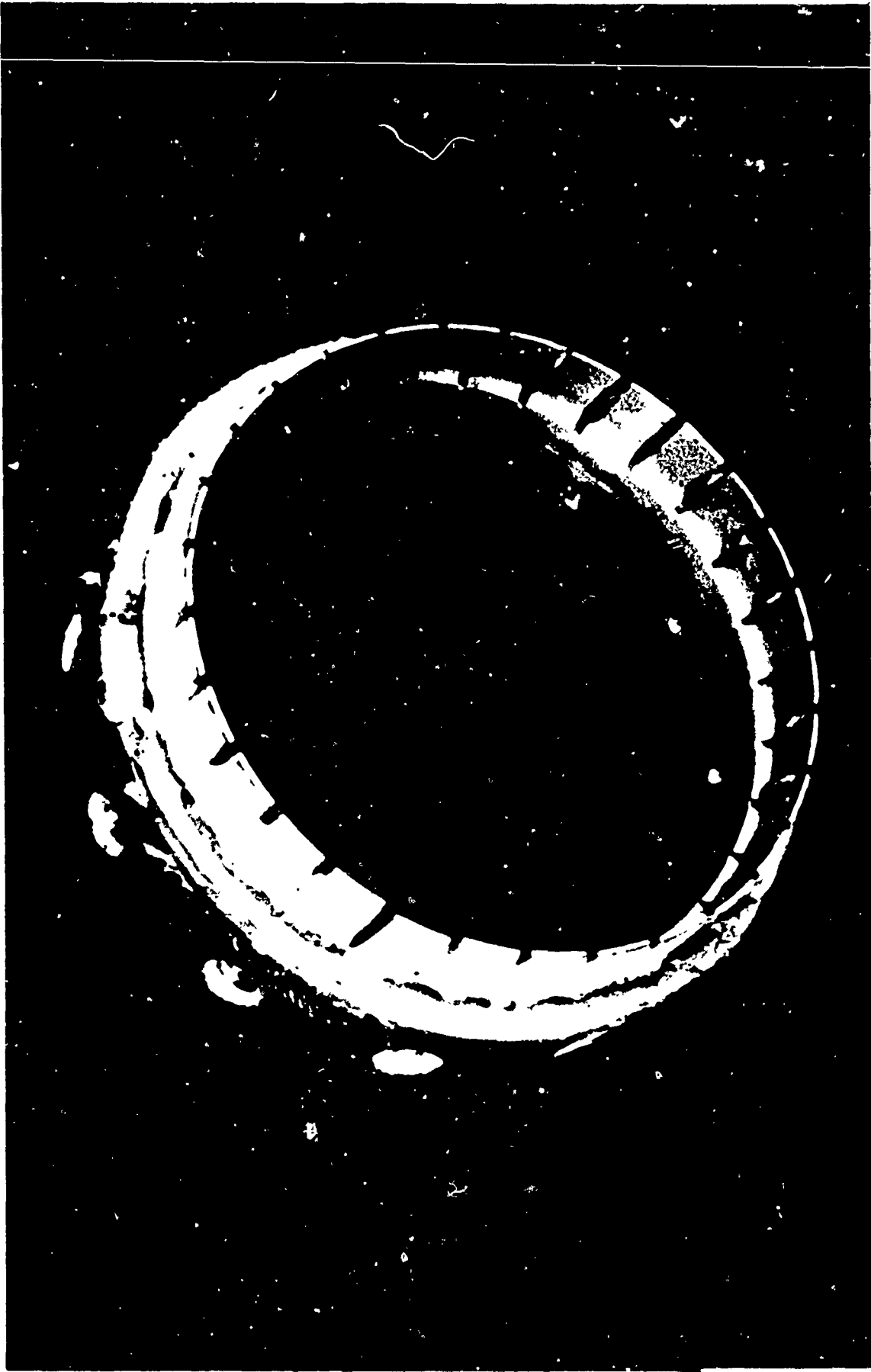


Figure 17. Ring Attachment From Pointed Dome After Run #6.



Figure 18. Pointed, Tip-glazed and Steel Tipped SCFS Domes Before Run #8.



Figure 19. Domes After Run #8.

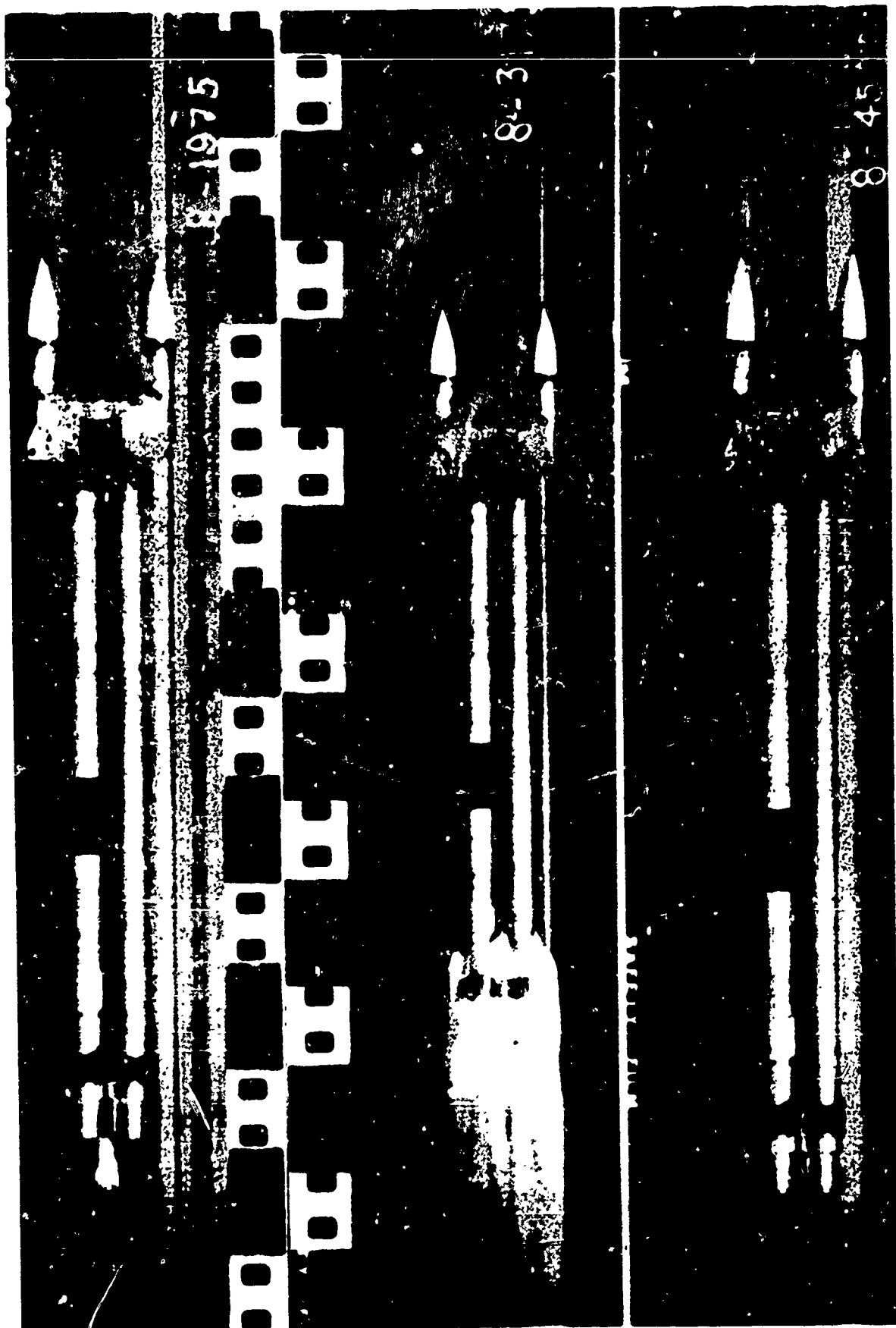


Figure 20. Synchronballistic Camera Shots of Run #8.

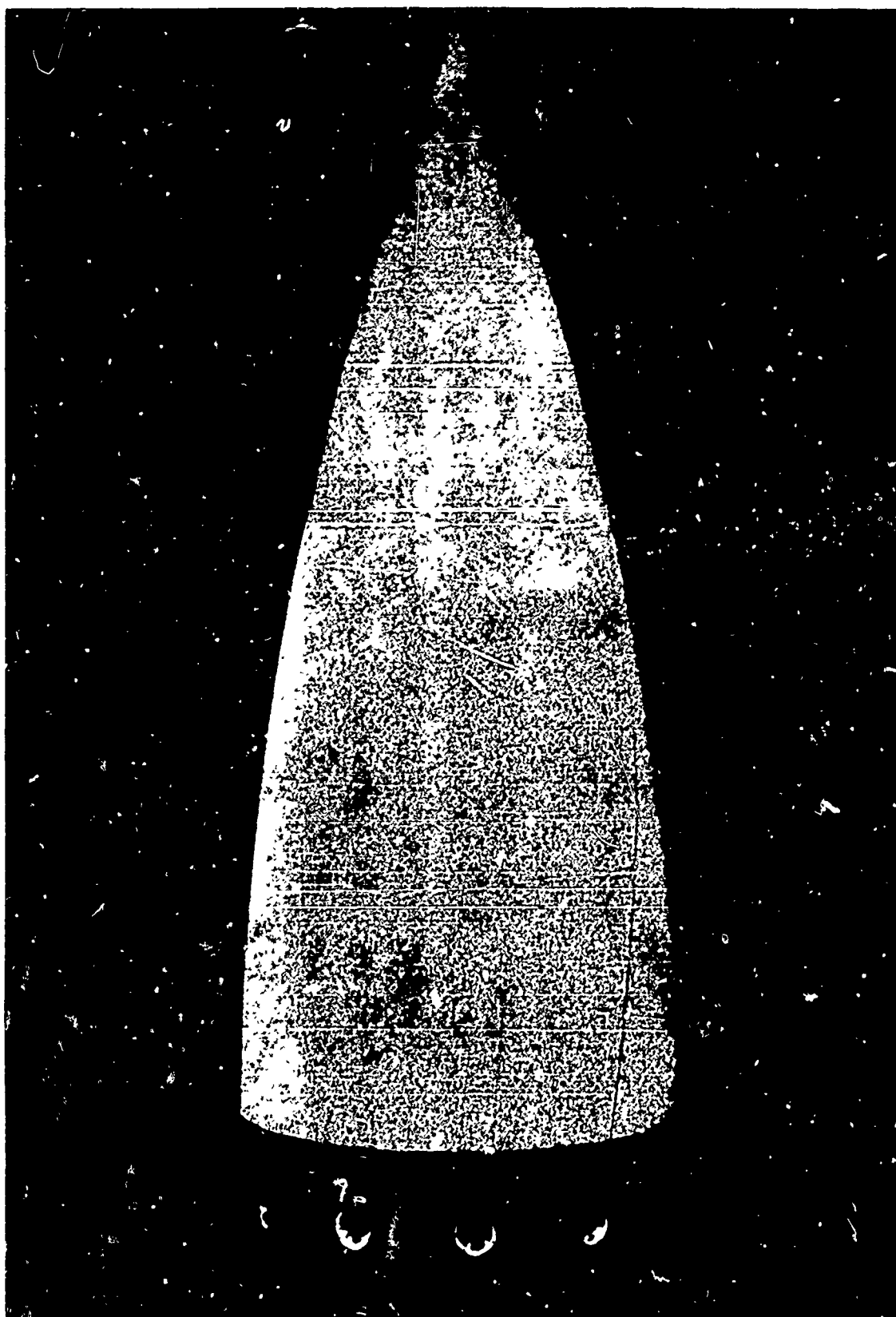


Figure 21. Pointed, Tip-glazed Dome After Run #8.

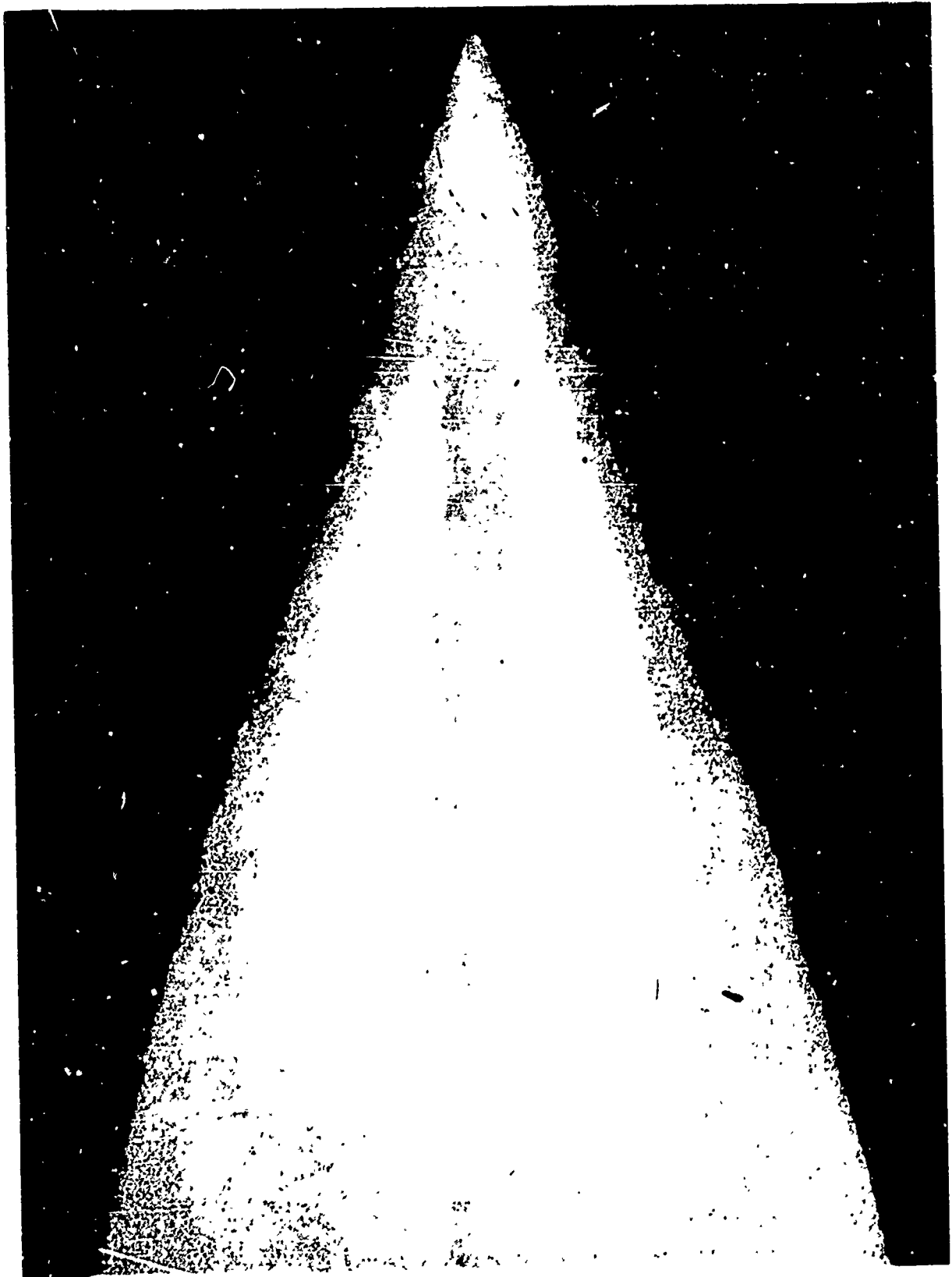


Figure 22. Closeup of Pointed, Tip-glazed Dome After Run #8.

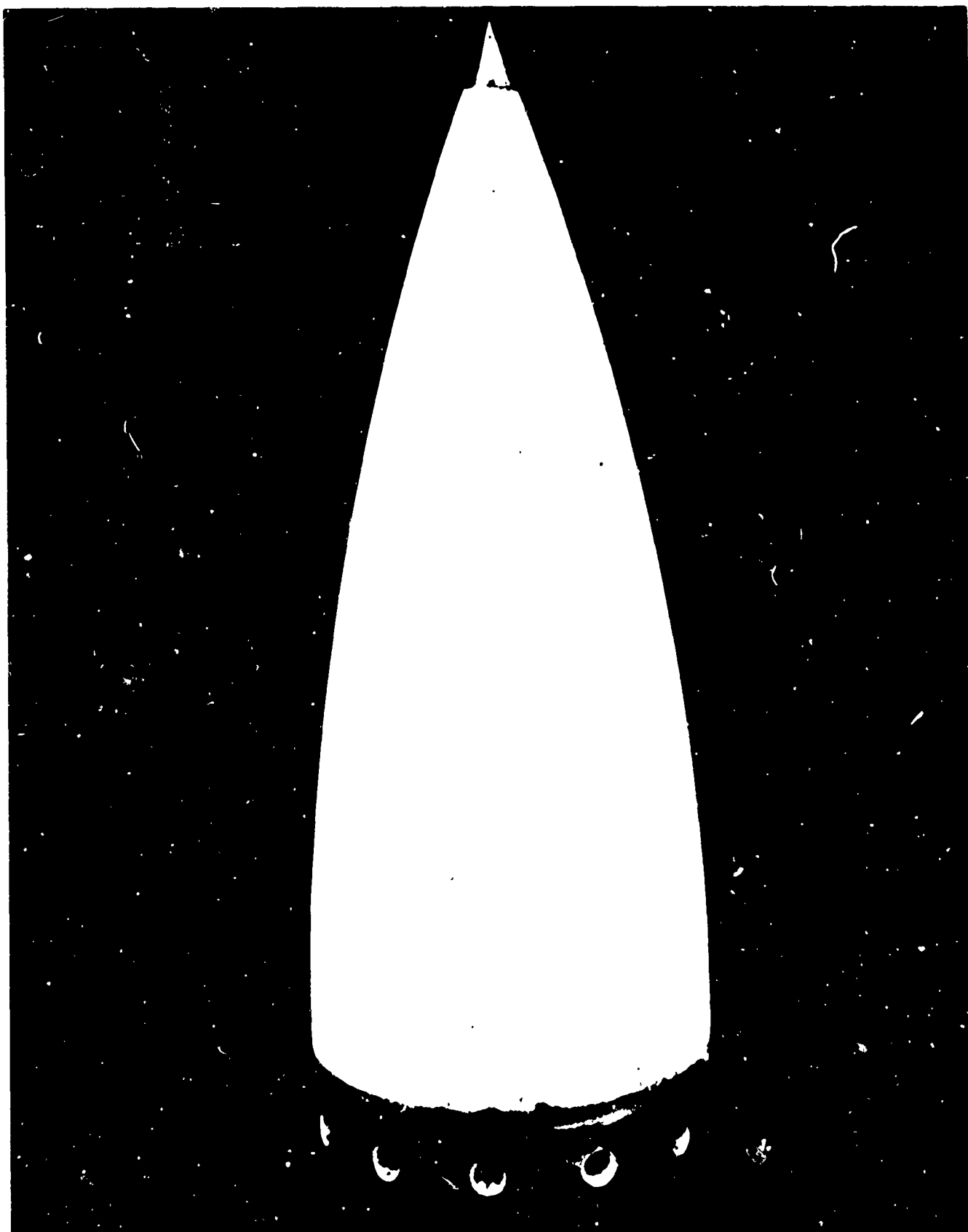


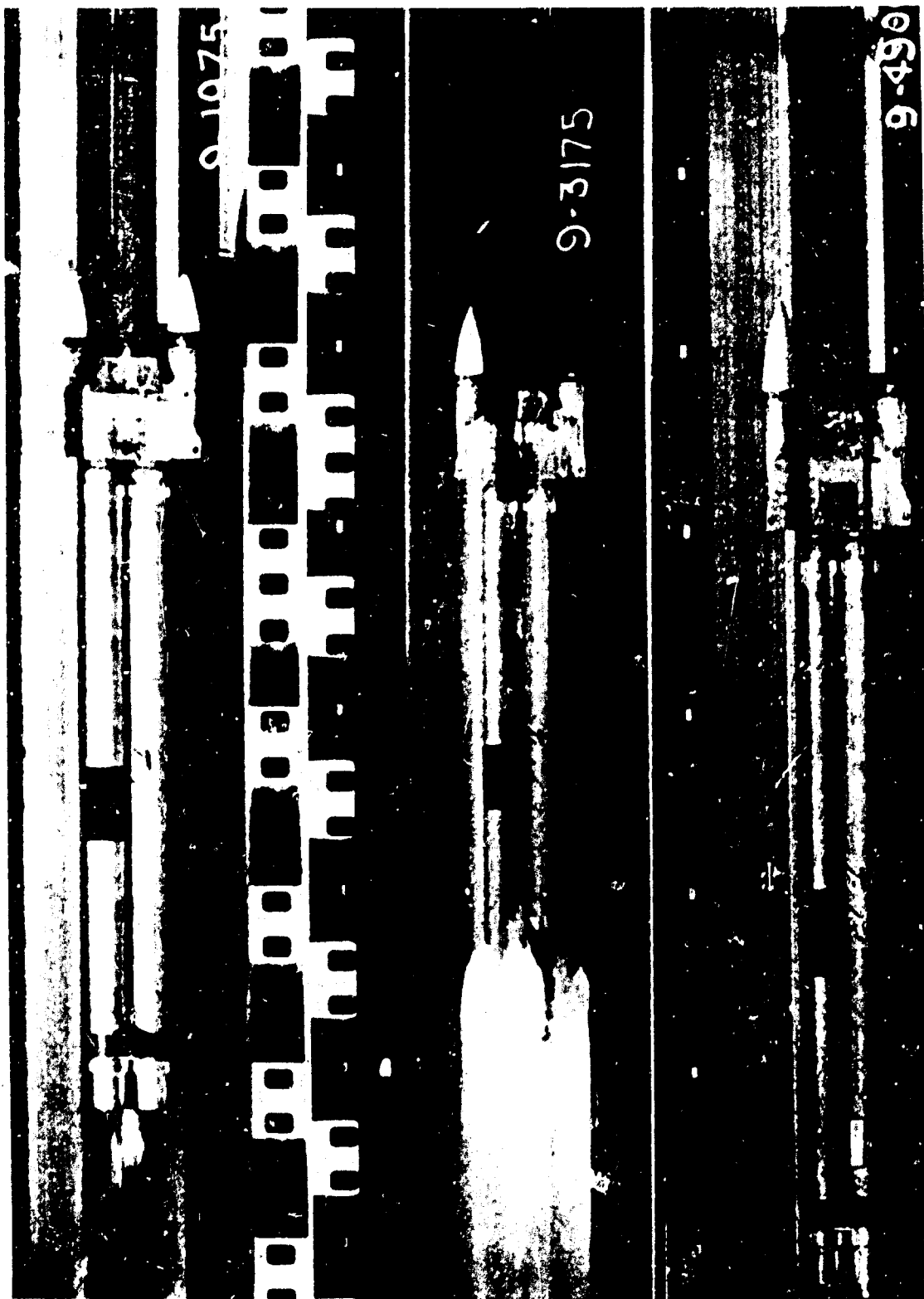
Figure 23. Steel Tipped Dome After Run #8.



Figure 24. Pointed, Tip-glazed Dome and Corning Fused Silica Dome Before Run #9.



Figure 25. Pointed, Tip-glazed Dome and Corning Ring After Run #9.



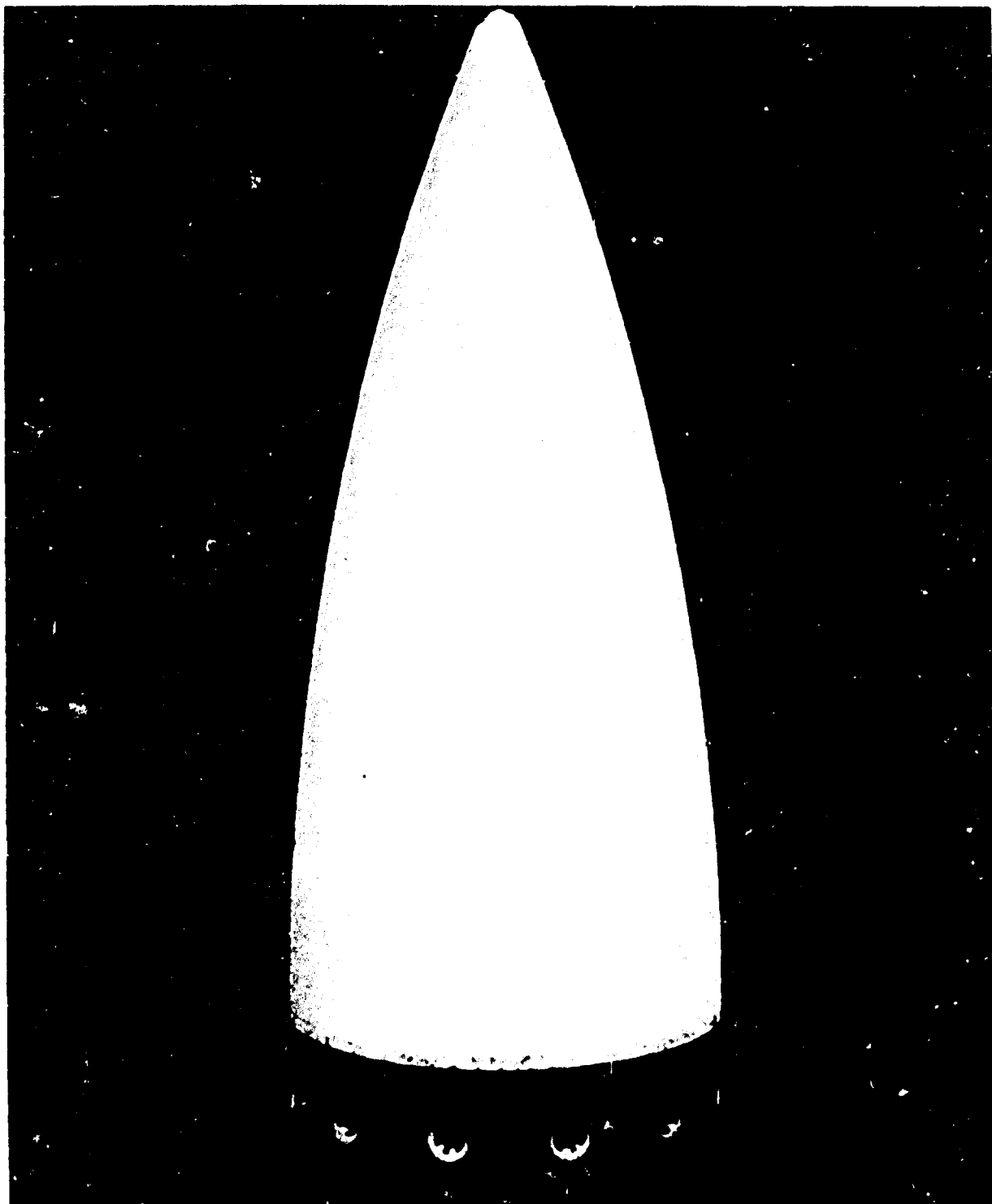


Figure 27. Pointed, Tip-glazed Dome After Run #9.